Alma Mater Studiorum - Università di Bologna

Human-Centric Wireless Communication Networks

Tesi di:
Riccardo Cavallari

Coordinatore:
Chiar.mo Prof. Ing. **Alessandro Vanelli-Coralli**
Relatori:
Chiar.mo Prof. Ing. **Roberto Verdone**
Dott.ssa Ing. **Chiara Buratti**

Esame anno finale 2016

Abstract

This thesis covers two main topics: the design and performance evaluation of Wireless Body Area Networks (WBANs), and the simulation and mathematical modeling of Delay Tolerant Networks (DTNs).

Different Medium Access Control (MAC) protocols for WBANs are implemented on dedicated hardware in order to evaluate, through extensive measurement campaigns, the performance of the network in terms of packet loss rate, delay and energy consumption. Novel solutions to cope with body shadowing and to improve the coexistence with other wireless technologies, are presented and evaluated. An analytic model for the CSMA/CA protocol defined in the IEEE 802.15.6 standard is also presented.

The benefits of offloading part of the traffic carried by a wireless backbone to a DTN composed of mobile nodes in a urban environment, is also investigated. A more analytic approach, mainly using tools from stochastic geometry and Markov chains theory, is used to develop a mathematical framework for the evaluation of the performance of routing rules for DTNs.

Contents

List of Figures

List of Tables

Introduction

This thesis presents the outcomes of the research carried out during my Ph.D. at the Department of Electrical, Electronic and Information Engineering "Guglielmo Marconi" (DEI) of the University of Bologna (Italy). Most of the research was conducted at DEI, however the research presented in Chapter 4 is the result of a collaboration with Assistant Prof. Stavros Toumpis at the Department of Informatics of the Athens University of Economics and Business (Greece), where I spent five months during the third year of the Ph.D.

Human-Centric Wireless Communication Networks: Concept

The general definition of *human-centric wireless communication networks* applies to all networks where the behavior of users plays a fundamental role in the performance of the network. Two types of human-centric wireless communication networks are studied in this thesis: Wireless Body Area Networks (WBANs) and Delay Tolerant Networks (DTNs).

WBANs are composed of receiving/transmitting nodes placed *in*, *on*, or *around* the human body. They are a particular type of Wireless Sensor Network (WSN) that collects data coming from the body and/or control

1

actuators placed on, or implanted in, the human body. The most common application of WBANs is in the field of healthcare, where nodes collect vital parameters (e.g., glucose levels), and may control an actuator accordingly (e.g., an insulin pump).

A DTN is a type of network without a dedicated infrastructure, and is characterized by being partitioned for most of the time. As a consequence, packets are delivered with large delays. DTNs are not tied to a specific implementation that involves the presence of people; historically, the paradigm of DTN was conceived to characterize the so-called *Interplanetary Internet* [3], used to connect spacecrafts. In the framework of this thesis, however, the nodes of the DTN are thought to be people moving in the same area (e.g., a city), and equipped with a short range wireless device (e.g., a smartphone with a Bluetooth transceiver). In this scenario, a DTN can be used to deliver delay-tolerant data from one location to another inside the area of interest. An example is the delivery of data coming from smart meters installed across the city generating data that need to reach a central gateway. The advantage of using a DTN is that the delivery of data comes "almost" for free, since no infrastructure needs to be deployed or maintained.

Problem Statement and Approach

The problems addressed for the two main topics, WBANs and DTNs, are different, as well as the approaches used to investigate them.

The design of a WBAN is challenging for several reasons. Among them, there is the presence of the human body, which creates non-ideal radio channel conditions between transmitter and receiver; the energy consumption, that must be kept as low as possible since typically WBAN nodes are battery-

powered; and lastly, the coexistence with other wireless technologies sharing the same radio resources of the WBAN. The designer can address these issues by acting on one or more layers of the ISO/OSI protocol stack. The work presented here is focused on the Medium Access Control (MAC) layer. The performance of a WBAN has been evaluated mainly with an experimental approach. A real WBAN has been designed and realized using an hardware platform tailored for WBAN applications, the whole protocol stack has been implemented in order to evaluate the performance of the network through extensive measurement campaigns. Novel solutions have been designed and applied to cope with the aforementioned issues. Different MAC protocols are studied and implemented. Some of them are taken from IEEE standards, namely IEEE 802.15.4 and IEEE 802.15.6; the former being the *de facto* standard for WSNs, and the latter is a relatively new standard (released in 2012) specifically made for WBANs. An original duty-cycling MAC protocol called Low Power Listening (LPL) is also presented and studied.

The part related to DTNs addresses two different problems: the offloading of delay-tolerant traffic from a wireless backbone to a DTN, and the analytic evaluation of the performance of different routing algorithms for DTNs. The two problems are addressed with simulations and analysis, respectively.

In the first case, a urban area with an already-deployed low-range wireless backbone is considered. The backbone is composed of nodes installed across the city, e.g., on lamp posts, that route packets from one location to another in a multihop fashion. The idea of exploiting a DTN composed of people moving around the city to carry part of the backbone traffic can be beneficial when the backbone is overloaded. However, if it is assumed that the backbone is interfered by the DTN, a tradeoff must be found in order not to degrade too much the performance of the whole system. This scenario has been studied

with simulations.

In the second case, a mathematical framework that uses tools from stochastic geometry and Markov chains theory is developed to evaluate the performance of different routing algorithms, for a mobile DTN where nodes move according to a Random Waypoint (RWP) mobility model. This work contributes in filling a gap in the literature for DTNs, where routing algorithms are studied mainly with a simulative approach.

Context: the WiserBAN Project

Most of the results presented in this thesis have been obtained in the framework of the large-scale Integrated Project (IP) "WiserBAN" [1], funded by the European Commission under the Seventh Framework Programme FP7. The aim of the project was to create an ultra-miniature and ultra-low-power RF micro-system for unobtrusive body-worn and implanted WBAN, targeting primarily lifestyle and biomedical applications.

The proposed research concerns WBAN communications at 2.45 GHz, with major focus on size and energy consumption issues, and uses a novel ad hoc radio architecture, where the minimization of the energy consumption is of primary importance.

The development of a dedicated communication protocol stack, as the one shown in Fig. 1a, is also one of the major project goals. Flexible and reconfigurable proprietary MAC/PHY solutions have to be designed and optimized for ultra low-power consumption, in compliance with already available standardized architectures used in WBAN communications.

At the application level, four industrial-driven wearable and implantable use cases are specifically addressed, representative of the great potential of

(a) Protocol stack.   (b) Use cases.
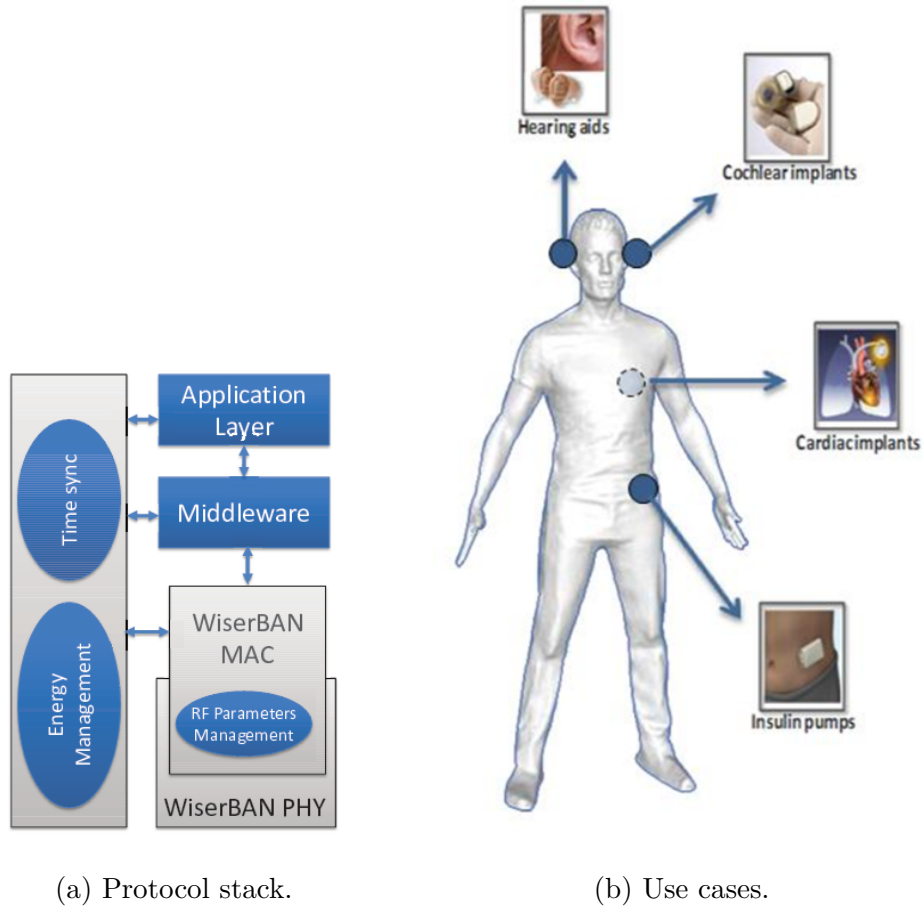
Figure 1: WiserBAN application use cases and protocol stack. Figure taken from [1].

WBANs for healthcare, bio-medical, and lifestyle applications (see Fig. 1b):

- *Hearing Aids* and *Cochlear Implants* use case: wireless connectivity is fundamental to improve performance and comfort of modern hearing systems. Therefor device miniaturization and low-power consumption are important issues to be addressed, together with enabling the transmission of different types of traffic, both streaming and non-streaming. Communication between hearing appliances and an external remote unit (e.g., a mobile phone) should be allowed, as well as bidirectional ear-to-ear transmissions.

- *Cardiac Implants* use case: it concerns people carrying cardiac implants in the context of remote monitoring of patients. Decreasing device power consumption leads to the reduction of battery size and hence of implant dimension, resulting in more comfort for the user. Wireless communication with an external remote controller should be considered.

- *Insulin Pumps* use case: a patch insulin pump for medication delivery is applied on the patient's skin, concealed under his clothes. Users interact with the pump using a remote controller, through a wireless link that should be easily established. Long-lasting batteries, as well as light and comfortable devices, are hence critical aspects to be accounted for.

Beyond these primary reference use cases, the WiserBAN technology, with its ultra-low-power and miniature radio microsystem, may be leveraged in other complementary application areas, such as ambient intelligence, home automation, entertainment, sports and fitness, motion capture, localization, and other related applications concerning WBANs and WSNs in general.

Structure and Contribution of the Thesis

The thesis is divided in two parts. The first part presents the work related to WBANs, while the second is about DTNs.

Chapter 1 introduces the topic, describing the current wireless technologies for WBANs, and discussing the main issues in a WBAN design, namely radio channel characterization, minimization of the energy consumption, and coexistence.

Chapter 2 that is devoted to the performance evaluation of WBANs. Although the main topic is presented in the third section, the chapter starts with a section devoted to the description of the reference WBAN that has been implemented, and continues with a section that presents an analytic model for the performance evaluation of the CSMA/CA protocol defined in the IEEE 802.15.6 standard. The outcome of this work is contained in the following published papers: [4], [5], [6], [7], [8], [9] and [10]; the last two being published in journals.

Part II is also divided in two chapters. The first section of Chapter 3 introduces the concept of DTNs, while the rest of it is about DTN offloading. After a description of the reference scenario, the MAC protocol and the offloading mechanism, the simulation results show the benefits brought by the introduction of the DTN offloading. This work is published in [11].

Chapter 4 presents the analytic framework developed to evaluate the performance of different routing rules for DTN. The performance is evaluated in terms of average packet speed towards the destination and average packet cost; a tradeoff between the two performance metrics is studied. Four routing rules are presented and one of them is completely analyzed using the proposed framework, while the other three are simulated. The comparison between analytic results and simulation proves that the framework models accurately the DTN, despite the fact that some approximations are done to make the model tractable. The work presented in this chapter has been submitted to [12].

Finally, the concluding Chapter 4.7 sums up the major achievements of the thesis and, for each chapter, suggests possible future research directions.

Part I

Wireless Body Area Networks

Chapter 1

Wireless Body Area Networks

The aim of this chapter is to introduce the concept of Wireless Body Area Networks (WBANs), to present three wireless technologies that can be employed to realize a WBAN, and to discuss the main issues related to the WBAN design. A more in-depth discussion on these aspects can be found in [7].

1.1 Definition and Taxonomy

A WBAN typically consists of a collection of low-power, miniaturized, either invasive or non-invasive devices with wireless communication capabilities that operate in the proximity of a human body. These devices can be placed in, on, or around the body, and are often wireless sensor nodes that monitor human body functions and characteristics from the surrounding environment.

On one hand, WBANs enable new applications and thus new possible markets with respect to Wireless Sensor Networks (WSNs); on the other hand, their design is affected by several issues that call for new paradigms and protocols.
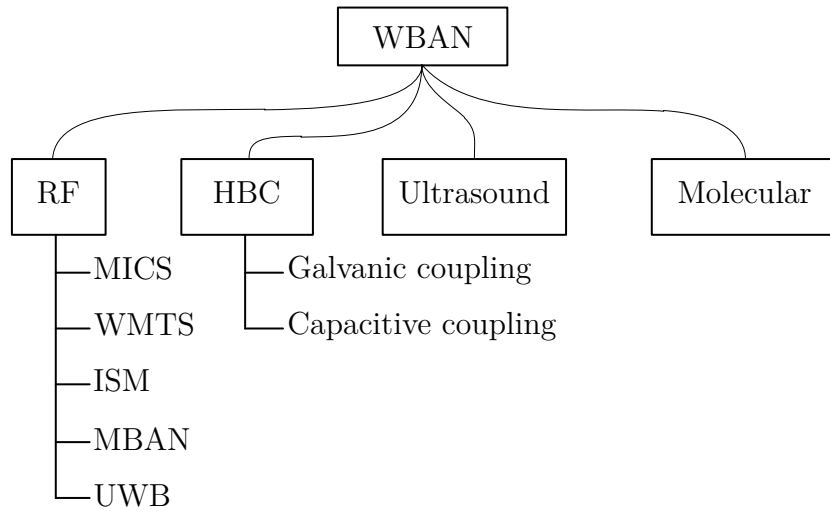
Figure 1.1: Taxonomy of WBANs.

The envisioned applications span from the medical field (e.g., vital signals monitoring, automatic drug delivery, etc.) to entertainment, gaming, and ambient intelligence areas. They create a set of technical requirements with a wide variety in terms of the expected performance metrics, such as throughput, delay and energy consumption; therefore, flexible architectures and protocols are needed.

1.1.1 Taxonomy

WBANs can be classified according to the wireless communication technology employed. This section presents on overview of these technologies, considering not only Radio Frequency (RF) solutions, but also other technologies, as Human Body communication (HBC), molecular communications and ultrasonic waves. This classification of WBANs is summarized in Fig. 1.1.

The majority of the works that can be found in the literature are about WBANs based on RF techniques, which can be classified according to the frequency band they operate in. Worldwide communication authorities reg-
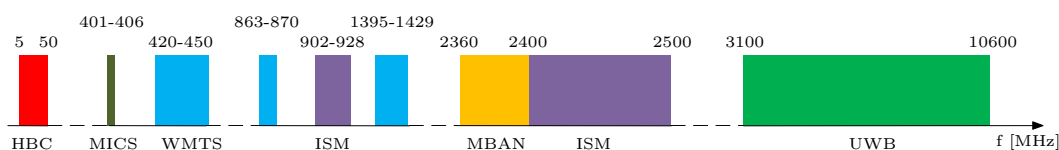
Figure 1.2: Some of the available RF bands for WBANs.

ulate the use of the frequency spectrum, however, it is not straightforward for the WBAN designer to choose the most appropriate band for the target application. To this end, the IEEE 802.15 Task Group 6 delivered a report providing an overview of frequency regulations for medical applications in different countries and regions [13]. The different bands are illustrated in Fig. 1.2 and described in the following.

Wireless Medical Telemetry System (WMTS) and Medical Implant Communications Service (MICS) bands are allocated exclusively for body-worn and implanted medical applications [14], which require simple point-to-point communication. They were introduced to overcome the range, bit rate and reliability limitations imposed by the magnetic coupling communication technology used in the early wireless medical devices. Within the MICS bands it is possible to achieve a bit rate up to 400 kbps and a communication range around 2 meters [15] to satisfy the requirements of application such as cardiac pacemakers, implanted defibrillators and neurostimulators. Applications like the swallable camera pill may require bit rate in the order of 1 Mbps, which are achievable in the WMTS band.

The unlicensed Industrial Scientific and Medical (ISM) bands are defined by the International Telecommunication Union (ITU) and are designated for purposes different from telecommunications. Some of them are subject to specific countries' radio regulations [16]. Being unlicensed, the ISM bands are prone to coexistence issues that must be taken seriously into account by the WBAN designer. The band between 2.4 and 2.5 GHz is often preferred

among the others because of its worldwide availability. An interesting action was taken by the Federal Communications Commission (FCC) on May 2012 to allocate 40 MHz of spectrum between 2.36-2.40 GHz on a secondary basis for a new Medical Body Area Network (MBAN) licensed service [17]. This will be an effective way to mitigate the interference experienced by devices working in the adjacent ISM unlicensed band.

Another option is Ultra-wide Band (UWB). An UWB signal is formally defined by the ITU as any signal that occupies more than 500 MHz of spectrum. The regulatory authority specifies, however, that the power spectral density shall not exceed -41.25 dBm/MHz, which is around 30 dB below the maximum allowed for a signal in the 2.4-2.5 GHz ISM band [13]. Some positive features that make UWB a good candidate technology for WBANs are the low susceptibility to multipath fading that improves the performance of indoor systems, the immunity to interference, and the very high bit rate (up to 500 Mbps). Moreover, intrinsically secure communication is possible thanks to the low energy and spectral density, which is below the noise floor of conventional receivers, and the simplicity of the transceiver architecture.

Although the work presented in this thesis is exclusively on RF WBANs, recent works have shown that other wireless communication paradigms can be applied in this framework.

One of these techniques is neither wireless nor wired, in fact; it uses the human body as communication medium. It is called *Human Body Communication* (referred to also as Intra Body Communication and Body Channel Communication). The signal propagation through the human body is possible by capacitive coupling of the human body to its surrounding environment, and galvanic coupling achieved by coupling alternate current into the human body. The benefits HBC can bring to a WBAN are: intrinsic security since

signals are confined to the person's proximity and receiving data requires body contact, the energy consumption can be kept as low as one order of magnitude compared to UWB at around 10 Mbps, and coexistence with other HBC WBANs is possible because the communication is confined in or in the immediate proximity of the human body. HBC technology defined in the standard IEEE 802.15.6 works in a band centered at 21 MHz with a width of 5.25 MHz. An extensive survey of HBC can be found in [18], while a general model for HBC is derived from Maxwell's equations in [19].

Considering in particular in-body WBANs, molecular and ultrasonic communications represent good alternatives to RF solutions. The former refers to the use of molecules as messages transferred between a transmitter and a receiver using nanotechnology [20], while the latter is based on the use of ultrasound, i.e. acoustic waves at non-audible frequencies [21].

Due to their intrinsic biocompatibility, diffusion-based *molecular communications* are promising for nanomedicine applications, such as restoration of the glucose feedback loop in diabetic patients, recognizing and destroying tumors with engineered bacteria, or even intracellular surgery with nanorobots [22]. On the other hand, their use brings crucial challenges that have to be addressed to allow the realization of reliable networks. Channel characteristics differ significantly from those of the classic RF medium in terms of propagation delays, noise, applicable modulations, and achievable capacity. The nature of molecular movement (based on Brownian motion) has to be taken into account when designing MAC and routing solutions, which have to be as simple as possible, given the very low memory and processing capabilities of nanomachines [22].

Ultrasonic waves can overcome some of the limits of RF propagation inside the human body, such as the high attenuation values. They have been

used in the last decades as the preferred technology solution for underwater communications and they are thus considered a suitable option for enabling communications inside the human body, which is mostly made up of water [21, 23]. Proper design choices have to be made at the physical (PHY), Medium Access Control (MAC), and network layers to achieve high capacities and to realize WBANs based on ultrasonic communications.

1.2 Applications and Requirements

The ability to deploy wireless sensor nodes on the human body leads to the opportunity of developing a large number of applications in several fields. This section starts by presenting a set of possible applications for WBANs, and then continues with a discussion of the requirements imposed by these applications.

1.2.1 Applications

Healthcare

At a first glances healthcare is the most promising field of application for WBANs. Several non-intrusive sensors deployed inside or on the human body allow the patients and the doctors to continuously sample biomedical signals [24]. Events that require prompt assistance, like heart attacks and epileptic seizures, can be detected and even predicted thanks to the continuous monitoring of the heart and brain activities, respectively. WBANs cannot only detect fatal events and anomalies, they can also improve the lifestyle of hearing and visually impaired people by means of hearing aids, cochlear implants andartificial retinas, respectively [25–27]. The following is a non-exhaustive list of applications that can benefit from WBAN usage: electro-

16

cardiogram (ECG), electroencephalogram (EEG), electromyogram (EMG), pulse oximetry, drugs delivery, monitoring of postoperative conditions, temperature, glucose level, toxins, blood pressure, etc.

Sports and Entertainment

A real-time log of vital parameters like blood pressure, heart beat, blood oximetry and posture can improve fitness and sport experiences. This is because users can gather information concerning their sport activity and then use them to prevent injuries and plan future training to improve their performance.

WBANs bring more realism in the user experience in the field of entertainment. Motion capturing techniques make it possible to track the position of different parts of the body by means of a network of gyroscopes and accelerometers wirelessly connected to a central node and worn by the user. The real-time information about the motion allows the user to use his/her body as a controller in videogames. Moreover, the film industry takes advantage of motion capture along with post-production techniques to realize highly realistic digital movies where actors play the role of non-human subjects [28].

Military and Defence

Network-Enabled Capability (NEC) is the name of the long-term research program aimed at achieving enhanced military capabilities through the use of information systems [29]. New capabilities added by a WBAN will enhance the performance, at both individual and squad level, of soldiers engaged in military operations. At individual level, a set of sensors can monitor vital parameters and provide information about the surrounding environment in order to avoid threats, while information taken at squad level will make

the commander able to better coordinate the squad actions and tasks. Spatial localization techniques and communication between different WBANs (inter-WBAN communications) play an important role in this field, as well as security in order to prevent sensitive information from being acquired by the enemy [30].

1.2.2 Requirements

Developing a WBAN is a challenging task because of the broad range of requirements imposed by the applications described in Sec. 1.2.1. The most important requirements, as recommended by the IEEE TG6 [31], are detailed in this section. Some of them are better analyzed and discussed in the following sections.

Bit rate and Quality of Service (QoS)

The bit rate requirement varies on a very broad range depending on the application and on the type of data to be transmitted. It goes from less than 1 kbps (e.g., temperature monitoring) to 10 Mbps (e.g., video streaming). The bit rate can refer to a single link or to multiple links, when several devices transmit/receive information to/from one coordinator at the same time (e.g., multiple leads ECG).

High levels of QoS should be guaranteed in medical and military applications. Appropriate error correction and interference-avoidance methods should be implemented at the MAC and PHY layers to reduce the bit error rate (BER). Other important parameters are the end-to-end delay, the delay variance and the capability to provide fast and reliable reaction to emergency situations. Furthermore, for this kind of WBAN the capability to handle traffic with different priority levels is important [31]. In Table 1.1 a

18

Table 1.1: Bit rate and QoS requirements for some WBAN applications [2].

Application	Bit rate	Delay	BER
Deep brain stimulation	< 320 kbps	< 250 ms	< 10^{-10}
Drug delivery	< 16 kbps	< 250 ms	< 10^{-10}
Capsule endoscope	1 Mbps	< 250 ms	< 10^{-10}
ECG	192 kbps	< 250 ms	< 10^{-10}
EEG	86.4 kbps	< 250 ms	< 10^{-10}
EMG	1.536 Mbps	< 250 ms	< 10^{-10}
Glucose level monitor	< 1 kbps	< 250 ms	< 10^{-10}
Audio streaming	1 Mbps	< 20 ms	< 10^{-5}
Video streaming	< 10 Mbps	< 100 ms	< 10^{-3}
Voice	50 - 100 kbps	< 100 ms	< 10^{-3}

list of requirements for different WBAN applications is collected.

Range and Topology

The communication range should not be larger than a few meters (3 to 6 m) for most of the applications, as presented in [32]. Thus, a star topology is usually enough; however, the human body can represent an obstacle itself for the radio propagation, especially for the implanted nodes. In this case, a multi-hop communication scheme must be established and a relaying technique should be used in order to exploit node spatial diversity. The number of nodes forming the WBAN, including the coordinator, ranges from two (e.g., glucose meter) to dozens (e.g., motion tracking suit, multi-leads ECG) and can vary at run time. Therefore, the network should implement reliable association and disassociation procedures to guarantee at any time the knowledge of the current network members.

Security

Security is of primary importance, especially for what concerns medical and military applications, and it should be addressed in terms of privacy, confidentiality, authorization, and integrity [32]. However, conventional data encryption mechanisms or authentication processes are not perfectly suitable for these kind of networks due to limited processing power, memory, and energy of WBAN nodes. A promising solution in this context is the use of biometric identification based mechanisms [33, 34].

Antenna and Radio Channel

Antenna design can be a very critical issue and research on miniaturization should target efficient solutions [35], always considering the proper trade-off between antennas sizes and their efficiency. Moreover, the presence of the human body cannot be neglected since it affects antenna's radiation and polarization characteristics, according to the specific on-body position of each device [36, 37]. A good radio channel characterization is therefore mandatory in order to design an antenna able to provide the proper radiation properties. The impact of the radio channel on network performance is discussed in Sec. 1.4.1.

Energy Consumption

The energy consumption requirement is very dependent on the nature of the application. However, WBAN devices are generally battery-powered and the battery lifetime is required to be up to several years for implanted devices (e.g., pacemakers require at least five years) [38]. Ultra-low power designs for radio transceivers and MAC protocols are essential. A common technique for the latter at the expense of end-to-end delay is lowering the duty cycle, which

allows devices to be in sleep mode (i.e., the transceiver and CPU shut down) for most of the time. Energy scavenging could also be an option to lessen the need for a battery [39, 40]. Energy consumption issues are addressed in Sec. 1.4.2.

Coexistence

Most WBANs are designed to operate in the license-free ISM band centered at 2.45 GHz. This is an overcrowded radio band; indeed, Wi-Fi (IEEE 802.11), Bluetooth, IEEE 802.15.4/ZigBee and other standards operate in this band. Many WBAN applications (e.g., medical applications) require very high reliability, especially when an emergency or alarm traffic has to be established, therefore techniques to avoid or reduce interference should be studied and implemented. Coexistence issues are addressed in Sec. 1.4.3.

1.3 Wireless Technologies for WBANs

This section describes three wireless technologies that can be used to realize a WBAN. The first two, IEEE 802.15.4 and IEEE 802.15.6, are standard technologies that define the two bottom layers of ISO/OSI protocol stack, namely PHY and MAC layers; whereas the third, Low Power Listening (LPL), is a proprietary MAC algorithm. As well as in the rest of the thesis, the focus is on the MAC layer and specifically, on the channel access algorithms.

1.3.1 The IEEE 802.15.4 Standard

IEEE 802.15.4 defines a wireless technology for Wireless Personal Area Networks (WPANs). This standard targets applications characterized by short-

Beacon   Beacon

CAP	CFP	Inactive
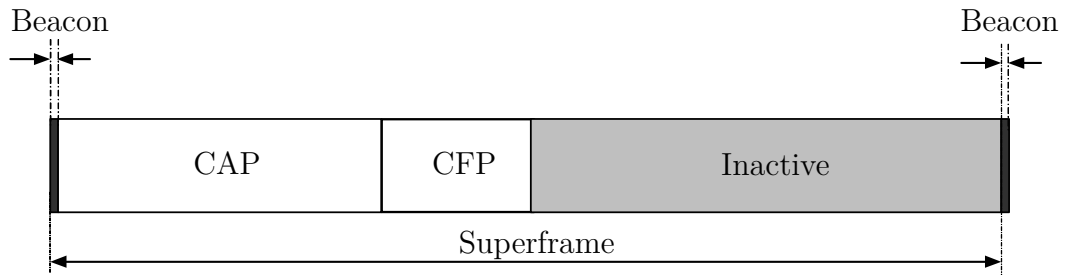
Superframe

Figure 1.3: IEEE 802.15.4 Superframe structure.

range (up to 100 m), relaxed throughput, and latency requirements. The key features of IEEE 802.15.4 wireless technology are low complexity, low cost, low power consumption, low bit rate transmissions, to be supported by cheap, fixed or mobile devices. The main field of application of this technology is WSNs. The network topologies supported are star, tree and mesh [41].

IEEE 802.15.4 specifies a total of 27 half-duplex channels across three frequency bands, organized as follows: i) The 868 MHz band with a single channel at a bit rate of 20 kbps; ii) The 915 MHz band, where ten channels, each with a bit rate of 40 kbps are available; iii) The 2.45 GHz ISM band with sixteen channels at bit rate equal to 250 kbps.

At the MAC layer, the IEEE 802.15.4 defines two operational modes, namely *beacon-enabled* and *non beacon-enabled*, which correspond to two different channel access mechanisms. In the beacon-enabled mode the access to the channel is managed through a superframe (SF) (see Fig. 1.3), which is defined as the period of time between two beacon packets. Beacons are transmitted by the WPAN coordinator, which is also managing the SF. The SF may contain an inactive part, allowing nodes to go into sleeping mode; whereas the active part is divided into two more periods: the Contention Access Period (CAP), where a slotted Carrier Sense Multiple Access with Collision Avoidance (CSMA/CA) protocol is used, and the Contention Free Period (CFP), where guaranteed time slots can be allocated to specific nodes

22
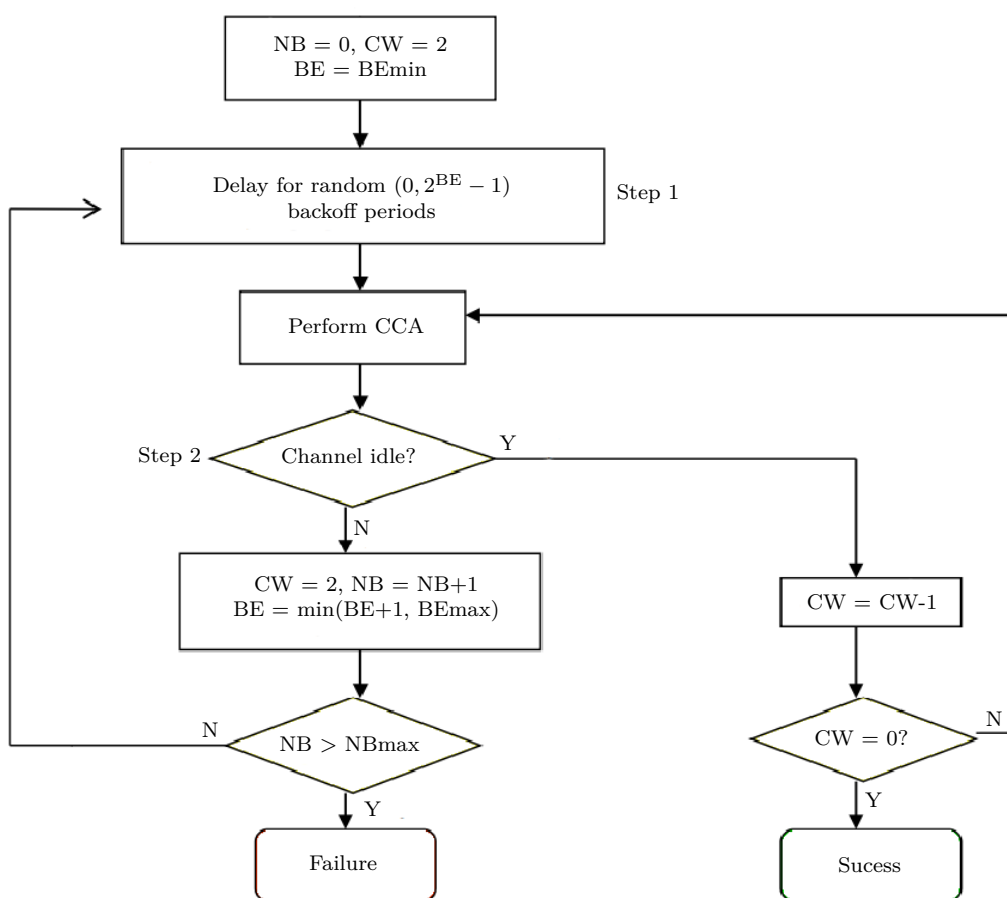
Figure 1.4: IEEE 802.15.4 slotted CSMA/CA algorithm.

in the network by the coordinator.

The CSMA/CA algorithm, see Fig.1.4 is implemented using units of time called backoff periods of fixed duration equal to 320 μs. Each node maintains three variables for each transmission attempt: NB, CW and BE. NB is the number of times the CSMA/CA algorithm was required to backoff while attempting the current transmission. CW is the number of backoff periods that need to be clear of channel activity before the transmission can start. BE is the backoff exponent related to the maximum number of backoff periods a node will wait before attempting to assess the channel. The algorithm follows

the following steps. First, NB, CW, and BE are initialized to 0, 2, and BE_{min}, respectively. Upon reception of the beacon, any activity is delayed (backoff state) for a random number of backoff periods in the range (0, $2^{BE} - 1$) (step 1). After this delay, channel sensing is performed for one backoff period (step 2). If the channel is assessed to be busy, CW is set to 2 and NB and BE are increased by 1, with the restriction that BE cannot be larger than BE_{max}. If the value of NB is lower than NB_{max}, the algorithm returns to step 1; otherwise the algorithm will unsuccessfully terminate, meaning that the node does not succeed in accessing the channel. If the channel is assessed to be idle, instead, CW is decremented by 1 and compared with 0. If CW>0, the algorithm returns to step 2; otherwise a transmission may start.

In the non beacon-enabled mode nodes only use an unslotted CSMA/CA protocol [42].

1.3.2 IEEE 802.15.6 Standard

The IEEE Task Group TG6 was established in November 2007 to realize a standard specifically designed for WBANs, namely IEEE 802.15.6, whose final version was released in February 2012 [43]. Due to the broad range of possible applications, three different PHYs have been defined:

- *Narrowband (NB) PHY:* A compliant device shall be able to support transmission and reception in at least one of the following optional frequency bands: 402-405 MHz, 420-450 MHz, 863-870 MHz, 902-928 MHz, 950-958 MHz, 2360-2400 MHz and 2400-2483.5 MHz. The maximum bit rate is 971.4 kbps.

- *UWB PHY:* There are two frequency bands. The lower one between 3.25 and 4.75 GHz and the higher one, between 6.6 and 10.25 GHz.
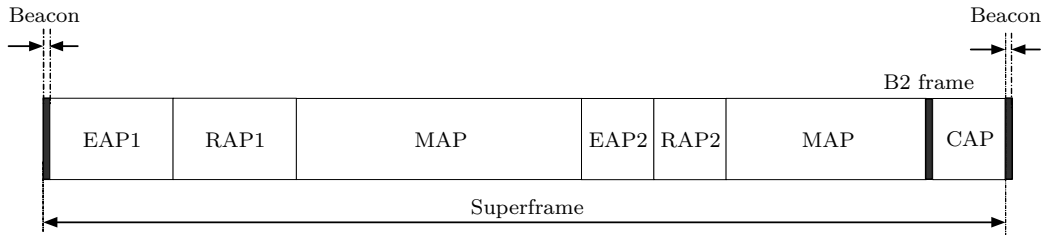
Figure 1.5: Example of IEEE 802.15.6 superframe.

Both of them are subdivided into operating channels of 500 MHz bandwidth. UWB PHY is specifically designed to offer robust performance for high quality, low complexity and ultra low power operations. The maximum bit rates is 15600 kbps.

- *HBC PHY:* This PHY solution uses the human body as a communication medium. The band of operation is centered at 21 MHz with a bandwidth of 5.25 MHz. The maximum bit rates is 1312.5 kbps.

The transmission range is limited to 3 m for in-body applications and has to be at least 3 m for body-to-body applications. The network topology is allowed to be a star or at most a 2-hops tree.

Although different PHY solutions are presented, the standard offers a single MAC protocol. The WBAN coordinator decides in which one of the following access modes to operate:

- *Beacon mode with superframe*: The coordinator establishes a common time base by sending beacon packets that define the beginning of an active SF (see Fig. 1.5). It shall also divide each SF into access phases, and defines their specific duration. In the Exclusive Access Phase (EAP), used only for the transmission of emergency data, Random Access Phase (RAP) and Contention Access Period (CAP) nodes use CSMA/CA or Slotted ALOHA algorithms. In the Managed Access

Period (MAP), the coordinator may schedule intervals, or poll nodes. The B2 frame is intended, among the other things, to announce the beginning of the CAP period [43].

- *Non-beacon mode with superframes*: In this mode, the coordinator defines only one MAP per SF, and it may organize the access to the medium as explained above for the MAP phase in the beacon enabled access mode.

- *Non-beacon mode without superframes*: A coordinator may provide an unscheduled allocation interval. After determining that the next frame exchange will take place in non-beacon mode without SF, a node shall treat any time interval as a portion of EAP1 or RAP1 and employ CSMA/CA based random access to obtain a contended allocation.

IEEE 802.15.6 CSMA/CA Algorithm

The CSMA/CA algorithm defined in this standard is represented in Fig. 1.6. The node attempts to gain access to the channel selecting a backoff counter (BC) among the equiprobable values in the interval [0-CW(UP)]. CW is the Contention Window value, it can vary between a maximum and minimum that are dependent on the data type and its User Priority (UP); larger CW values are set for data with less stringent requirements. If the channel is sensed as idle for a minimum interval of time the node shall decrease its BC by one for each idle CSMA/CA slot[1] that follows, and once BC reaches the value 0, the node obtains a contended allocation during which the frame transmission takes place. The BC freezes to a specific value when the channel is sensed as busy, and the countdown is resumed as soon as the channel

---

[1]The duration of a CSMA/CA slot depends on the PHY layer configuration.
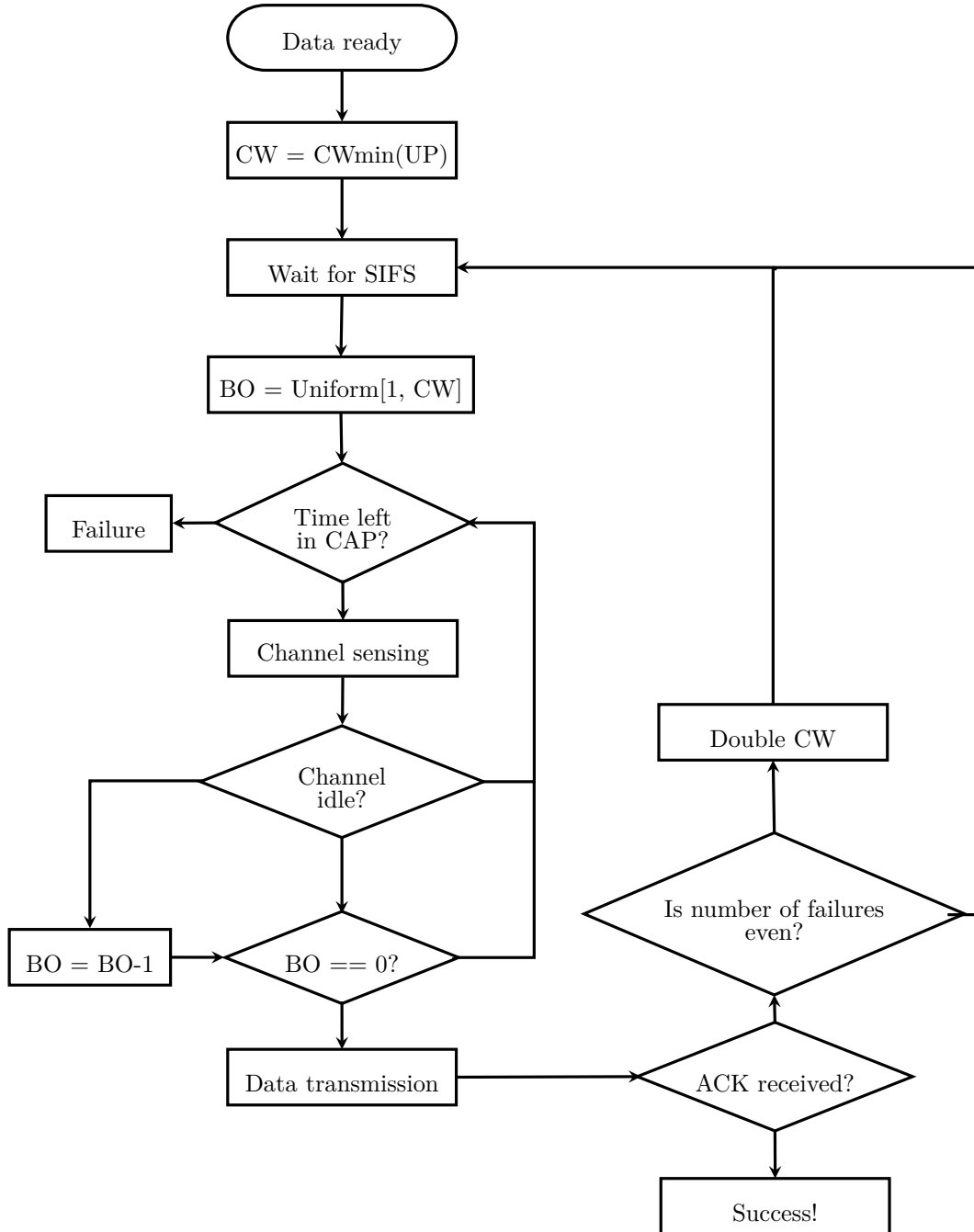
Figure 1.6: IEEE 802.15.6 CSMA/CA algorithm.

returns in idle condition. The CW value is set according to the result of the last contention attempt, following specific assignment rules. Note that, differently from the IEEE 802.15.4 CSMA/CA in beacon-enabled mode, the access to the channel is not slotted, i.e., a node wishing to transmit a packet does not have to wait until the beginning of the next slot to initiate the backoff procedure. Moreover, there are no limits in the maximum number of attempts that can be make to access the channel. This limit exists in IEEE 802.15.4 and it is equal to NB_{max}.

The IEEE 802.15.6 Slotted ALOHA

The slotted ALOHA algorithm works as follows. A node transmits the packet in a given slot if $z \leq CP[UP]$, where z is a random variable uniformly distributed in $[0,1]$, and CP is the Contention Probability value, which is set according to the result of the last contended allocation, and whose value depends on the data UP (smaller for lower priority data). The duration of the slot shall be large enough to guarantee the packet to be transmitted and the acknowledgement (ACK) (if requested) to be received.

1.3.3 Low Power Listening (LPL)

Preamble sampling, also referred to as Low Power Listening (LPL), is a key technique used by a large number of MAC protocols to save energy. In LPL nodes save energy by keeping their radios off most of the time to reduce idle listening. An extensive survey of MAC protocols, with a section dedicated to preamble sampling protocols can be found in [44].

Two solutions have been mainly considered in the literature [45,46]: transmission of a single long preamble and transmission of a burst of short preambles. The second solution is more energy efficient since it prevents the over-
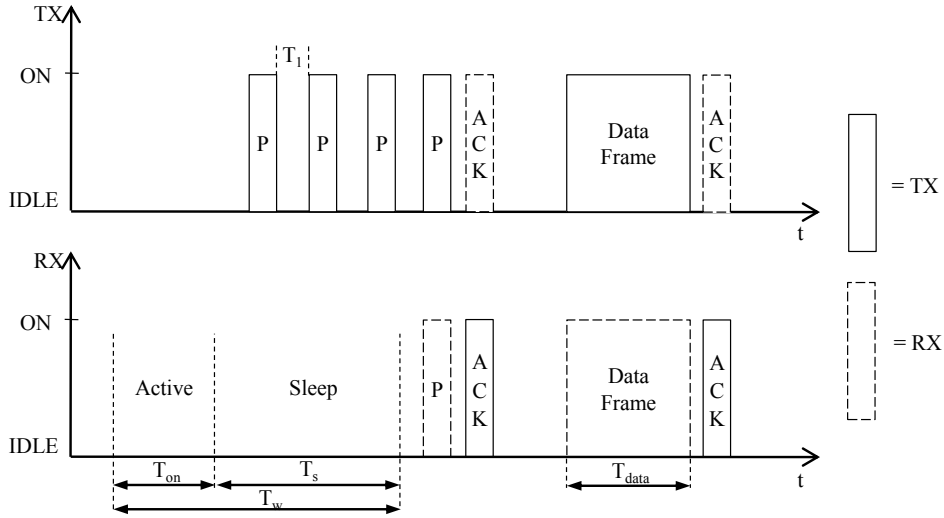
Figure 1.7: The LPL mechanism.

hearing problem by dividing the single long preamble into a series of short preamble packets, each one containing the address of the target node.

Fig. 1.7 depicts how the LPL works. Devices that do not have a packet to transmit, save energy by alternating sleeping and active phases, whose durations are denoted as T_s and T_{on}, respectively. Each node wishing to send a data to a given receiver, or to a set of receivers, will transmit a burst of short preamble packets, separated by an interval of time T_1, intended for the reception of the ACK. To check the status of the channel the node will listen the channel for T_{on} before the transmission of the first preamble, in order to ensure that no other devices are transmitting preambles. To be sure that the intended destination node receives at least one preamble, the transmitter has to send preambles for at least the duration of the sleep period of the destination node. Once the preambles are sent, which contain the addresses of all the intended receivers, the transmitter will wait for the ACK from all these devices. When a node wakes up and receives a short preamble packet, it reads the target node address that is included in the packet: if the node is not

the intended recipient, it returns to sleep immediately. On the other hand, if the node is the intended recipient, it replies with an ACK and receives the incoming data packet.

1.4 Main Challenges in WBAN Design

This section serves as an introduction to critical aspects that must be taken into consideration in the design of a WBANs, in particular the impact of the radio channel, the energy consumption and the coexistence are those aspects on which this research is focused. A quantitative discussion on their impact on the performance of a WBAN is presented in the next chapter.

1.4.1 Radio Channel

Devices forming a WBAN are placed on the human body or even implanted in it. In order to realize systems optimized for body centric communications, a deep knowledge of the radio channel is of utmost importance.

Depending on the locations of the wireless nodes, four different types of propagation channel are identified.

- *In-body*: nodes are implanted in the human body (e.g., pacemaker, cochlear implant). The authors of [47] present a propagation model for a channel of this type.

- *On-body*: nodes are located on the human body (e.g., hearing aid, insulin pump). This is the reference channel for the experimental activity that is presented in this thesis. Propagation models for this type of channel are described in [36, 48].

- *Off-body*: one node is on the human body, while the other is in its proximity (e.g., ECG that transmits data to a laptop) [49].

- *Body-to-body*: nodes are located on the human bodies of different people (e.g., nodes placed on different members of a military squad) [50].

The main unwanted effect of the presence of the human body is the *shadowing*, i.e., the fluctuation of the received signal power. As a consequence, packets may not be received and must be retransmitted. This increases the energy consumption of the nodes and the delay with which packets are received. The shadowing may be different for the different links between the nodes of the WBAN; moreover it will be time-variant as the subject moves.

1.4.2 Energy Consumption

The most promising applications for WBANs are in the field of healthcare, as pointed out in Sec. 1.2.1. When one or more devices are implanted or worn be a person, it is of great importance to reduce the stress caused by the battery replacement/recharge, which in some cases may require surgery. The problem of reducing energy consumption can be tackled by designing energy efficient PHY and MAC layers, the latter being the focus of this work.

As widely addressed in the literature, there are several factors that contribute to the energy inefficiency from a MAC perspective. They include collisions, *overhearing*, and *idle listening* [44, 51]. Collisions increase the energy consumption by making retransmissions necessary. Idle listening occurs when a node listens to an idle channel to receive possible traffic, while overhearing happens when one node receives a packet that is intended to other nodes. If the traffic load is centrally managed, overhearing and idle listening can be prevented, but in the case of contention-based MAC protocols, these

issues should be accounted for.

LPL is a valid solution to minimize the energy consumption, however it can increase the delay significantly: a proper tradeoff between delay and energy consumption must be found. Moreover, due to the overhead represented by the preamble packets, LPL is effective for applications characterized by infrequent transmissions.

1.4.3 Coexistence

The coexistence issue arises when different wireless technologies share the same radio resources.

The ISM band at 2.45 GHz is worldwide available and unlicensed, which makes it attractive and, as a consequence, very crowded. Coexistence of WBANs with other systems operating in this band (e.g., IEEE 802.11 (Wi-Fi), Bluetooth, IEEE 802.15.4) is of primary importance to guarantee reliability of a WBAN. WBANs are often characterized by low transmission power, primarily for reasons of energy efficiency. On the other hand, Wi-Fi systems are prone to use a higher transmission power (typically 20 dBm) than WBANs in order to cover wide areas. Moreover, the traffic generated by a Wi-Fi network is usually very intense and Wi-Fi networks are ubiquitous. For all these reasons, WBANs should implement techniques that guarantee reliability of the network in the presence of strong interference. Several works that explore this aspect of the WBAN design can be found in the literature; among them [52] and [53] consider the coexistence between IEEE 802.15.4 and IEEE 802.11.

A coexistence problem may arise also between different WBANs operating close to each other (e.g., in hospitals). The IEEE 802.15.6 standard considers this issue and provides two mechanisms, namely beacon shifting and channel

hopping [43, Section 6.13], to mitigate it. Channel hopping has also been introduced for IEEE 802.15.4 by the IEEE 802.15.4e amendment [54].

1.5 Conclusions

This chapter starts by giving a broad overview of the WBAN concept, WBAN common applications and requirements. The focus then, moves to the MAC protocols for this kind of wireless networks. Two standard technologies (IEEE 802.15.4 and IEEE 802.15.6) are briefly presented, along with one proprietary solution optimized for low power consumption (Low Power Listening). Three main issues in the design of a WBAN are identified; namely, the impact of the human body on the radio channel characteristics, the energy consumption, and the coexistence with other wireless technologies.

In the next chapter, the impact of these issues on the performance of a WBAN is quantified through an extensive measurement campaign. Moreover, novel solutions to cope with these problems are presented and evaluated.

Chapter 2

Performance Evaluation of MAC Protocols for WBANs

The performance evaluation is an important phase of the WBAN design. It aims at quantitatively characterizing a set of key performance metrics that help to understand whether or not the WBAN satisfies the application requirements.

This chapter describes the reference scenario and architecture of the WBAN implemented for the WiserBAN project, the methodology and the results of the performance evaluation. Although most of the work is of experimental nature, a mathematical model for the performance evaluation of the IEEE 802.15.6-based MAC protocol is also presented.

2.1   Reference Architecture, Scenario and Performance Metrics

This section presents the reference scenarios considered for the performance evaluation, the architecture of the WBAN and the set of performance metrics.
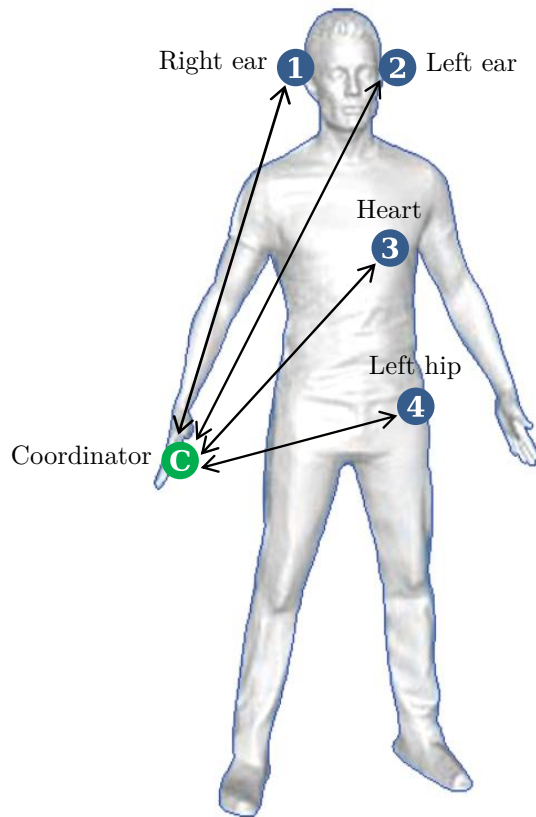
Figure 2.1: The position of the nodes for the reference WBAN.

2.1.1 Scenario

Two reference scenarios are considered: "on-body" and "on the table". The "on-body" scenario is taken from the WiserBAN project specifications, where up to four end-devices (EDs) are located on the human body and connected to a coordinator according to a star topology, as depicted in Fig.2.1. The location of the four EDs corresponds to the four WiserBAN use cases: two EDs are placed on the ears (hearing aid), one on the chest (cardiac implant), and one on the hip (insulin pump). For those measurements that aim to evaluate the MAC protocols performance, the "on the table" scenario is used. In this case, devices still form a star topology, but instead of being placed on a
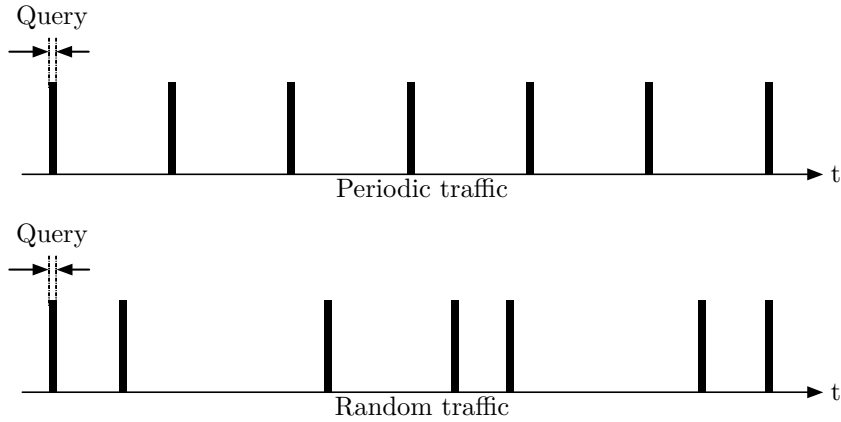
Figure 2.2: Traffic schemes used to evaluate the WBAN performance.

human body, they stay on a table in order to ensure ideal channel conditions (no body shadowing, no fading, etc.) and to guarantee the repeatability of the measurement conditions. Moreover, in order to avoid near-field propagation issues, the distance between the devices is larger that the wavelength.

The experimental measurements and the mathematical analysis consider a contention-based access. The SF, when present, is composed of beacon period, CAP and inactive period. The experimental measurements concerning the LPL protocol involves only two devices, since the protocol is not meant for contention access.

The traffic is always query-based: the coordinator broadcasts a query packet to the EDs at a given rate, and the EDs reply to the query with a data packet. Two query-based traffic schemes are considered, in the first one the query is sent at fixed rate, while in the second one the query is sent at random instants of time while preserving a minimum and maximum temporal distance between two queries. The interval of time between two query packets is called packet generation interval. The two traffic schemes are called "periodic" and "random", respectively; Fig. 2.2 illustrates how the queries are sent in the two traffic schemes.

Table 2.1: PHY Layer Characteristics

Name	Modulation	Bit rate	Band	Rx sensitivity
CC2530	O-QPSK	250 kbps	2400-2483.5 MHz	-97 dBm
icycom	FSK	200 kbps	863-928 MHz	-105 dBm

2.1.2 Architecture

The architecture of the reference WBAN follows the simplified ISO/OSI model showed in Fig. 2.3.
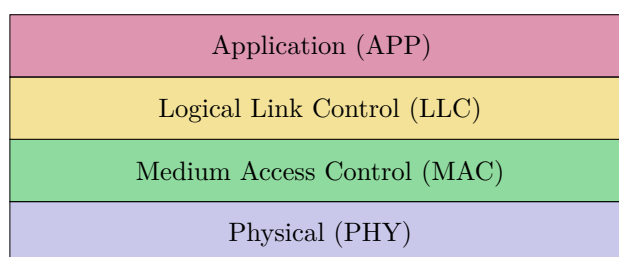
Figure 2.3: ISO/OSI model of the reference WBAN design.

Physical Layer (PHY)

The physical later is responsible for the transmission and reception bit streams over a physical medium, i.e., the radio channel.

In the experiments two different PHY layers are used. The first one is a IEEE 802.15.4 2.4 GHz compliant PHY implemented by the CC2530 Texas Instrument System-on-Chip (SoC) [55]; the second is a proprietary PHY layer implemented by icycom, a SoC tailored for WBAN applications developed by CSEM [56]. Their main characteristics are summarized in Table 2.1.

Medium Access Control Layer (MAC)

The main function of the MAC layer is to control the access to the radio channel. The MAC layer is also responsible for the association and disassociation of devices to the network, the maintenance and synchronization of the network.

The reference WBAN implements a flexible MAC layer inspired mainly from the IEEE 802.15.4 [42] and IEEE 802.15.6 [43] standards, but also implements a LPL mode. The network can operate in SF and in LPL mode; the transition between the two modes is managed by the coordinator.

The SF is defined as the time interval between two subsequent beacon packets and is managed by the coordinator. It is composed of four periods.

- Beacon period. This period, is dedicated to the reception of the beacon, therefore it has a fixed duration.

- Contention Free Period (CFP). During this period nodes access the channel in a TDMA fashion using dedicated time slots assigned by the WBAN coordinator. The duration of the period depends on the number of nodes in the network, since each node has its time slot.

- Contention Access Period (CAP). During this period, the access to the channel is contention-based. The CAP is characterized by the algorithm the node use to access the channel. Three algorithms have been tested: IEEE 802.15.4 CSMA/CA, IEEE 802.15.6 CSMA/CA and IEEE 802.15.6 Slotted ALOHA.

- Inactive period. During this period, nodes are in sleep mode, that is, they turn off most of their peripherals, including the radio, to save energy.

39

To optimize the usage of the radio channel, the coordinator can change at runtime the structure of the SF and the duration of each period. All the information regarding the incoming SF is contained in the payload of the beacon packet; in this way each node becomes aware of the new SF structure.

The LPL mode is described in detail in Section 1.3.3.

Link Control Layer (LLC)

The LLC layer guarantees to the upper layers a given Quality of Service (QoS) and allows data streams with different QoS requirements to coexist.

The LLC is a piece of software implemented by a set of primitives that creates an interface from the application towards the MAC layer, in this way the application does not need to be aware of how to set the MAC parameters (e.g., priority, retransmission, use of CFP or CAP, etc.) to ensure a given QoS for all the data streams that are active at the same time.

The logical representation of a data stream is called *flow*. A flow is a logical communication channel characterized by a set of QoS requirements. Flows can be opened and closed by the application layer with dedicated LLC primitives, moreover, multiple flows must coexist at the same time; the LLC may refuse to open a new flow if the QoS cannot be guaranteed. Each flow has a packet queue associated to it that is filled by the application layer and emptied by the MAC layer.

To give an example, consider an application that streams a phone call to a hearing aid and, at the same time, monitors a cardiac implant. Audio streaming and monitoring traffic have different QoS requirements, the first one has a strict requirement on the delay, while the second one is more sensitive to packet losses. The application layer will open two different flows characterized by different QoS levels; from that moment on, the LLC will be

in charge of setting the MAC parameters that guarantee that the QoS levels are always satisfied for the two flows.

Application Layer (APP)

The APP layer is on the top of the ISO/OSI model. On the coordinator side it is realized as an Android application that runs on a tablet or on a smartphone (see Fig. 2.4). The application interacts with the user and translates user commands to LLC primitives and vice-versa.

On the ED side the APP layer is a software that processes received data and generates data to be transmitted.

In the measurements, the WBAN coordinator runs the full protocol stack described in this section, while the EDs run a lighter stack where the LLC is not present. This is because in a star topology the EDs communicate only with the coordinator, so there is no need to handle multiple flows.

2.1.3   Performance Metrics

The performance of the WBAN is evaluated according to the following metrics:

- Packet Loss Rate (PLR). It is the ratio between the total number of lost packets and generated packets. Packets can be lost due to collision or because their time-to-live (TTL) has expired.

- Success Probability. It is the probability that a node successfully transmits a packet. It is complementary to the PLR.

- Averaged Delay. It is the period of time that goes from the generation of the data packet at the ED side to its correct reception at the coordinator side, averaged over all received packets. The delay accounts for the
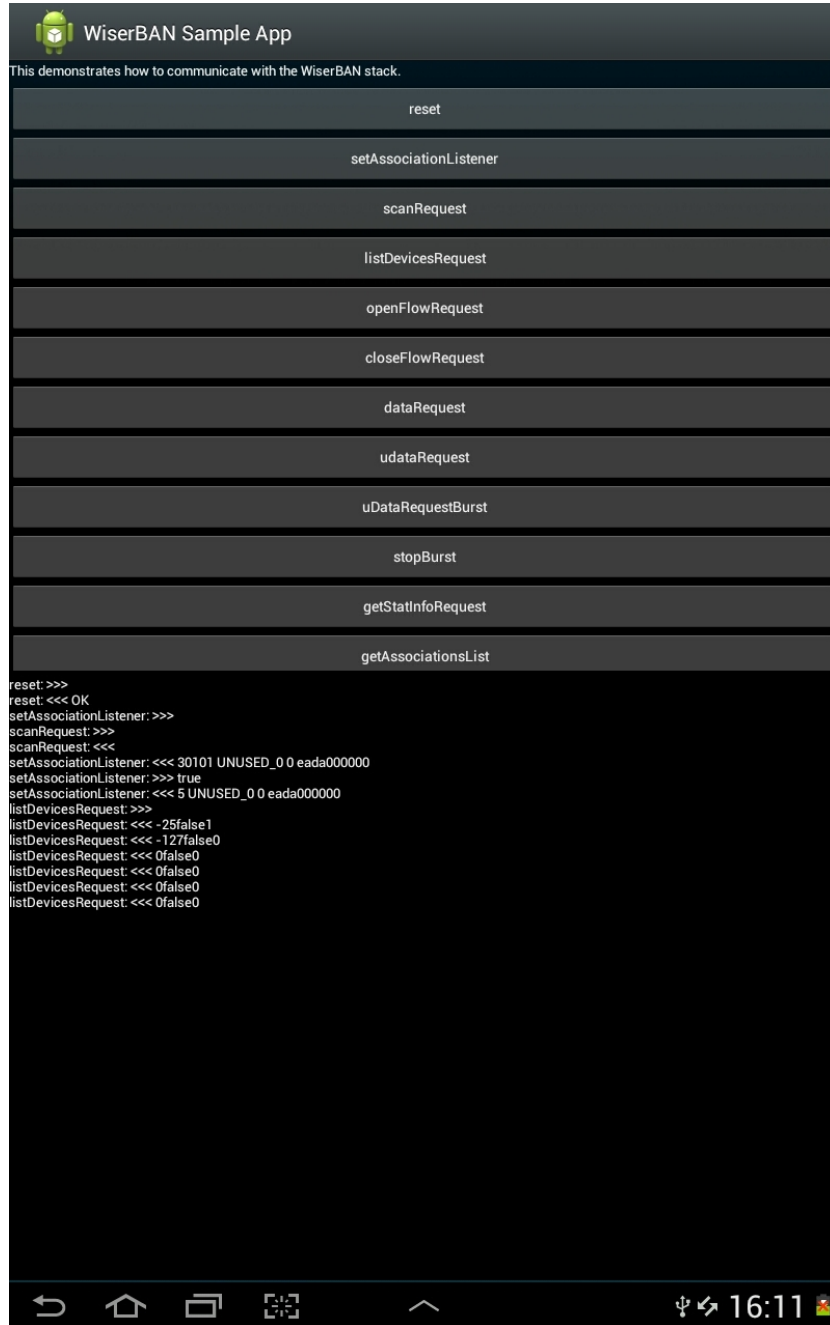
Figure 2.4: Screenshot of the WiserBAN testing application that runs on Android devices.

time needed for accessing the channel, transmitting the packet and the acknowledgement, the data processing time, and for the turn-around times, that is the time needed to switch the transceiver from receive to transmit mode and vice-versa. Lost packets are not accounted in the average.

- Throughput. It measures the amount of useful information that is delivered to the APP layer of the coordinator per unit of time. It is measured in bit/s. The useful information is contained in the payload of the data packet; all the other received bytes (PHY and MAC headers) are overhead. The throughput is calculated as

$$T = \frac{(1 - PLR) \cdot z \cdot N}{T_q},$$

the quantity z is the payload size, N is the number of EDs and T_q is the SF duration.

- Energy consumption. It is the average amount of energy required to transmit a packet that is correctly received. It is measured in mJ/packet.

2.2 Analytic Model for MAC Performance in WBANs

This section describes an analytic model for the characterization of the performance of the CSMA/CA algorithm with priority defined in the IEEE 802.15.6 standard, in the case of periodic query-based traffic, when the beacon acts as query packet.

The authors of [57] and [58] studied IEEE 802.15.6-based WBANs. They derived delay and throughput using a Markov chain model both in saturation and non-saturation regimes. The mathematical models presented therein are not suitable for periodic query-based applications where the Markov property does not apply, therefore a different approach is needed. Although the model is very simple, it gives the designer an idea on the lower bound of the performance of the network, and can be considered a starting point for the development of more complex mechanisms to optimize the assignment of the priority values to the different nodes in the network subject to QoS constraints. The comparison of the analytical results with experimental and simulation results demonstrate that the model captures the behavior of the protocol.

The CSMA/CA algorithm is described in details in Sec. 1.3.2 and the relation between the minimum and maximum value of the parameter CW and the UP value is reported in Table 2.2.

2.2.1 CSMA/CA Analytic Model

The performance of the IEEE 802.15.6 CSMA/CA is evaluated in terms of success probability and delay.

The success probability $P_s^{(k)}$ is the probability that an ED starts in slot

Table 2.2: UPs and CSMA/CA contention window values.

Priority	**UP**	**CW$_{\mathbf{min}}$**	**CW$_{\mathbf{max}}$**
Lowest	0	16	64
	1	16	32
	2	8	32
	3	8	16
	4	4	16
	5	4	8
	6	2	8
Highest	7	1	4

k a successful transmission, i.e., without collision, toward the coordinator.

The model is valid under the following assumptions: i) there are no hidden terminals, i.e., all nodes can "hear" each other; ii) the capture effect is negligible, that is collisions always result in packets loss; iii) to reduce the energy consumption retransmissions are not allowed; iv) nodes are perfectly synchronized by means of the reception of the beacon packet sent by the coordinator. The model captures the probability $P_s^{(k)}$ and the average delay for network composed of N EDs with fixed UP value, a packet transmission time D_{tx} of 3 slots, and the probability $P_s(UP_i)$ that a node with UP value UP_i starts a successful transmission for a network composed of N nodes for any D_{tx} and UP values.

The node behavior can be represented as a finite state transition diagram with three types of state: *Idle*, *Backoff* and *Transmission*. The node is in the Idle state until the reception of the query, after that the node moves to a Backoff state. The Backoff state is characterized by the pair (c, k) where c is the value of the backoff counter at time slot k, and each time slot has a duration of 355 μs. When the backoff counter eventually reaches zero, the

node moves to the state Transmission, characterized only by the time slot k. The node will remain in Transmission for D_{tx} slots.

The state diagram for $UP = 4$, corresponding to $CW = 4$, and transmission time $D_{tx} = 3$ slots is shown in Fig. 2.5, where $P_f^{(k)}$ and $P_b^{(k)}$ are the probabilities for the channel to be free and busy, respectively, during slot k.

According to the protocol, before receiving the query the node is in Idle state; as soon as the query is received, the node sets its backoff counter to a random integer, c, uniformly and randomly distributed in the interval $[1, CW]$ and moves to state $(c, 1)$, with probability $1/CW$. Since during the first slot the channel is always free, the node then moves to the next state with probability 1. Let us consider a node that with probability $\frac{1}{4}$ selects $c = 2$: from the Idle state it moves to state $(2, 1)$ and with probability 1 to state $(1, 2)$. At the beginning of time slot 2, the node senses the channel free with probability $P_f^{(2)}$ and busy with probability $P_b^{(2)}$. In the first case the node will start the transmission at slot 3, whereas in the second case it will move from state $(1, 2)$ to state $(1, 2 + D_{tx})$ because a transmission from a competing node that started at 2 lasts until slot 4. Then the next move will be toward state $(3 + D_{tx})$ with probability 1, in fact according to slotted CSMA/CA there will always be a free slot after a frame transmission.

The state diagram is used to derive $P_s^{(k)}$ for all the possible slots k, bearing in mind that all the events whose probabilities are $P_f^{(k)}$ and $P_b^{(k)}$ are not independent. Note that k varies in the range $\{2, \dots, k_{\max}\}$ where:

$$
k_{\max} = \begin{cases} (N - 1)D_{tx} + CW + 1, & \text{for } N \le CW, \\ (CW - 1)D_{tx} + CW + 1, & \text{otherwise.} \end{cases}
$$

In the following, $n = N - 1$ will denote the number of nodes competing with the reference one to access the channel, as P_{ci} the probability that the
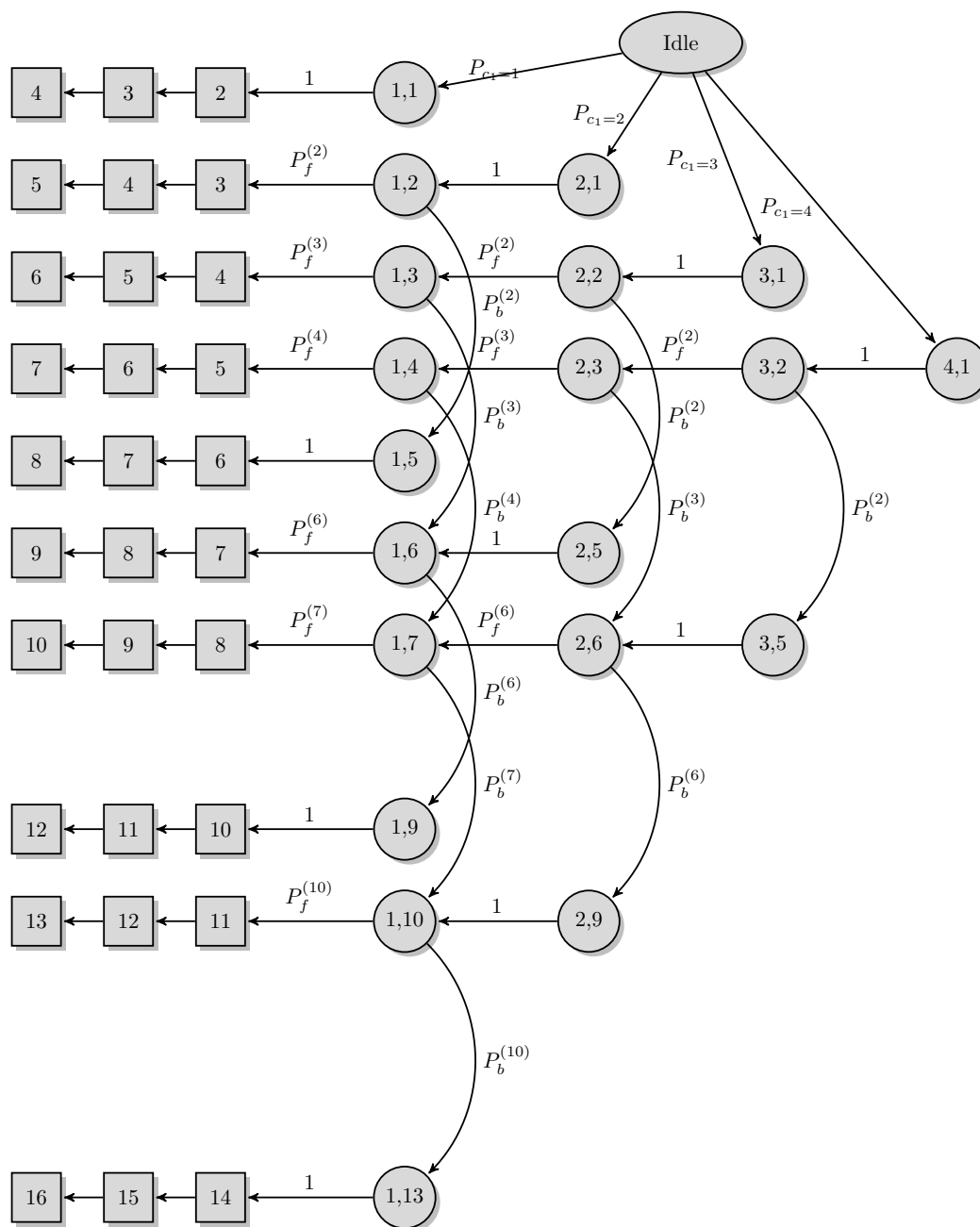
Figure 2.5: Example of diagram for UP 4 and transmission time $D_{tx} = 3$. Circles denote Backoff states, Square denote Transmission states.

reference node sets its backoff counter to z, and as $P_{n_{ci}=0}$ the probability that the number n_{ci} of competing nodes that set its backoff counter to i is zero. The values of $P_s^{(k)}$ for $UP = 4$ and $D_{tx} = 3$ are given by (2.2.1), where $P_{A,B}$ is the probability of $A \cap B$, where A and B are events. Note that $P_s^{(1)} = P_s^{(9)} = P_s^{(12)} = P_s^{(13)} = 0$.

$$
\begin{aligned}
P_s^{(2)} &= P_{c1} P_{n_{c1}=0}, \\
P_s^{(3)} &= P_{c2} P_{f_2, n_{c2}=0}, \\
P_s^{(4)} &= P_{c3} P_{f_2, f_3, n_{c3}=0}, \\
P_s^{(5)} &= P_{c4} P_{f_2, f_3, f_4, n_{c4}=0} = 0, \\
P_s^{(6)} &= P_{c2} P_{b_2, n_{c2}=0}, \\
P_s^{(7)} &= P_{c3} \left(P_{f_2, b_3, n_{c3}=0} + P_{b_2, f_6, n_{c3}=0} \right), \\
P_s^{(8)} &= P_{c4} \left(P_{b_2, f_6, f_7, n_{c4}=0} + P_{f_2, f_3, b_4, n_{c4}=0} + P_{f_2, b_3, f_7, n_{c4}=0} \right), \\
P_s^{(10)} &= P_{c3} P_{b_2, b_6, n_{c3}=0}, \\
P_s^{(11)} &= P_{c4} \left(P_{b_2, b_6, f_{10}, n_{c4}=0} + P_{b_2, f_6, b_7, n_{c4}=0} + P_{f_2, b_3, b_7, n_{c4}=0} \right), \\
P_s^{(14)} &= P_{c4} P_{b_2, b_6, b_{10}, n_{c4}=0}.
\end{aligned}
\tag{2.2.1}
$$

The probabilities in (2.2.1) depend on how the N nodes set their backoff counters when they receive the query. In fact, among the N^{CW} possible choices of backoff counter values that the N nodes can make, only a subset of them allows the reference node to transmit successfully in a given slot. For example, $P_s^{(14)}$ imposes the following conditions: i) the backoff counter of the reference node is set to 4, ii) none of the other n competing nodes sets its backoff counter to 4, iii) transmissions from the competing nodes are detected to start at slots 2, 6 and 10. Conditions ii) and iii) are satisfied if among the competing nodes at least one chooses 1, at least one chooses 2 and at least one chooses 3, but none of them chooses 4, which results in

$$P_{b_2,b_6,b_{10},n_{c4}=0} = P\left(n_{c1} \geq 1, n_{c2} \geq 1, n_{c3} \geq 1, n_{c4} = 0\right).$$

According to the latter considerations the joint probabilities in (2.2.1) can be generalized as follows

$$
\begin{aligned}
P_{n_{c1}=0} &= P\left(n_{c1} = 0, n_{c2} \geq 0, n_{c3} \geq 0, n_{c4} \geq 0\right), \\
P_{f_2,n_{c2}=0} &= P\left(n_{c1} = 0, n_{c2} = 0, n_{c3} \geq 0, n_{c4} \geq 0\right), \\
P_{f_2,f_3,n_{c3}=0} &= P\left(n_{c1} = 0, n_{c2} = 0, n_{c3} = 0, n_{c4} \geq 0\right), \\
P_{f_2,f_3,f_4,n_{c4}=0} &= P\left(n_{c1} = 0, n_{c2} = 0, n_{c3} = 0, n_{c4} = 0\right), \\
P_{b_2,n_{c2}=0} &= P\left(n_{c1} \geq 1, n_{c2} = 0, n_{c3} \geq 0, n_{c4} \geq 0\right), \\
P_{f_2,b_3,n_{c3}=0} &= P\left(n_{c1} = 0, n_{c2} \geq 1, n_{c3} = 0, n_{c4} \geq 0\right), \\
P_{b_2,f_6,f_7,n_{c4}=0} &= P\left(n_{c1} = n, n_{c2} = 0, n_{c3} = 0, n_{c4} = 0\right), \\
P_{b_2,b_6,n_{c3}=0} &= P\left(n_{c1} \geq 1, n_{c2} \geq 1, n_{c3} = 0, n_{c4} \geq 0\right), \\
P_{b_2,b_6,f_{10},n_{c4}=0} &= P\left(n_{c1} \geq 1, n_{c2} \geq 1, n_{c3} = 0, n_{c4} = 0\right), \\
P_{b_2,b_6,b_{10},n_{c4}=0} &= P\left(n_{c1} \geq 1, n_{c2} \geq 1, n_{c3} \geq 1, n_{c4} = 0\right).
\end{aligned}
\tag{2.2.2}
$$

Note also that $P_{f_2,b_3,n_{c3}=0} = P_{b_2,f_6,n_{c3}=0}$, $P_{b_2,f_6,f_7,n_{c4}=0} = P_{f_2,f_3,b_4,n_{c4}=0} = P_{f_2,b_3,f_7,n_{c4}=0}$, and $P_{b_2,b_6,f_{10},n_{c4}=0} = P_{b_2,f_6,b_7,n_{c4}=0} = P_{f_2,b_3,b_7,n_{c4}=0}$.

Let $\eta = \{1, 2, \ldots, CW - 1\}$ be the number of values of the backoff counter for which n_{ci} has to be zero when considering one of the $P_s^{(k)}$, that is how many values cannot be chosen among the CW possible. As an example, for $P_s^{(14)}$, $\eta = 1$ because only the value 4 cannot be chosen by the competing nodes.

It is now possible to derive the probabilities (2.2.1):

$$P_s^{(2)} = \frac{n!}{4^N} \sum_{x=0}^{n} \sum_{y=0}^{n-x} \frac{1}{x!y!(n-x-y)!}$$

$$P_s^{(3)} = \frac{n!}{4^N} \sum_{x=0}^{n} \frac{1}{x!(n-x)!}$$

$$P_s^{(4)} = \frac{1}{4^N}, \quad P_s^{(8)} = 3\frac{1}{4^N}$$

$$P_s^{(6)} = \frac{n!}{4^N} \sum_{x=1}^{n} \sum_{y=0}^{n-x} \frac{1}{x!y!(n-x-y)!}$$

$$P_s^{(7)} = 2\frac{n!}{4^N} \sum_{x=1}^{n} \frac{1}{x!(n-x)!}$$

$$P_s^{(10)} = \frac{n!}{4^N} \sum_{x=1}^{n-1} \sum_{y=1}^{n-x} \frac{1}{x!y!(n-x-y)!}$$

$$P_s^{(11)} = 3\frac{n!}{4^N} \sum_{x=1}^{n-1} \frac{1}{x!(n-x)!}$$

$$P_s^{(14)} = \frac{n!}{4^N} \sum_{x=1}^{n-2} \sum_{y=1}^{n-1-x} \frac{1}{x!y!(n-x-y)!}$$

$$(2.2.3)$$

Depending on η, the probabilities in (2.2.2) can be generalised as

$$P\left(n_{cx} = n, n_{cy,z,w} = 0\right) = \frac{1}{4^N}, \text{ if } \eta = 3$$

$$P\left(n_{cx} \geq i, n_{cy} \geq j, n_{cz,w} = 0\right) = \frac{n!}{4^N} \sum_{x=i}^{n-j} \frac{1}{x!(n-x)!}, \text{ if } \eta = 2$$

$$P\left(n_{cx} \geq i, n_{cy} \geq j, n_{cz} \geq k, n_{cw} = 0\right)$$

$$= \frac{n!}{4^N} \sum_{x=i}^{n-j-k} \sum_{y=j}^{n-x-k} \frac{1}{x!y!(n-x-y)!}, \text{ if } \eta = 1$$

$$(2.2.4)$$

Success Probability

The state diagram can be used to derive $P_s(UP_i)$: the probability for a frame to be successfully transmitted with UP value UP_i, that is the probability for a sender node to grant the access to the medium and transmit the frame

without collision, whatever the slot is. The latter probability is equal to:

$$P_s(UP_i) = \sum_{k=1}^{k_{\max}} P_s^{(k)}(UP_i) = \left(1 - \frac{1}{CW_i}\right)^n \tag{2.2.5}$$

where $P_s^{(k)}(UP_i)$ for the case $UP_i = 4$ is given by equations in (2.2.1). The latter equation can be extended to the case where nodes have different user priorities as follows. Assume now the network is composed of $N = \sum_{i=0}^{7} n_i$ nodes, where $\{n_0, n_1, \ldots, n_7\}$ is the set of transmitting nodes, n_i is the number of nodes with UP value UP_i. CW_i is the value of the contention window CW for a node with UP value UP_i as shown in Table 2.2, and δ_{ij} is the Kronecker delta.

$$P_s(UP_i) = \frac{1}{CW_i} \sum_{j=1}^{CW_i} \prod_{k=0}^{m:CW_m \geq j} \left(1 - \frac{1}{CW_k}\right)^{n_k - \delta_{ki}} \tag{2.2.6}$$

The rationale behind (2.2.6) is that the condition for a frame to be successfully received is that the value of the backoff counter of the sender node is unique among the set of backoff counter values of the other nodes.

Average Delay

The delay is modeled as $D = xT_s + D_{tx}T_s$ where x is a sample of the discrete random variable representing the number of slots (of duration T_s) the node spends in the backoff phase of CSMA/CA and D_{tx} is the transmission time in slots, which depends on the size of the frame.

The average value of the delay $\mathbb{E}[D]$ is given by:

$$\mathbb{E}[D] = \sum_{k=1}^{k_{\max}-1} (kT_s + D_{tx}T_s) P_s^{(k+1)} \tag{2.2.7}$$

Table 2.3: $P_s(UP_i)$ for $N = 3$ and different UP values.

Node UP	Model	Experiment
0	0.88	0.88
2	0.82	0.81
4	0.82	0.81
0	0.89	0.89
4	0.70	0.70
7	0.70	0.70

2.2.2   Numerical Results

The model is validated using a custom CSMA/CA simulator written in C and through a set of experiments with the icycom platform. The network is composed of one coordinator and three EDs. In order to satisfy assumptions iii) and iv) the devices have been programmed to generate one data frame at the beginning of the CAP, the number of retransmission is set to zero, and the devices were placed at the same distance from the coordinator such that the capture effect is negligible and there is no hidden terminal problem (assumptions i and ii). The results of the experiments are averaged over 5000 generated packets and are shown in Fig. 2.6, along with the results obtained with the model. $P_s(UP)$ is pictured as function of UP values for a network where all the three EDs share the same UP value. It can be seen that the results of the model can be reproduced in the experiments. In Table 2.3 is reported a comparison of the success probability obtained from the model and from the experiments, for two 3-EDs networks where each ED has a different UP value (see Table 2.3).

Fig. 2.7 shows the analytic results of the success probability as function of the number of EDs N, for five networks where senders have the same UP
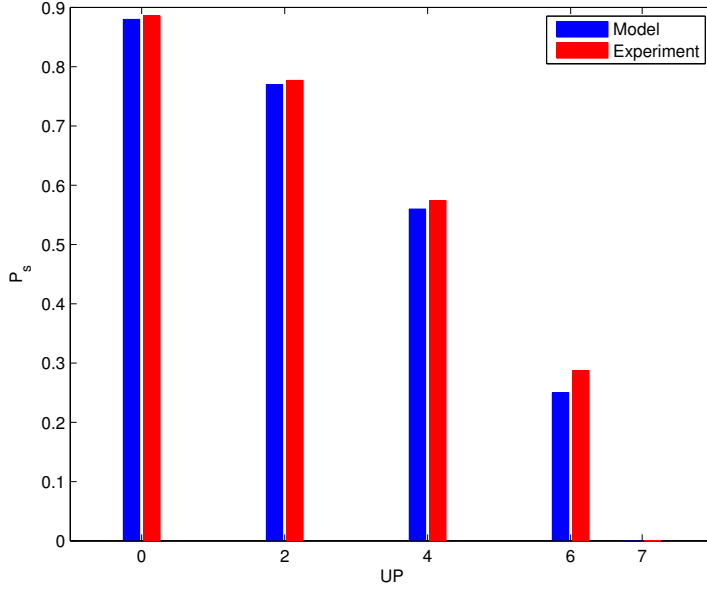
Figure 2.6: $P_s(UP_i)$ for for a network of 3 senders with the same UP values.

value.

Another situation in which (2.2.6) can be useful is when the designer wants to understand how much the performance degrades when a new sender is added to the set of transmitting nodes. Fig. 2.8 shows three examples where, considering the initial array of EDs $\{n_s, 0, n_s, 0, n_s, 0, n_s, 0\}$, different UP values are assigned to the new ED that joins the network. The metrics shown here is the average success probability defined as $\overline{P_s} = \frac{1}{N} \sum_{i=0}^{7} n_i P_s(UP_i)$.

Regarding the delay, a set of measurements has been performed with the icycom platform to validate the analytic model. The results are shown in Fig. 2.9 along with the outcome of the model. The difference between the two curves is due to the processing time at the receiver side which is not taken into account by the model and increases with the payload size. The cumulative distribution function (CDF) of the delay obtained with the model and with a
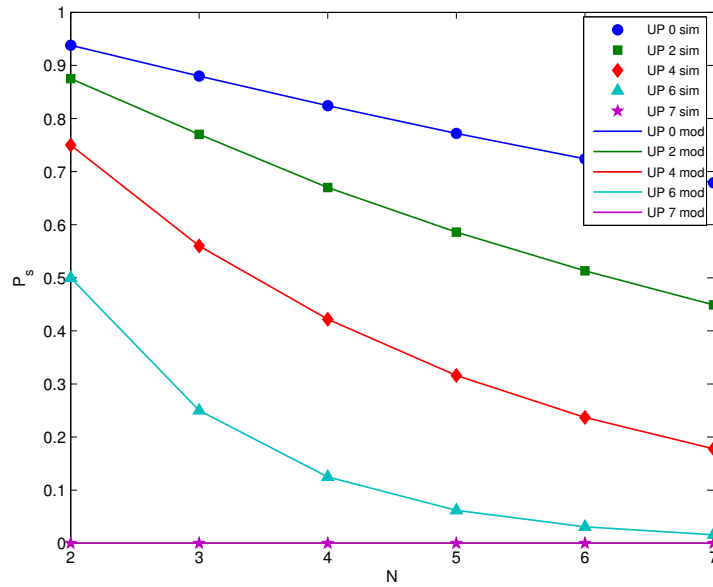
Figure 2.7: P_s for $N = 2, \ldots, 7$ where EDs use the same UP values.
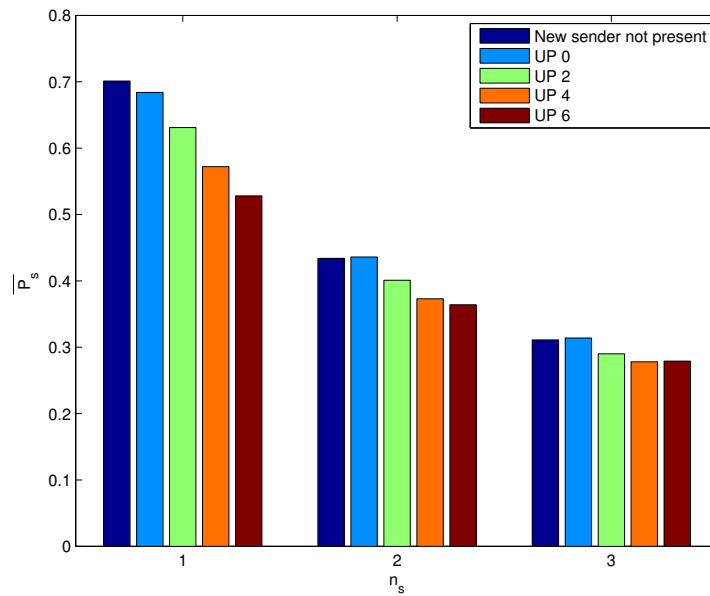
Figure 2.8: $\overline{P_s}$ when a new ED is added to the network.

Figure 2.9: $\mathbb{E}[D]$ for $N = 3$, UP=4 for different payload size.

CSMA/CA simulator is reported in in Fig. 2.10 for different number of EDs N.

2.3 Experimental Performance Evaluation

This section presents the experimental evaluation of the performance of a WBAN.

There are several works in the literature that deal with the performance evaluation of WBAN. Among them [59] is focused on the evaluation of the energy consumption, delay and throughput of WBANs used in healthcare applications; the same metrics are evaluated in [60] for WBANs based on the IEEE 802.15.4 standard.

The extensive measurement campaign that is described in this section has
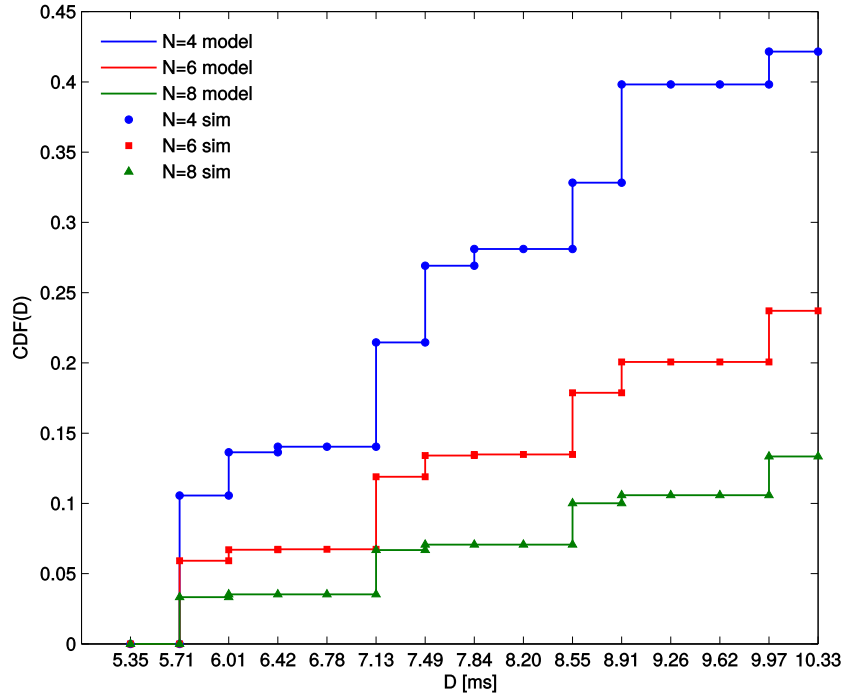
Figure 2.10: Cumulative distribution function of the delay for different values of N and for a payload size of 100 Bytes.

been performed in the framework the WiserBAN project. Unless otherwise stated, measurements are done with the "on the table" scenario and with the periodic query-based traffic scheme (see Section 2.1).

2.3.1 Body Shadowing

A WBAN operates in close proximity of the human body; this often results in a degradation of performance due to the negative impact that the human body has on the propagation channel. This effect is called *body shadowing* and it results in an additional attenuation between the transmitter and receiver. This attenuation can be such that the received power is below the receiver sensitivity; when this happens, packets are lost, and consequently the PLR increases. This effect can be alleviated by increasing the maximum number

Table 2.4: MAC and PHY parameters setting.

Parameter	Value
$BE_{\min}$	3
$BE_{\max}$	3
$NB_{\max}$	4
Retransmissions	3
Tx Power	-22 dBm
I_{on}	20.5 mA
I_{idle}	6.5 mA
V_{DD}	3 V

of retransmissions. However, this has the negative effect of increasing the delay and the energy consumption.

To quantify the effect of the body shadowing the on-body scenario is reproduced (see Fig. 2.1). During the experiments, the subject was walking back and forth in an office environment.

The Texas Instrument CC2530 IEEE 802.15.4-compliant devices [55] are used in these measurements with MAC and PHY parameters reported in Table 2.4. The results are averaged over 10000 transmitted packets in order to be statistically acceptable.

Fig. 2.11 shows the results for the PLR as a function of the packet payload size for each link between the ED and the coordinator. As expected, the best link is the one connecting the coordinator and the right ear (Link 1), while the worst link is the one between the coordinator and the left ear (Link 2). This is because of the shadowing effect introduced by the subject's head: indeed, nodes in Link 1 are always in line-of-sight, while nodes in Link 2 are always in non-line-of-sight. Links 3 and 4 have intermediate performance because the propagation is shadowed by the human body roughly for half of
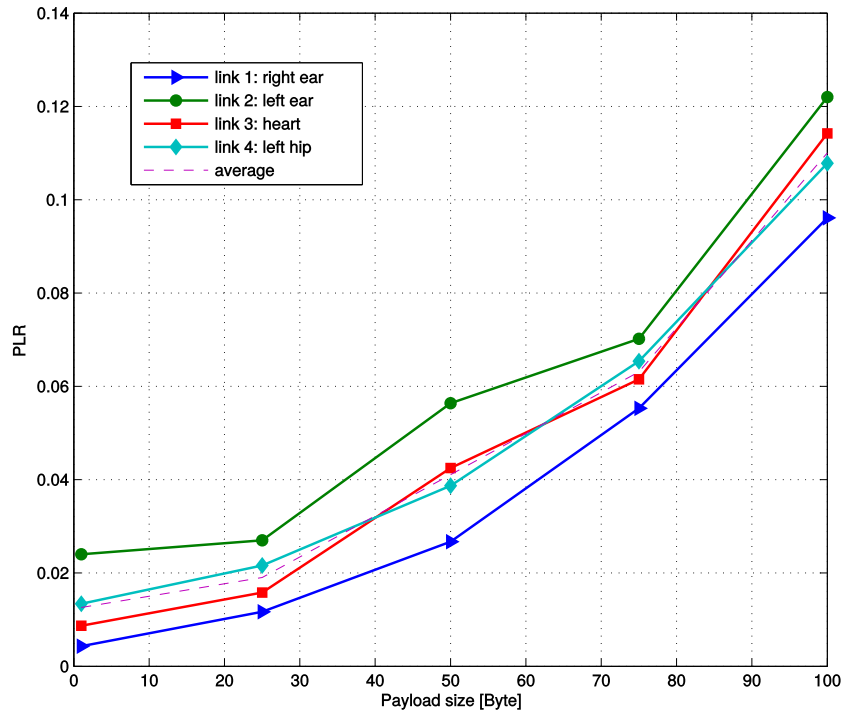
Figure 2.11: PLR for different links of Fig. 2.1.

the duration of the experiment, due to the typical swinging movements of the arm while walking.

Data Aggregation

A packet is usually retransmitted immediately after its first failed transmission, however this is not always the most effective solution. If, for example, a packet is lost due to connectivity issues caused by the shadowing effect of the body, to retransmit the packet immediately after the transmission is useless, since the channel will be most probably in the same conditions due to the slow movements of the subject. Moreover, all the energy spent for retransmitting the packet is wasted. Assuming that the person wearing the WBAN is walking, the body movement generates an alternation of situations in which nodes are in visibility and in which nodes are shadowed by the body.
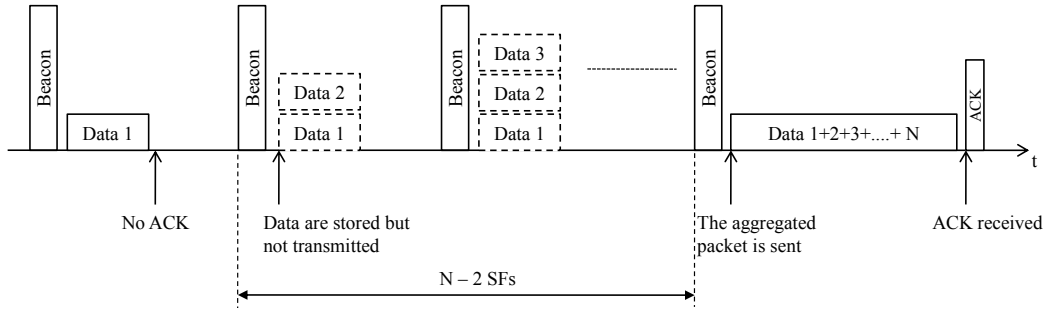
Figure 2.12: Example of the data aggregation strategy.

This is mainly due by the typical arm movements performed during walking. Therefore, it is possible to take advantage of the movement and avoid packets transmissions in those intervals of time during which there is a lack of visibility, and defer the transmission of those packets when the good channel conditions between nodes is gained again.

Based on the above intuition, the following data aggregation strategy has been implemented. When a device does not receive the ACK from the coordinator, instead of retransmitting the packet in the same SF, it will wait for a given number of SFs, during which it will only store the generated data, without transmitting them. After a given number of SFs, the node will try to transmit a single packet, containing the lost data plus all the data generated and not transmitted, in an aggregated packet. The quantity N_a denotes the number of packets aggregated. Therefore, once a packet is lost, the node will only store data for the following $N_a - 2$ SFs and at the $(N_a - 1) - th$ SF after the loss it will transmit a packet with a payload containing the N_a aggregated packet. N_a is limited by the MAC Protocol Data Unit (MPDU) maximum size. This mechanism is depicted in Fig. 2.12.

The number N_a can be optimized such that the PLR is minimized. The existence of an optimal value can be motivated as follows: when N_a is too small, there is still correlation between the channel condition experienced by
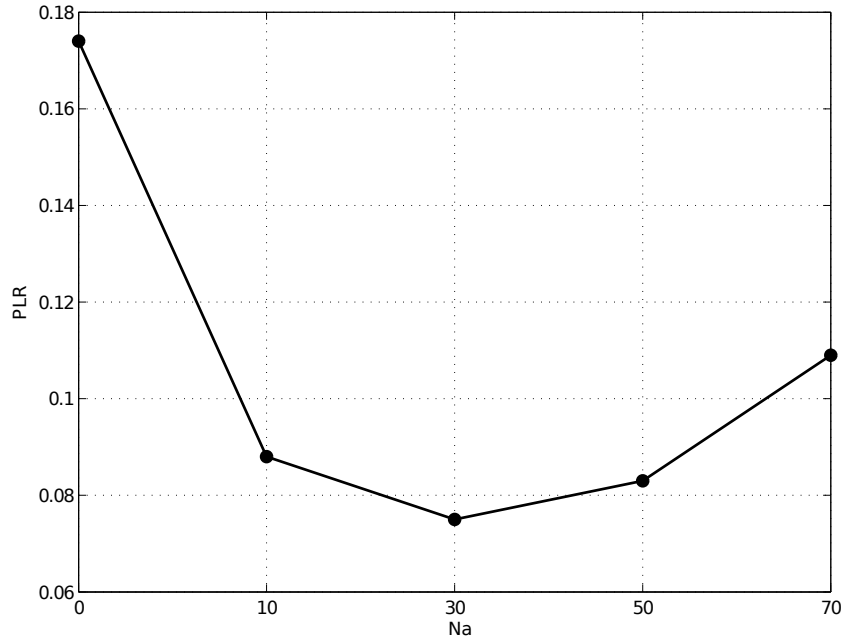
Figure 2.13: Optimal value of N_a.

the transmission and the one experienced by the retransmission; when N_a is too large, the size of the transmitted packet becomes very large, therefore collisions are more likely to occur. This optimum is shown in Fig. 2.13 in the case of payload size equal to 1 byte. As can be seen from the Figure, the optimum value is equal to 30 aggregated packets, which means, approximately, that the duration of the inactive interval for the radio transceiver is 900 ms, when accounting for the SF duration.

Fig. 2.14a shows the PLR as function of the payload size when the number of maximum retransmissions is set to three and zero, and when data aggregation in used; in this case the maximum number of retransmission is set to three. It can be seen that the data aggregation strategy performs better in terms of PLR with respect to the other cases; moreover it is more energy efficient. In fact, thanks to aggregation, nodes can save energy, assuming that they switch off the radio during all the SFs where they just have

(a) PLR vs payload size.

(b) Average energy consumption per SF vs number of aggregated packets.
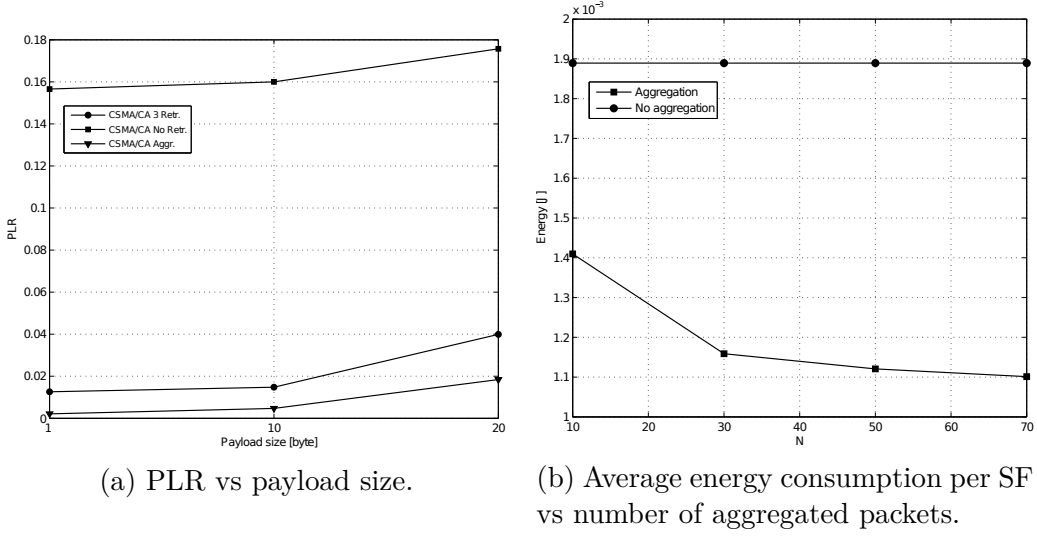
Figure 2.14: PLR and energy consumption for the data aggregation strategy.

to store information data. To this end, Fig. 2.14b shows the average energy consumption per SF for a CC2530 node. The straight line is the average energy consumption per SF for a node when no aggregation strategy is used; it is computed as

$$E_{\text{no\_aggr}} = V_{\text{DD}} \cdot I_{\text{on}} \cdot T_{\text{SF}} = 1.89 \, \text{mJ}, \qquad (2.3.1)$$

where it is assumed that the transceiver is always on during the SF, draining I_{on} [55], V_{DD} is the supply voltage, and T_{SF} is the SF duration. The energy spent by the node performing aggregation is calculated as

$$E_{\text{aggr}} = \frac{N_{\text{act}} \cdot E_{\text{no\_aggr}} + N_{\text{inact}}(I_{\text{idle}} \cdot T_{\text{CAP}} + I_{\text{on}} \cdot T_{\text{b}}) \cdot V_{\text{DD}}}{(N_{\text{act}} + N_{\text{inact}})}, \qquad (2.3.2)$$

using the following assumptions: while performing aggregation, the node just receives beacons, draining I_{on}, and keeps the transceiver off during the rest of the SF, draining I_{idle}; N_{act} and N_{inact} are obtained from the experiments and represent the number of SFs during which the node is not performing

aggregation, and during which is performing aggregation, respectively. $T_{\mathrm{b}} = 640\,\mu s$ is the beacon reception time and T_{CAP} is the CAP duration; notice that $T_{\mathrm{beacon}} + T_{\mathrm{CAP}} = T_{\mathrm{SF}}$. The difference between the two curves is not very large, since, according to our protocol, nodes perform data aggregation only when a packet is lost, that is not for all the duration of the experiment. This is done to avoid increasing the average delay. In case the requirements of the application in terms of latency are not stringent, the aggregation procedure could be implemented to a larger extent, bringing better performance in terms of both PLR and energy consumption.

2.3.2   PLR, Delay and Throughput

Most of the experimental measurements were intended to evaluate the performance of contention channel access algorithms of the IEEE 802.15.4 and IEEE 802.15.6 standards, and LPL.

The measurements are performed using the CSEM icycom platform and using a network composed by a maximum number of three EDs managed by one coordinator. The duration of the SF is set to 75 ms and only CAP is present with a duration of 60 ms; the remaining time is dedicated to the reception of the beacon (5 ms) and to the inactive period (10 ms). Unless otherwise specified, the maximum number of retransmission is set to three.

What follows is the comparison of the performance in terms of PLR, average delay and throughput, for the three contention access algorithms.

The results for the PLR as a function of the payload size are reported in Fig 2.15a. As expected, Slotted ALOHA performs worse than CSMA/CA because of the lack of the sensing phase, so collisions cannot be avoided. From the comparison between the two CSMA/CA algorithms, it can be observed that the one implemented according IEEE 802.15.6 has better performance;

(a) Periodic traffic.

(b) Random traffic. PLR in %.
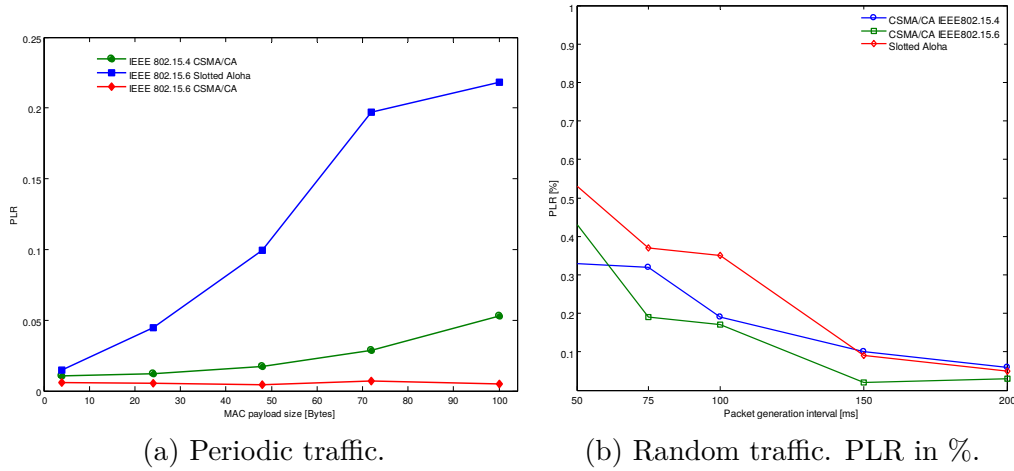
Figure 2.15: Comparison of the PLR for three different contention access algorithms.

this is because there is no limitation on the maximum number of attempts to sense the channel after finding it busy, in contrast to IEEE 802.15.4 where the parameter NB_{max} limits the amount of retries. This limitation makes the algorithm discard those packets for which the channel has been sensed busy more than NBmax times. Moreover, the amount of packets discarded grows with the size of the packet, since larger packets keep the channel busy for longer, and this explains the increase of the PLR with the increase of the payload size. On the other hand, the IEEE 802.15.6 exhibits a flat PLR since the CAP is long enough to fit all the possible retransmissions and there is no limitation on the amount of times the channel has been sensed busy.

Fig. 2.15b shows the PLR as a function of the packet generation interval for the three CAP algorithms when queries are generated according to the random schemes. Thanks to the randomness in the packet generation instants, collisions are less likely to happen. Since all the three algorithms achieve similar performance, it is possible to conclude that the PLR can be kept below 1% even for high traffic intensities.

(a) Periodic traffic.

(b) Random traffic.
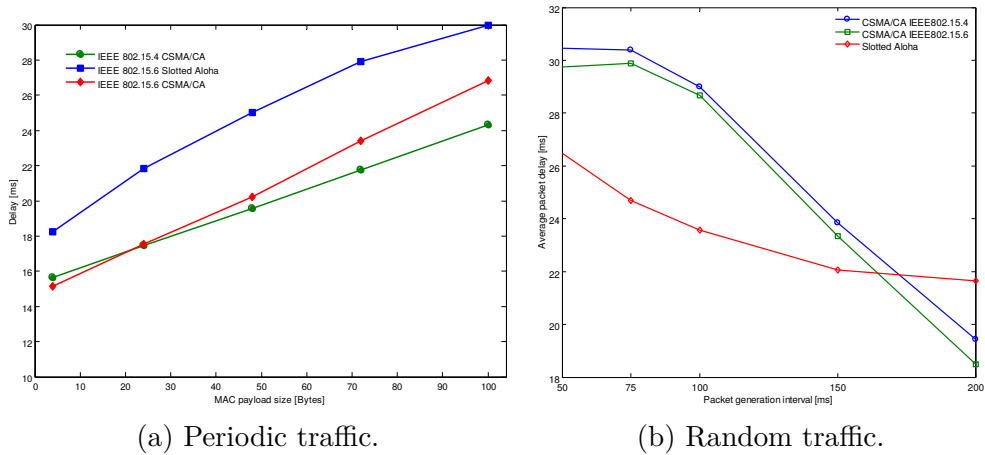
Figure 2.16: Comparison of the average delay for three different contention access algorithms.

The delay results for the periodic traffic scheme are shown in Fig. 2.16a. Slotted ALOHA performs worse than CSMA/CA because collisions are not avoided, so delay increases as a larger number of packets are retransmitted. The two curves related to CSMA/CA show that the two algorithms have more or less the same performance, however, since there is no limitation on the number of times the channel can be sensed as busy, the IEEE 802.15.6 algorithm waits more, on average, before transmitting the packet with respect to the IEEE 802.15.4 algorithm.

Fig. 2.16b shows the average packet delay as a function of the packet generation interval for three algorithms when the random traffic schemes is used. For low traffic intensities (big packet generation interval) the CSMA/CA based algorithms perform better than Slotted ALOHA. When the traffic is low, nodes using CSMA/CA will always find channel free, so the transmission will begin almost immediately after the packet is generated. This is not true for Slotted ALOHA, because even when a node is alone in the network it will still transmit in a slot with a given probability. The only reason why the delay increases with traffic intensity is because of the collisions, which
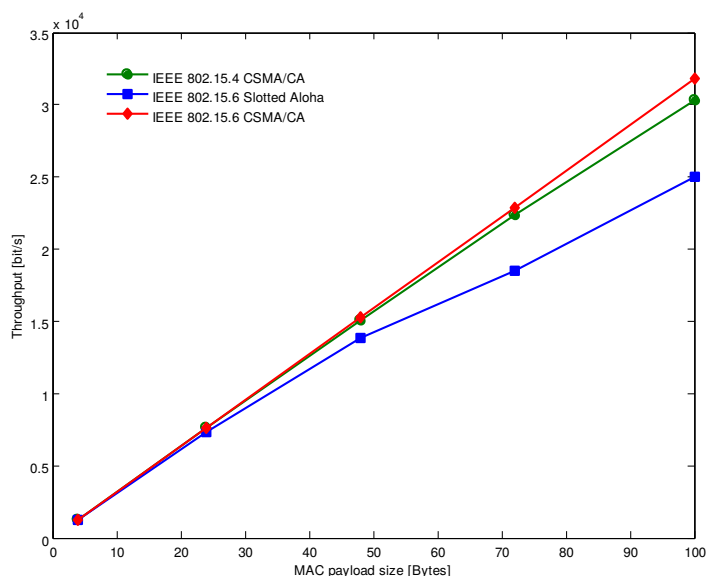
Figure 2.17: Network throughput (periodic traffic).

lead to more retransmissions. In CSMA/CA based algorithms the increase in delay is due to backoff.

The network throughput for the periodic traffic is shown in Fig. 2.17. It can be seen that up to 50 bytes of payload size all the three protocols have a quite similar behavior. As the payload size increases, the Slotted Aloha slot duration needs to be increased such that the packet can be fit in it. Maintaining the CAP size fixed leads to lower number of slots which further leads to lower number of retransmission attempts. In this conditions, collisions are the cause of the performance degradation with respect to CSMA/CA based protocols.

A dedicated set of measurements on the icycom platform has been done to investigate the dependence of the PLR and delay on the User Priority (UP) in the CSMA/CA algorithm from the IEEE 802.15.6 standard. In this measurements the SF duration is set to 75 ms, beacon period is 5 ms, CAP
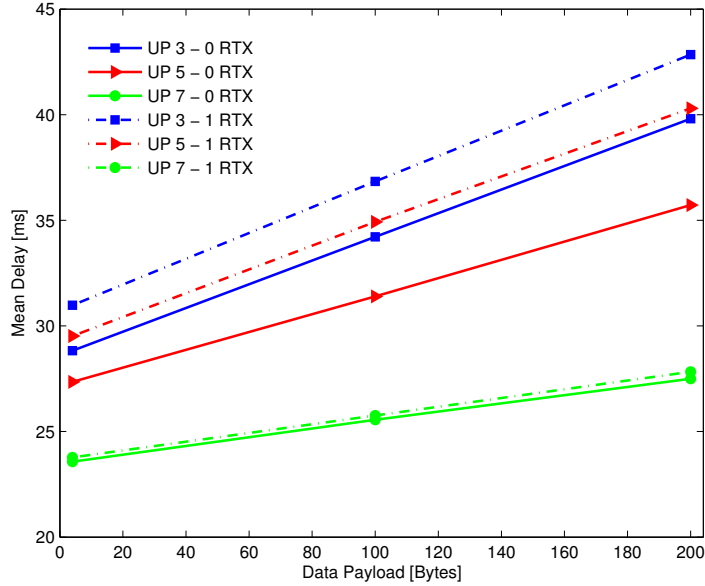
Figure 2.18: Average delay for a three nodes-network, each one with different UP values: node 1-UP 3; node 2-UP 5; node 3-UP 7.

is 60 ms and inactive period is 10 ms.

Fig. 2.18 shows the average packet delay per node as a function of the payload size of the transmitted packets. The three nodes forming the network have different UP values. Two sets of curve are shown for different values of retransmissions allowed. Node 3, being the one with UP 7, experiences the lowest average delay since its $CW_{\min}$ is 1 so it is always the first node to start the transmission. On the other hand Node 1 and Node 2 have higher $CW_{\min}$ values, which leads to higher delay since the backoff time is longer. When the number of retransmissions increases from zero to one, in order to decrease the PLR, the average packet delay increases.

Fig. 2.19 presents the average packet delay for a three-nodes network as function of the payload size and for different values of UP, in this case the three nodes have the same UP value. The maximum number of retransmis-
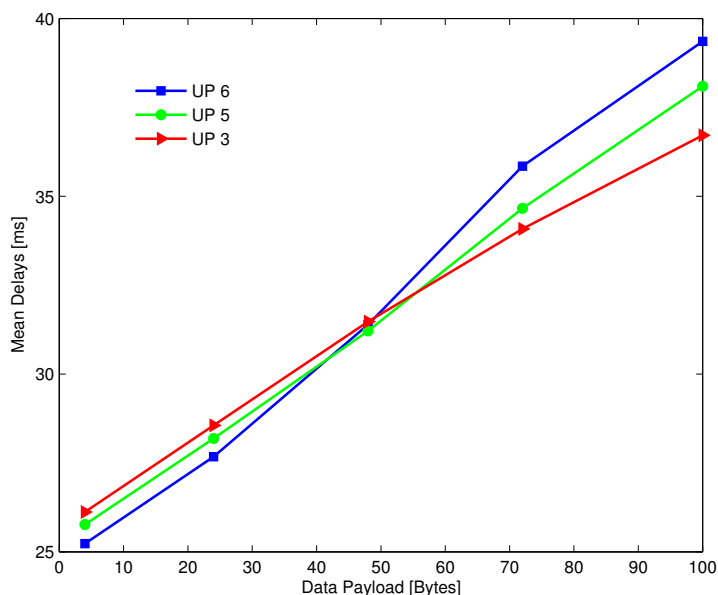
Figure 2.19: Average delay for a three nodes-network, each one with the same UP value.

sions is set to three. It can be seen that for low values of payload size, the average delay is mainly due to the the backoff period, therefore it decreases by increasing UP. On the other hand, when the payload size is large and UP increases, more packets are retransmitted since collisions are more likely to happen. This has greater impact on the average delay than the backoff period.

For what concerns the PLR analysis, it is interesting to observe the impact of UP. Fig. 2.20 shows PLR as a function of the payload size for different priorities. When the number of retransmissions is larger then two the PLR gets much better, which happens because the value of CW is doubled after an even number of failures. Moreover the PLR has an almost flat behavior because CAP lasts enough to fit the transmissions and retransmissions of all the nodes in the network. Therefore, the PLR is determined by the

67
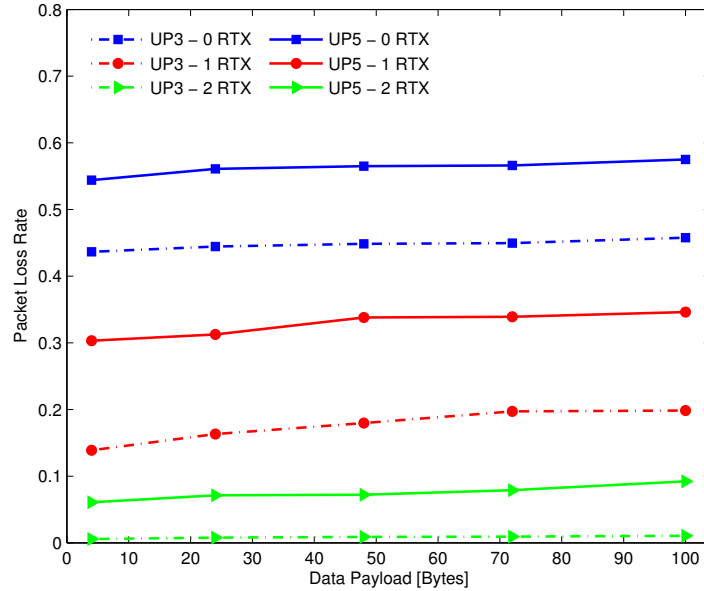
Figure 2.20: PLR for a three nodes-network with the same UP and different number of retransmissions.

probability that at least two devices choose the same random number of backoff periods, and this is independent from the payload size.

2.3.3 Energy consumption

This section present the results of the comparison between the energy consumption of IEEE 802.15.6 CSMA/CA and Slotted ALOHA; IEEE 802.15.4 CSMA/CA has not been considered since there are no relevant differences from IEEE 802.15.6 CSMA/CA. The average energy per packet is calculated as the total energy spent divided by the number of generated data packets and averaged among the devices. A dedicated software module is embedded into the protocol stack to calculate the energy consumption in real time. It measures for how long the radio stays in the different radio states (receive, transmit and off) and multiplies these values with the voltage supply (3 V)
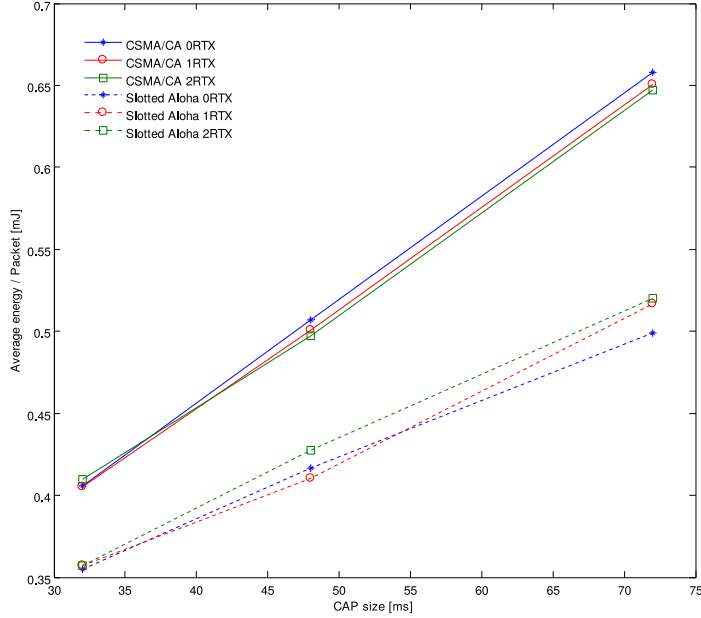
Figure 2.21: Comparison of the energy consumption of IEEE 802.15.6 CSMA/CA and Slotted ALOHA as function of the CAP duration and for different number of retransmissions.

and the current draws in each state, this method is taken from [61]. The current values have been measured in advance. Fig. 2.21 presents the average energy consumed per transmitted packet as a function of CAP duration for Slotted ALOHA and CSMA/CA. The energy consumption increases with CAP duration since the fraction of time in which the radio is active increases. It can also be seen that the energy consumption practically does not depend on the maximum number of retransmissions. This is due to the characteristics of the platform on which the experiments are performed. Indeed, the current draw in reception and transmission by the icycom board are very similar. Moreover, when there is no packet to be transmitted a node listens the channel, therefore the energy consumption does not depend significantly on the number of transmissions in CAP. Finally, CSMA/CA consumes more

69

(a) CSMA/CA, CAP duration 32 ms.

(b) CSMA/CA, CAP duration 72 ms.

(c) Slotted ALOHA, CAP duration 32 ms.

(d) Slotted ALOHA, CAP duration 72 ms.
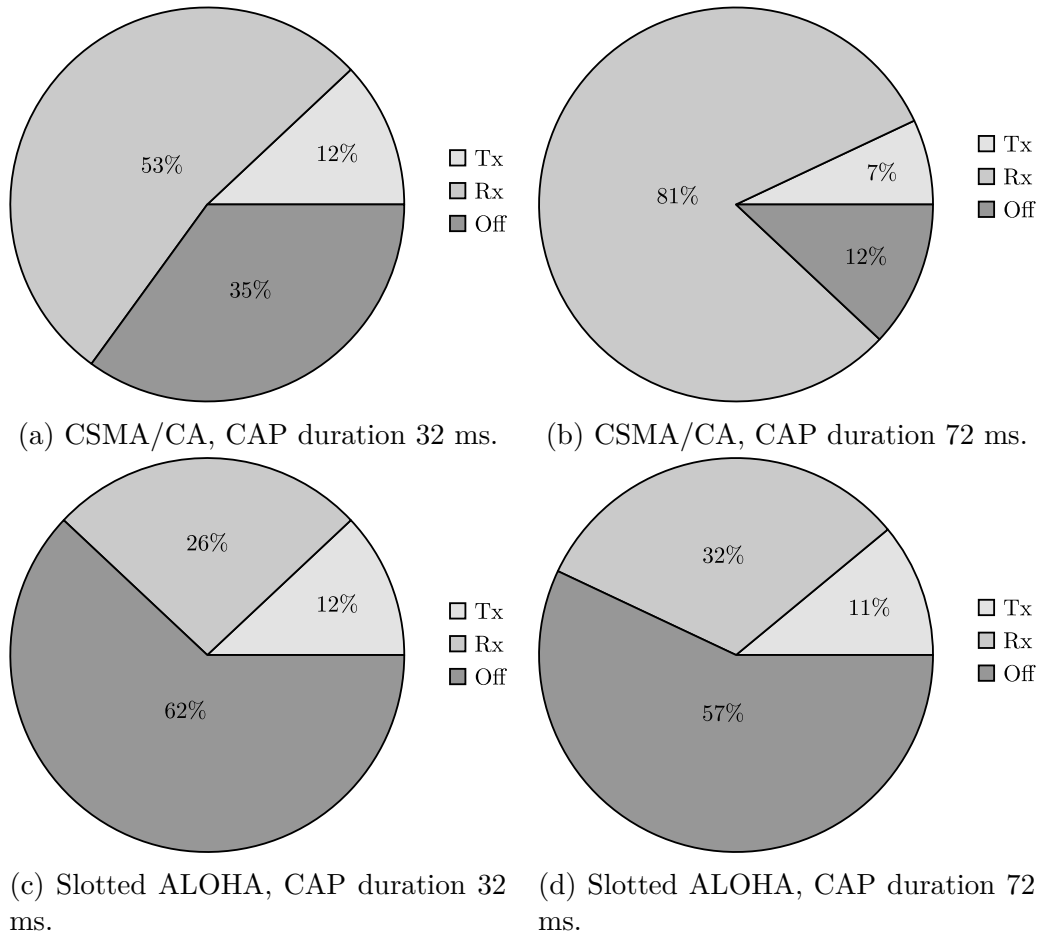
Figure 2.22: Distribution of the energy consumed in the different radio states for IEEE 802.15.6 CSMA/CA and Slotted ALOHA for different CAP durations.

energy than Slotted ALOHA because of the sensing mechanism, but also because of its unslotted nature which leads to abundant idle listening. In fact, if there are no packets to be transmitted, a node stays in receive mode for all the duration of the CAP. On the other hand, Slotted ALOHA avoids idle listening because a node knows that transmissions start only at the beginning of a slot. If it does not receive anything at that time, a node keeps the radio off for the rest of the slot, thus saving energy.

In order to properly understand the differences between Slotted ALOHA

Table 2.5: IEEE 802.15.4 and LPL energy measurements parameters.

	IEEE 802.15.4		LPL
SF duration	100 ms	T_W	100 ms
CAP duration	50 ms	T_{on}	3 ms
Beacon duration	5 ms	T_p	3 ms
Inactive duration	45 ms	**Inactive duration**	3 ms

and CSMA/CA schemes it is not enough to look at the average energy consumption only; it is important to understand how this energy is spent. Fig. 2.22 shows the fractions of energy spent in different radio states for the two access schemes and different CAP durations. The number of retransmissions in this measurement is set to zero to make the analysis of the results easier. When CSMA/CA is used, the fraction of energy spent in reception increases with the CAP duration. This is simply because a node stays in receive mode even if there is nothing to receive. This is not true for Slotted ALOHA since it limits idle listening; in fact, at the beginning of each slot the node senses the channel, if there is nothing to be received, it will go to sleep for the rest of the slot.

It is interesting to compare now the energy consumption for a standard protocol and for LPL. What follows is the comparison between IEEE 802.15.4 beacon-enabled CSMA/CA and LPL, as described in Section 1.3.3.

In these measurements the network consists of a coordinator and an ED. The payload size of the data packet is set to 100 bytes. The important parameters for the two protocols are summarized in the Table 2.5; their values are such that the delay is below 100 ms. Fig. 2.23 shows the average energy consumption per packet as a function of the packet generation interval. It can be seen that the average energy consumption per packet increases with the packet generation interval because more energy is spent while there is
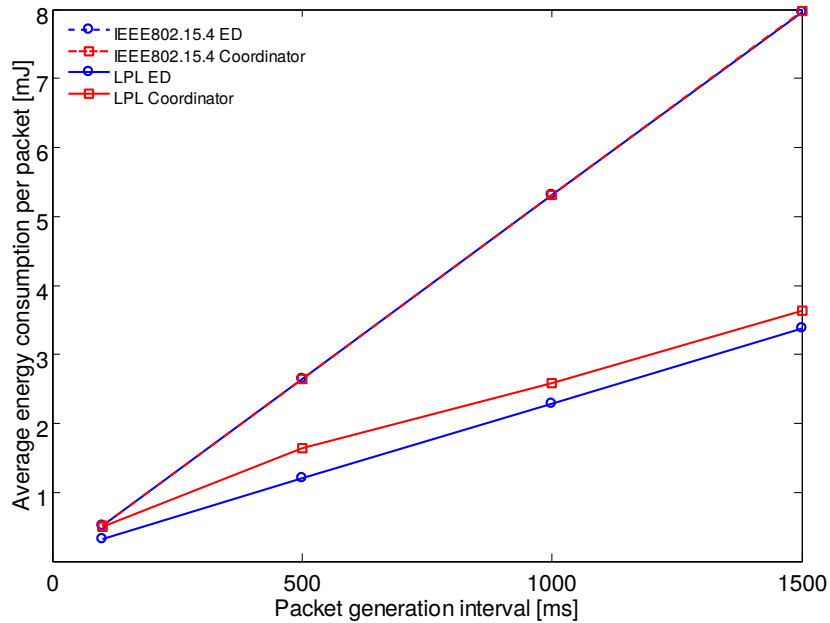
Figure 2.23: Average energy consumption per packet for IEEE 802.15.4 and LPL.

no packet exchange, in other words the experiment lasts longer while the number of packets exchanged is the same. Notice that the slopes of curves related to the two protocols are different. In the case of LPL, when there are no packets to transmit duty cycle is only 3%, while in the case of IEEE 802.15.4 it is 55%. This makes the increase in idle listening more significant in the case of IEEE 802.15.4.

The distribution of the energy consumption on different radio states for the two protocols is reported in Fig. 2.24. It shows the ability of LPL to reduce idle listening as only 18% of the energy is spent in reception compared to 66% in case of IEEE802.15.4.

Fig. 2.25a presents the average energy consumption per hour as a function of packet generation interval for the two considered protocols. In the case of IEEE 802.15.4 the average energy consumption per hour is almost constant, because the most of the energy is consumed in idle listening during CAP,

(a) CSMA/CA.

(b) LPL.
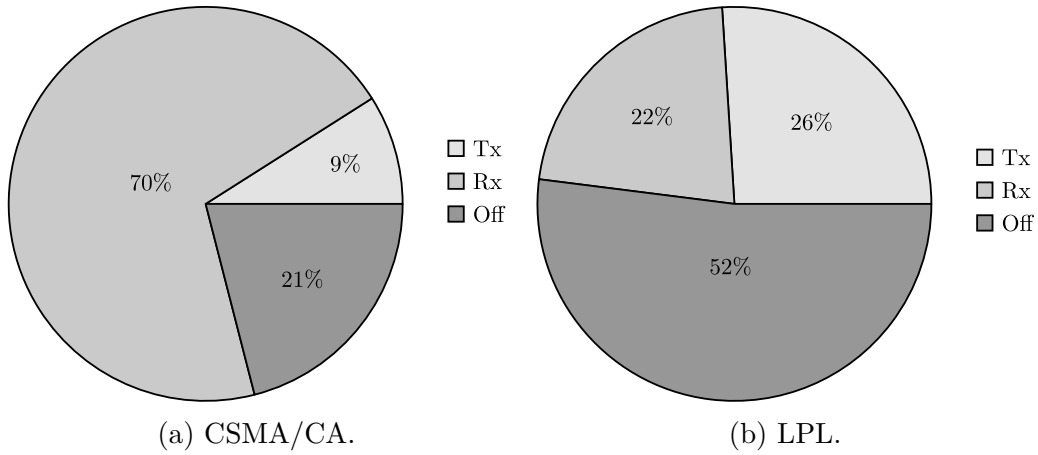
Figure 2.24: Distribution of the energy in the different radio states for IEEE 802.15.4 CSMA/CA and LPL.
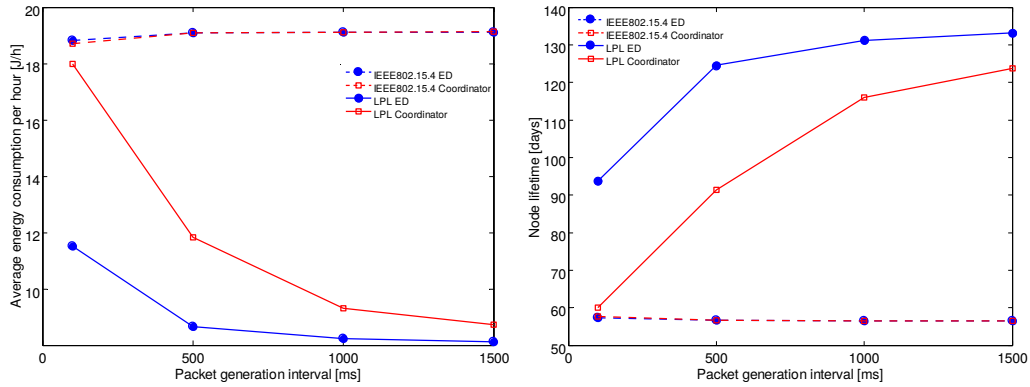
(a) Average energy consumption per hour.

(b) Node lifetime.

Figure 2.25: Average energy per hour and node lifetime for LPL and IEEE 802.15.4.

73
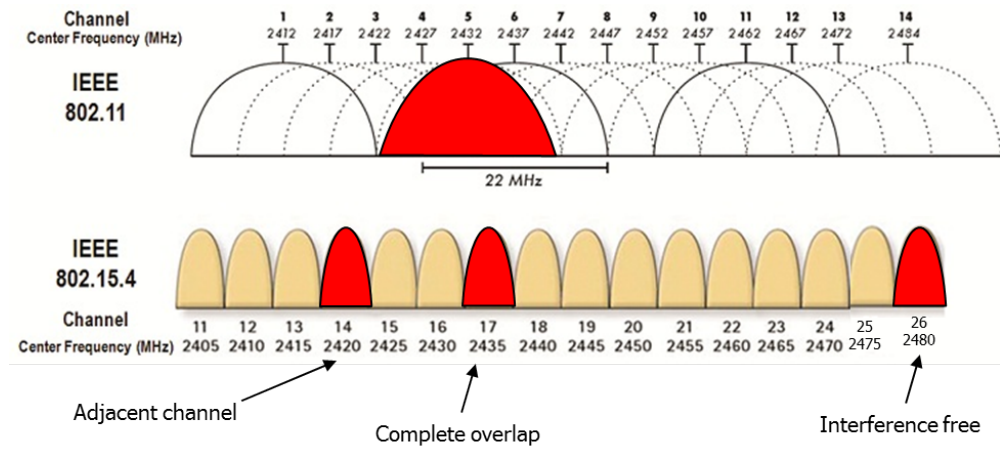
Figure 2.26: Radio channels for IEEE 802.15.4 and IEEE 802.11 (Wi-Fi).

which is independent from packet generation interval and flattens the curve. On the other hand LPL suffers much less from idle listening. This makes the packet generation interval significantly affect the energy consumption, the lower is the traffic intensity, the lower the energy consumption. Starting from Fig. 2.25a and considering a battery with a given capacity it is possible to estimate the node lifetime which is presented in Fig. 2.25b.

2.3.4 Coexistence

The ISM unlicensed band at 2.45 GHz is very crowded nowadays because of its worldwide availability. Coexistence of WBANs with other systems operating in this band (e.g., IEEE 802.11, Bluetooth, IEEE 802.15.4) is of primary importance to guarantee network reliability.

A set of experimental measurements has been done to evaluate the impact of a Wi-Fi network operating in the proximity of a WBAN compliant with the IEEE 802.15.4 standard.

The experimental setup consists of a Wi-Fi network composed of a router and a laptop, and an IEEE 802.15.4 network composed of one ED and one

coordinator located close to each other. The Wi-Fi network operates on channel 5 at 20 dBm (see Fig. 2.26), while the WBAN is tested on three different channels: channel 17, which overlaps with the Wi-Fi channel, channel 14, which is adjacent to the Wi-Fi channel, and channel 26, which is far away from the interfering Wi-Fi channel. The transmit power for the WBAN is set to 0 dBm. The experiments are performed with IEEE 802.15.4-compliant Texas Instrument devices (CC2530) in an indoor office environment.

(a) Web browsing.   (b) File downloading.
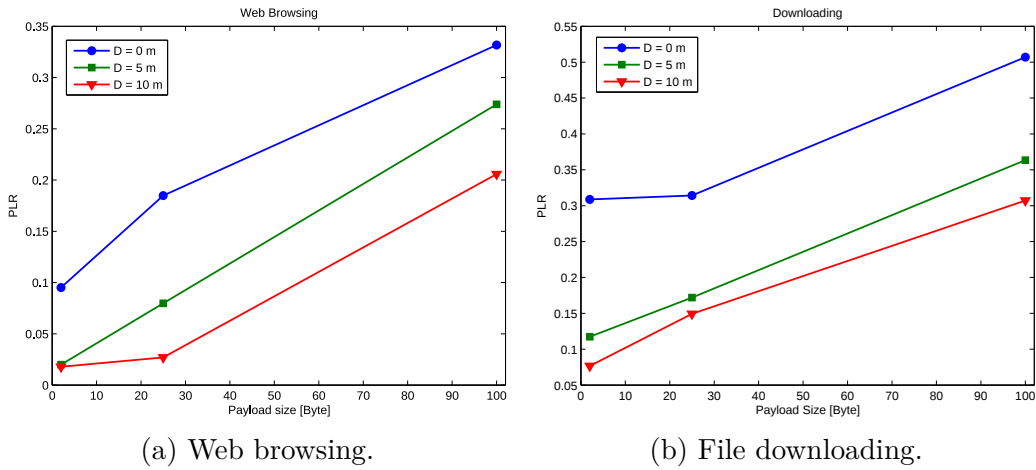
Figure 2.27: PLR vs payload size for a IEEE 802.15.4 WBAN operating in the proximity of a Wi-Fi network. The networks operate on two overlapping channels.

Fig. 2.27 shows the PLR as a function of the payload size experienced by the WBAN for different distances from the Wi-Fi network, and for two types of Wi-Fi traffic: web browsing and file downloading. The WBAN operates on channel 17, i.e., the channel overlapped to the Wi-Fi channel. As expected, the PLR increases when the distance between the two networks decreases and it is higher for the downloading traffic type than for the web browsing since the former is more intense than the latter. A preliminary experiment was carried out to test the PLR without interference, which was negligible. Therefore all the packet losses are due to collision with Wi-Fi packets or

(a) Web browsing.

(b) File downloading.
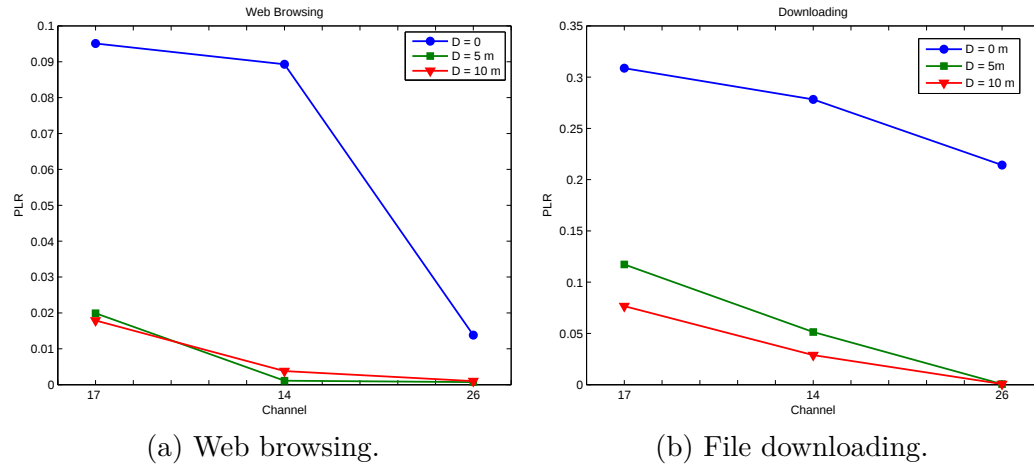
Figure 2.28: PLR vs payload size for a IEEE 802.15.4 WBAN operating in the proximity of a Wi-Fi network, for different WBAN operating channels. The WBAN packet payload is set to 2 byte.

impossibility to access the channel that is kept bust by the Wi-Fi network for most of the time.

Fig. 2.28 shows the PLR of the WBAN as function of the operating channel, and for different value of the distance between the two networks. The figure shows that even on the adjacent and on the farthest channel, the spurious emissions of the Wi-Fi network have an impact on the WBAN reliability, at least for the downloading traffic type.

From the preceding two figures, it is clear that a WBAN can hardly work in the proximity of a Wi-Fi network. To solve this problem the WBAN should implement *frequency agility*: the ability to change channel when the one currently in use is too busy. An example frequency agility technique can be the following. When the WBAN coordinator realizes that the current channel is too intefered, it selects a less busy channel and instructs the EDs to migrate to that channel.

Fig. 2.29 shows the PLR of a WBAN as function of the distance from the WiFi network when frequency agility is used and when is not. A great
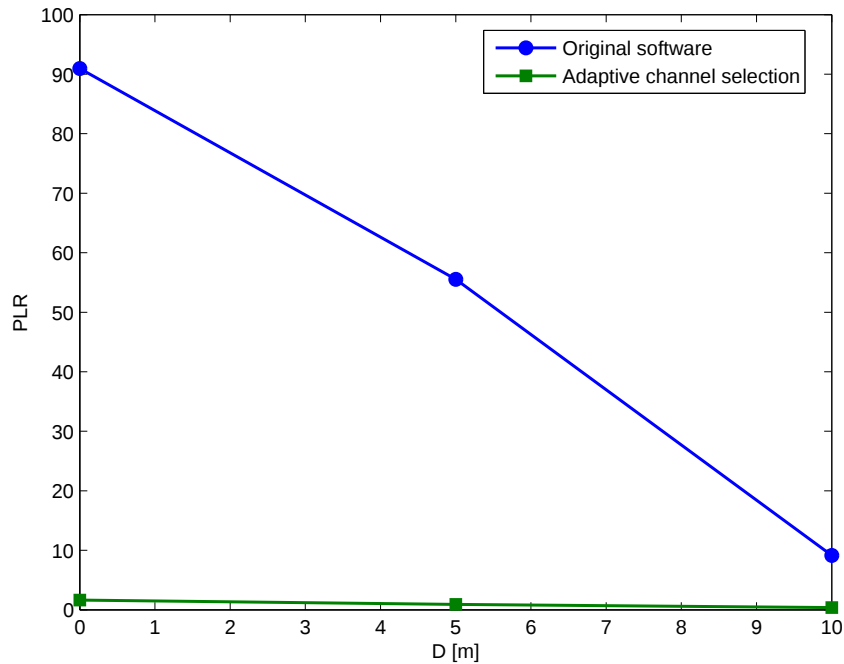
Figure 2.29: PLR for a WBAN in presence of a WiFi network when frequency agility is used and when is not.

improvement can be achieved by implementing this simple technique.

2.4 Conclusions

This section has the main objective to present the results of an extensive measurement campaign aimed at the evaluation of the performance of the WiserBAN reference WBAN; the latter, being described in detail in the first section of the chapter. The performance are evaluated in terms of PLR, average delay and energy consumption; the effect of the design issues presented in Section 1.4 are evaluated and discussed, along with novel solutions to mitigate their negative effects on the performance of the WBAN.

Part II

Delay Tolerant Networks

Chapter 3

A Wireless Backbone with Delay-Tolerant Offload

This chapter opens the second part of the thesis, which addresses the topic of Delay-Tolerant Networks (DTNs). The main purpose of this chapter is to introduce DTNs and to present a solution in which a fixed wireless backbone for Internet of Things (IoT) applications offloads part of its traffic to a DTN under certain circumstances. The work presented in this chapter is based on simulations, while the next chapter presents a mathematical approach to DTN performance evaluation, in a related setting.

3.1   Introduction to Delay-Tolerant Networks and their Applications

Delay-Tolerant Networks (DTNs) (also called Opportunistic Networks) [62–64] are characterized by the absence of a dedicated infrastructure that connects communication sources and destinations, and may lack continuous network connectivity. As a consequence of this, end-to-end paths between com-

munication sources and destinations do not exist most of the time due to node mobility, obstacles in the wireless propagation, and other adverse factors. This leads to a significant increase of the average delay with which the destination receives the information sent by the source with respect to connected networks (e.g., the Internet); therefore DTNs are suitable for applications that can "tolerate" such a delay.

The most challenging aspect of DTNs is *routing*, i.e., the definition of algorithms that specify how packets are exchanged between nodes, in order to reach their destinations. The main paradigm for routing algorithms in DTNs is the *"store-carry-and-forward"*. According to this paradigm, a node that receives a packet not intended for it, will *store* the packet in its memory and will *carry* it until a node that satisfies the routing conditions is met; when this happens, it will *forward* the packet to the newly encountered node. Of course, the packet is immediately forwarded to the destination as soon as a carrier gets in contact with it.

In the design of routing algorithms for DTN, the main focus is almost always in the minimization of the delay with which packets reach their destinations. The minimization of the delay usually comes at the expenses of some cost, therefore a delay/cost tradeoff must be considered. The cost can be in terms of energy consumption or radio resource usage. Epidemic routing [65], in its simplest form, is an example of algorithm that minimizes the delay at the expenses of the radio resource usage. According to this algorithm, a node that receives a packet forwards its replicas to the nodes it meets from that time on. Intuitively the delay is minimized in this way; however, the cost in term of radio resources is high due to the elevated number of transmissions between nodes; moreover, nodes need large buffers to store the packets they receive. A counterexample could be a naive protocol for which the source

transmits the packet only to the destination once it is met. In this case the cost is minimized, but the delay can be extremely high, or, even worse, the packet might never be delivered.

It is clear that between these two extreme examples there is room for improvement. In the last twelve years, a large number of routing algorithms has been proposed; [66] and [67] are comprehensive surveys on the subject.

The DTN concept can be applied whenever there is no infrastructure for the communication between nodes. One of the first envisioned applicative scenarios is the Interplanetary Internet, where the nodes of the network are spacecrafts [3].

Examples of terrestrial applications are military ad hoc networks, where end-to-end connectivity between nodes may not exist due to operation in hostile environments, and in emergency situations, especially after a natural disaster, when the communication infrastructures may be damaged and the use of DTNs may help in delivering information and assisting the rescuers [68]. Recent examples of applied DTNs are instant messaging applications that run on smartphone and exchange short messages without accessing the Internet [69]; recently, these applications have been used by people to communicate when the local authorities shut down social networks, usually during political protests [70].

Other applications arise in the context of the IoT, where delay-tolerant data need to be delivered to a central sink; an example can be a smartmeter for which it is important that the data arrives to the sink, but it is less relevant when the data arrives.

The rest of this chapter presents a solution based on the idea of offloading part of the traffic carried by a wireless multi-hop backbone to a DTN in order to improve its throughput in a smart city scenario. Indeed, under

some circumstances, one or more nodes of the backbone may be congested and this could lead to packet losses; in order to overcome such situations, the backbone may decide to offload part of its traffic to the mobile nodes on the street (pedestrians and vehicles), thus forming a DTN that delivers the offloaded data to a sink.

3.2 A Wireless Backbone with Delay Tolerant Offload

The amount of machine-to-machine traffic is predicted to increase by 82% by 2017 [71] and part of this increase is due to smart city applications. Smart city traffic comes from fixed and mobile sensors deployed across the city; the information is carried in data packets that are usually very small and may have loose requirements in terms of throughput and delivery delay. The most immediate solution to route data packets towards a sink would be to use the cellular network because of its omnipresence, especially in urban areas. However, the cellular network is not intended for traffic of this kind: in fact, it is mainly made for applications that require high throughput and very low delay (e.g., audio and video streaming, web browsing). Therefore, using it might be extremely suboptimal in terms of bandwidth usage. Other possible solutions are wireless multi-hop networks and the application of the paradigm of DTN.

A wireless multi-hop network, that can be used in place of the cellular network, is composed of low cost, low-range and low data-rate devices (e.g., based on the IEEE 802.15.4 standard [42]) typically arranged in mesh or tree topology [72]. On one hand, the advantage of this kind of networks is their simplicity that turns into low installation and maintenance cost; on the other

hand, the main drawbacks are the low performance (delay and throughput) and the low robustness: if a single node is in outage, it could be impossible to deliver part of the data. Outage can be due to interruption of the power supply, a data buffer overflow, and coexistence issue with other wireless technology that shares the same radio resources: it is common that this kind of networks operate in the unlicensed Industrial, Medical and Scientific (ISM) band centred at 2.45 GHz which is also used by Wi-Fi, Bluetooth, and other technologies.

The main advantage of a DTN is that it almost "comes for free" since it requires no infrastructure. A typical example of a DTN for data delivery in a urban environment is the network that uses the Bluetooth interface of smart phones carried by the people to exchange data packets: data are exchanged when two persons are inside the transmission range of each other (in the example of Bluetooth, 10 m). The main drawback of DTNs is the very long delivery delay and low throughput since contacts among people are difficult to predict, thus the design of a well performing routing algorithm is a big challenge.

The idea explored in this chapter is to exploit the DTN to improve the performance of the wireless multi-hop backbone network in charge of routing the traffic from a source node to a sink. In our urban reference scenario, the low power, low data-rate wireless backbone is composed of devices installed on lamp posts while the DTN is composed of people moving on the streets carrying smart phones equipped with the same low range wireless technology as the one employed by the backbone. The work presented in this chapter aims to answer the following questions: i) in a situation in which the offered data traffic is larger than the backbone throughput, how can the overall throughput improve when excess data are offloaded to the DTN? ii) if the

backbone and the DTN share the same band and the latter generates other traffic (unrelated to the backbone traffic), how does the interference generated by the DTN impact the performance of the lamp post backbone?

3.2.1 Related Work

In the literature there are several papers that deals with DTN offloading applied to cellular traffic, but none of them adopts the DTN paradigm to offload IoT traffic.

In [73] the authors propose and evaluate an architecture that exploits a DTN composed of 500 taxis to migrate data traffic from cellular networks to metropolitan WiFi access points. The results is that even with a sparse WiFi network the delivery performance can be significantly improved. In [74] a mathematical framework to study the problem of multiple mobile data offloading under realistic network assumptions is presented to account for heterogeneity of mobile data and limited storage of the offloading DTN nodes. The economic benefits generated by DTN offloading of cellular data is studied with a game theoretic approach in [75]; the authors concludes that DTN offloading is economically beneficial for both the provider and users. As DTN offloading increases the delay with which data are delivered, the users' satisfaction may be compromised; therefore, the authors of [76] investigate the tradeoff between the amount of traffic being offloaded and the users' satisfaction. They also provide an incentive framework to motivate users to leverage their delay tolerance for cellular traffic offloading.

3.2.2 Reference Scenario

The system presented here targets the delivery of data coming from a set of source nodes spread across the city to a central sink node. Source nodes can

be different kind of sensors (light, temperature, noise, pollution, etc...) while the sink can be a gateway that collects these data and makes them available on the Internet.

The objective is to evaluate through simulations the performance of the system in terms of throughput and average delay. In order to do so, a simplified urban scenario is considered: a Manhattan grid where each portion of the road is composed of two lanes for vehicles and two sidewalks for pedestrians; the total width of the road is 12.5 m, the area of the grid used in the simulation is about 100,000 m^2. Vehicles and pedestrians move according to their own mobility model as described later. The backbone is composed of a set of devices installed at the top of the lamp posts of the central street; lamp posts are placed on one sidewalk 25 m away from each others and they are 8 m high. One source node and one sink are considered; the former coincides with the first lamp post while the latter coincides with the last lamp post at the end of the street as depicted in Fig. 3.1.

Two kinds of mobile nodes are considered: vehicles and pedestrians.

Vehicles' mobility traces has been obtained with SUMO [77]. SUMO is a microscopic road traffic simulator that simulates accurately vehicles that are moving on a road network; being a microscopic simulator, it simulates the movements in a very realistic way, for example it reproduces the queues at the intersections, overtaking and so on. Simulations are done such that a fixed number of vehicles is always present in the scenario and such that at each intersection each vehicle chooses one of the possible directions with the same probability. Vehicles travel at a maximum speed of 13.9 m/s (50 km/h).

Pedestrian mobility has been generated using the dedicated module of the ONE simulator [78]. A fixed number of pedestrians move on the sidewalks
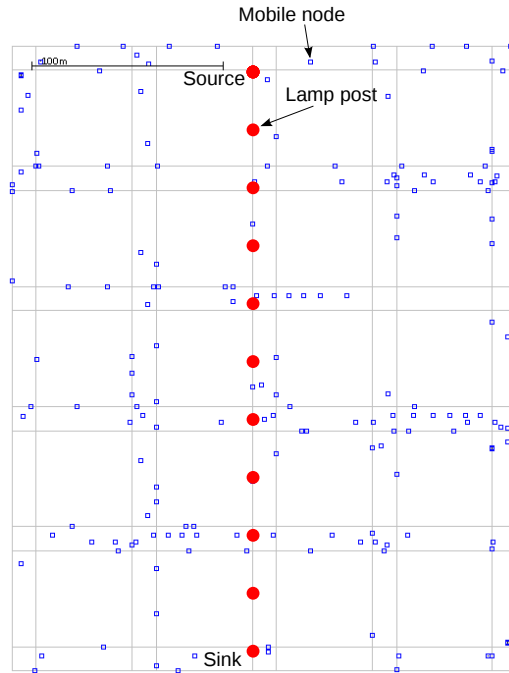
Figure 3.1: Reference scenario. Blue dots denote mobile nodes, red dots denote lamp posts.

(represented by a straight line), at a random speed uniformly distributed between 0.5 and 1.5 m/s. Their initial positions are uniformly distributed over the whole sidewalk length. As in the case of vehicles, when a pedestrian reaches an intersection, it chooses the next direction uniformly among the possible ones, but differently from vehicles, microscopic effects such as queues and regulated road crossings are not simulated. Such a simple model allows us to draw some theoretical observations, as discussed in the next Sec. 3.2.5.

3.2.3   Backbone MAC protocol

The backbone uses a combination of Frequency Division Multiple Access (FDMA) and Time Division Multiple Access (TDMA) schemes to access the channel. Each node of the backbone has been assigned an address from 0
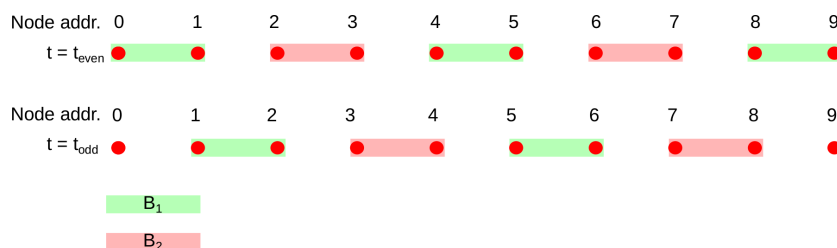
Figure 3.2: Illustration of the MAC mechanism; transmission of packets is always from the left node to right node inside the same band.

(the node at the first lamp post) to $N_l = 10$ (the node at the last lamp post). Time is divided into slots, whose duration is enough to accommodate a packet transmission and slots are numbered starting from 0. During even (odd) time slots the nodes with an even (odd) address transmit to the next node in line with an odd (even) address. In order to avoid that two contiguous transmitter-receiver pairs interfere each others, two radio bands, B_1 and B_2, are used: each transmitter-receiver pair operates in a band different from the one used by its two neighbours. The MAC mechanism is illustrated in Fig. 3.2.

3.2.4 Offloading Mechanism

Data packets are generated at the first lamp post and need to be routed towards the last lamp post through the wireless backbone. Assuming the backbone nodes have a finite buffer for incoming packets, the packets in excess will be discarded if the offered data traffic is larger than the backbone throughput. Since packets are generated only at the first lamp post, it will be the only one for which the buffer may become full. When this happens, the node will attempt to offload these packets to all the mobile nodes (pedestrians or vehicles) that are within its transmission range.

Once a packet is offloaded, it stays in the buffer of the mobile node until

89

the latter gets in the transmission range of the destination of the packet, that is, the last lamp post. This is the simplest approach to delay-tolerant networking; alternatively one can implement a routing algorithm, from a simple one, like the already mentioned epidemic routing, to more complex ones.

3.2.5   Numerical Results

This section presents the results obtained applying the described offloading mechanism.

With the MAC protocol described in Sec. 3.2.3 and a bit rate R_b, the maximum throughput S_{max} of the wireless backbone is $S_{max} = R_b/2$, since each node transmits for half of the slots[1]. It is also assumed that the mobile nodes generate interference on the same frequency bands of the wireless backbone; this affects the correct reception of packets at the backbone, therefore it limits the throughput. A packet is correctly received if the ratio between the useful signal and the interference is $C/I > 3$ dB, the value of C in Watt is calculated as

$$C = kd^{-\beta}, \tag{3.2.1}$$

where $d = 25$ m is the distance between two lamp posts, $\beta = 2$ is the path loss exponent and $k = 10^{-4}$ W is the received power 1 m away from the transmitter. The interference I is calculated as the sum of the received powers coming from the set of transmitting mobile nodes; the same formula as before is used, however in this case it is $\beta = 3$ to account for the shadowing introduced by obstacles in between the mobile nodes and the lamp post (e.g., trees, buildings, etc.). The set of transmitting mobile nodes is a subset of all

---

[1]An ideal physical layer is assumed; the header in the data packet is neglected.

the nodes that are in the scenario, specifically, it is assumed that a mobile node transmits with probability t. This considerations leads to the following expression for the interference, in Watts,

$$I = \sum_{i=1}^{N} T_i k d_i^{-\beta},$$
(3.2.2)

where N is the total number of mobile nodes, d_i is the distance between the backbone node and the mobile node, T_i is a random variable that takes the values 1 with probability t, and 0 with probability $1 - t$, for each interfering source.

The first result is the analytic expression of the probability P_c for the backbone node on the first lamp post to have at least one pedestrian inside its coverage area. Only pedestrians are considered because it is simpler to compare the analytic results with the simulation since the mobility model for pedestrians is more random than the one of vehicles. The node displacement with respect to the sidewalks is depicted in Fig. 3.3: y_a and y_b represent the length of S, i.e., the portion of sidewalk inside the coverage area of the backbone node. They are $y_a = 2\sqrt{r^2 - h^2}$ and $y_b = 2\sqrt{r^2 - h^2 - w^2}$, respectively, where r is the transmission range, h is the height of the lamp post and w is the distance between the sidewalks. Since the pedestrians' positions are uniform identically and independently distributed (iid) random variables, the expression for P_c is:

$$P_c = 1 - P\left(\text{All the N nodes are outside } S\right)$$
$$= 1 - \left(\frac{L_s - y_a - y_b}{L_s}\right)^{N_p},$$
(3.2.3)

where N_p is the number of pedestrians in the scenario and L_s is the overall
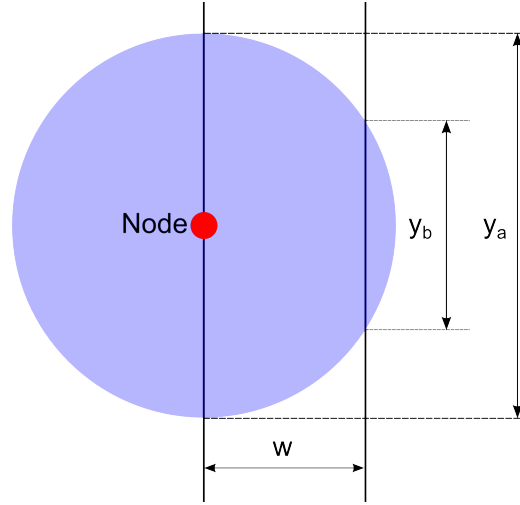
Figure 3.3: Top view of the portions of sidewalks covered by the backbone node coverage. The node is $h = 8$ m above the ground level.

length of the sidewalks in the grid; this value is set to 6400 m. Fig. 3.4 shows the comparison of P_c with respect to the transmission range obtained with (3.2.3) and the one from the simulation, in this case it is $N_p = 100$. The figure shows a good agreement between the simulation and the model.

The simulation results for the throughput as a function of the transmission range r for a scenario with 100 pedestrians and 100 vehicles, is shown in Fig. 3.5a. The offered throughput and the bit rate are set to 100 kbps; this leads to a backbone throughput of 50 kbps without interference, as it can be seen from the first point of the curve for $t = 0$ in Fig. 3.5a. When the intervention of the mobile nodes starts to become significant, the throughput increases up to 100 kbps when r is about 150 m, that is roughly the half of the length of the backbone. At this point, the two coverage areas of the source and sink nodes start overlapping, thus the offloaded data packet is immediately transmitted from the mobile node to the sink, no matter what is the route of the mobile node. Of course, the presence of the interference ($t > 0$) seriously affects the throughput.
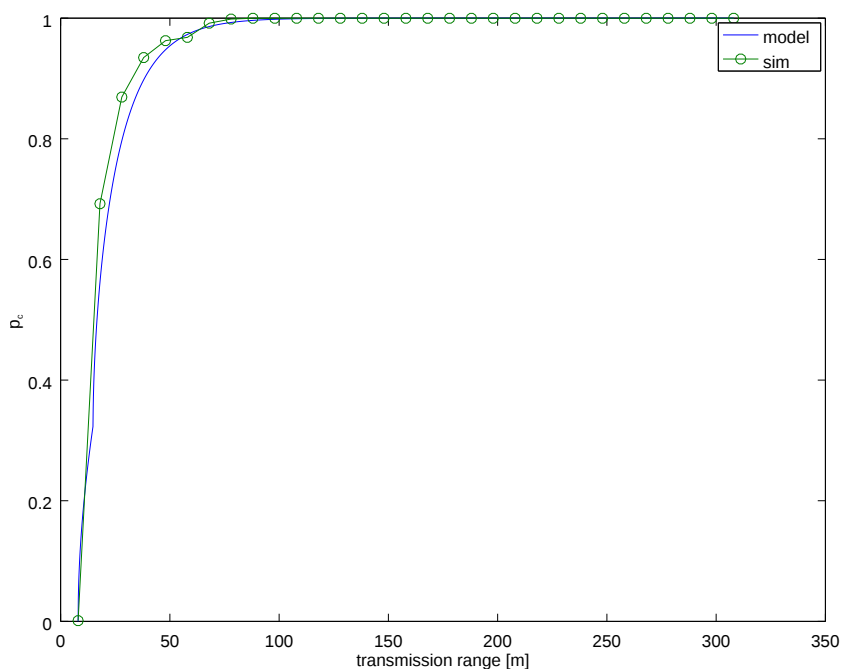
Figure 3.4: The probability P_c that a backbone node has at least one pedestrian in its coverage area, when the transmission range is r.

Fig. 3.5b shows the average delay as function of r; the average delay is measured as the time elapsed from the generation of the packet at the source node and the reception at the sink, averaged over the number of received packets. For small values of r, the delay is very small because its main contributor is the backbone. When r increases, more packets are offloaded to the mobile nodes, as seen before; this is a benefit for the throughput, but it also makes the average delay to increase significantly because of the travelling time of mobile nodes. After a certain value of r the average delay starts to decrease again since the two coverage areas of the source and the sink are getting closer and closer, so the mobile nodes need to travel less, in average, to reach the coverage area of the sink. These plots can be used to decide the most suitable value for the transmission range of the backbone and to find a tradeoff between throughput and delay.

93

(a) Throughput.
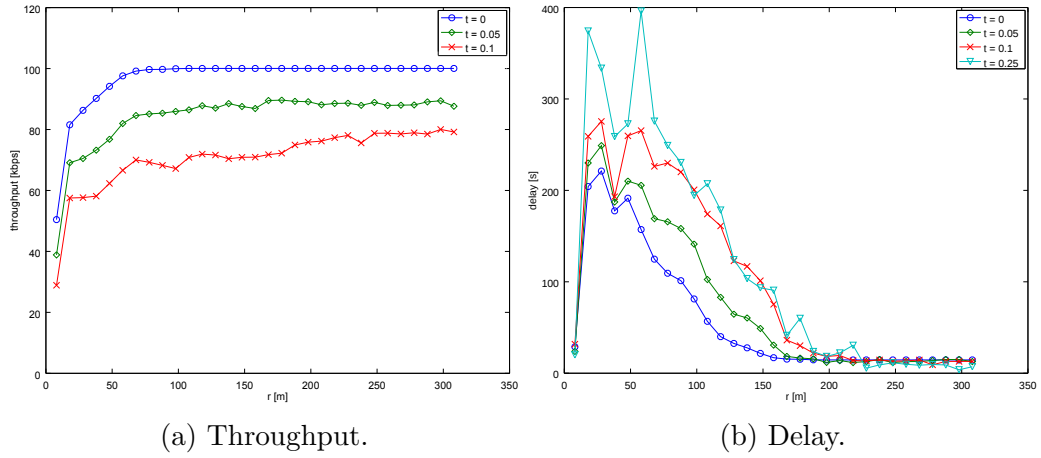
(b) Delay.

Figure 3.5: Throughput and delay as function of the transmission range r for different values of transmission probability.

The next results show the performance of the network when the number of mobile nodes change; for these results the assumption that packets are offloaded only to pedestrians holds, and the transmission range is set to 20 m. From Fig. 3.6a it can be seen that, as expected, the network throughput tends to the offered throughput when the number of pedestrians N_p gets larger that a threshold. However, when N_p increases, also the interference increases and has a strong impact on the throughput.

Fig. 3.6b shows the average delay versus N_p. In the case $t = 0$, the average delay tends to a value that is the time it takes a pedestrian to go from the source to the sink following the shortest path. This happens because when N_p tends to infinite, the probability that among the nodes that receive the offloaded packet, there is one of them going to the sink following the shortest path, tends to be 1.

(a) Throughput. (b) Delay.
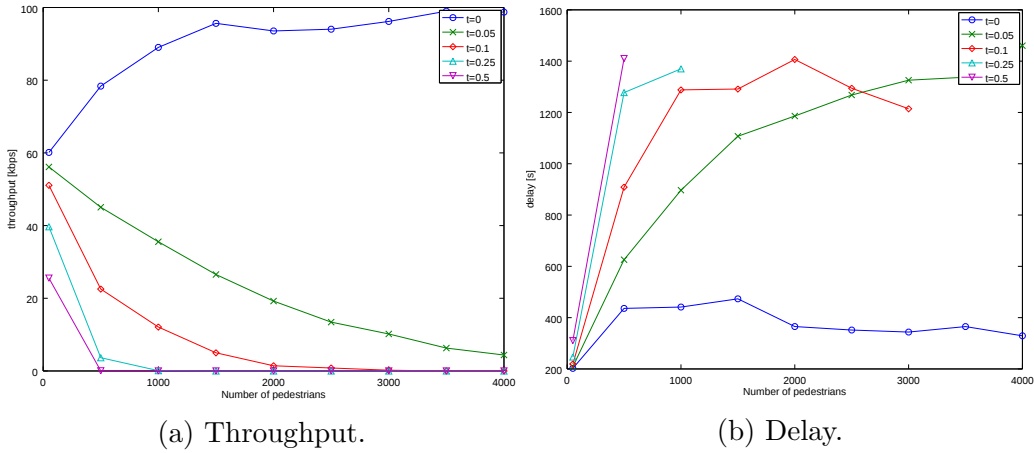
Figure 3.6: Throughput and delay as function of the number of pedestrian N_p for different values of transmission probability and for $r = 20m$.

3.3 Conclusions

This chapter evaluates the performance of a system for data delivery composed of a low-cost, low data-rate backbone that exploits the offload to a DTN in order to improve the performance of the whole system. The results is that the network throughput can be improved, at the expenses of the average delay, by just offloading those packets that otherwise would be discarded when the offered throughput is larger than the backbone throughput. The effect of the interference generated by the DTN on the throughput and delay is accounted for.

Overall, this work, although being preliminary, proves that the novel idea of offloading part of the traffic to vehicles and pedestrians, forming a DTN, is worth of further investigation.

Chapter 4

Cost/Speed Analysis of Mobile DTNs

Consider a network where an infinite number of nodes are moving in $\mathbb{R}^2$ according to a Random Waypoint (RWP) mobility model. Each node is equipped with a radio transceiver with transmission range R; a transmission across a distance d incurs a quadratic cost d^2. Assume, moreover, that a packet is generated at one node and must be delivered to a destination located at an infinite distance in the direction of the positive x-axis through a combination of wireless transmissions and physical transports on the buffers of nodes. A routing rules specifies when a node is eligible to carry the packet.

Given this setting, this chapter presents a mathematical framework that uses tools from stochastic geometry and Markov chains theory, to evaluate, with certain approximations, the tradeoff between the average speed with which the packet travels toward the destination and the average cost incurred. Simulations are used to verify the correctness of the analysis. The effects of the transmission range R and other parameters on the performance metrics are also investigated.

4.1 Related work

This work can be seen as an extension of [79], where a similar framework was developed; however, differently from [79], the mobility model used here includes the possibility of nodes occasionally changing their direction, which is more realistic but complicates the analysis significantly; furthermore, and in contrast to [79], a more precise analysis is conducted, coupling the existing stochastic geometry approach with a new Markov chain component. An upper bound of the information propagation speed, that holds irrespective of the routing protocol used, has been derived for different types of mobility models in [80]. This work is different from [80] because it does not provide bounds, but is focused on specific routing rules; moreover it considers the cost besides the propagation speed. In [81] the authors analyze the tradeoff between delay and cost for the delivery of a packet in a DTN for a number of known geographic routing rules; using network optimization tools, while in this work probabilistic analysis is used.

4.2 Network Model and Routing Rules

4.2.1 Network Model

An infinite number of nodes move in $\mathbb{R}^2$ according to the following RWP mobility model [82]: at time $t = 0$ nodes are placed on $\mathbb{R}^2$ according to a homogeneous Poisson Point Process (PPP) with density λ. Each node then selects a random direction and starts moving in that direction until a change of direction occurs at time T_1, when a new random direction is chosen; after time T_2 another change of direction occurs and a new random direction is chosen, and so on; this process continues forever. It is assumed that the

change-of-direction instants T_k form a homogeneous Poisson process with intensity r_0 and the new directions are uniformly distributed in $[-\pi, \pi]$. At all times nodes move at constant speed v_0 and independently of each other; as a conseguence, the displacement theorem [83, Theorem 1.3.9] applyes, therefore at any time the nodes constitute a PPP of density λ.

The focus is on a single *tagged* packet that is generated at a source node and must be delivered to a destination located at an infinite distance from the source in a specific direction which, for simplicity, is taken to be the direction of the positive x-axis, through a combination of wireless transmissions and physical transports on the buffers of nodes. The node that at a given time instant is carrying the packet is called the carrier. The exchange of a packet between two nodes separated by distance d is instantaneous and has a transmission cost $C(d) = d^2$. The transmission range of a node is denoted by R, and the circular region, of radius R centered at a node and moving with it is called the forwarding region (FR). A routing rule (RR) specifies under which conditions a packet is transmitted to another node; four example routing rules are presented in Section 4.2.4, but the analysis can be extended in a straightforward manner to a large class of other RRs. If at any time a node exists in the FR of the carrier node that satisfies the condition set by the RR for immediately receiving the packet, this node is called eligible.

It is clear that a tradeoff exists between packet speed toward the destination and cost: a RR that prefers wireless transmissions over physical transport leads to higher speed at higher cost with respect to a RR that prefers physical transport over wireless transmissions.

99

4.2.2 Stages

To perform the mathematical analysis, the travel of the packet toward the destination is divided in a sequence of stages indexed by $i = 1, 2, \ldots$. A stage is defined as a period of time during which the packet travels along a fixed direction. A stage ends when the packet changes direction of travel, which happens in four ways:

1. The carrier node meets an eligible node at the boundary of its FR.

2. A neighbor of the carrier, i.e., a node that is inside the FR of the carrier, becomes eligible.

3. The carrier changes direction and immediately an eligible node is found.

4. The carrier node changes direction but no eligible node is immediately found.

In the first three cases, the packet is transmitted to the eligible node, while in the last case no transmission takes place. When the packet is transmitted, it may happen that the node that has just received the packet already has other eligible nodes within its FR, the packet will be immediately transmitted to one of these nodes; this process may be repeated an arbitrary number of times; this scenario is called multihop packet forwarding. Since in this case the packet will change its direction a number of times at an instant, it is assumed that the new stage starts when the last node that has received the packet does not have any eligible node in its FR. This specific definition of stages is made for mathematical convenience in order to avoid stages with null duration.

A set of random variables (RVs) is introduced to describe a stage. In the following, RVs are denoted by capital letters, while small letters are used

Table 4.1: Notation

	Model parameters
λ	Density of the node PPP
v_0	Node speed
r_0	Node turning rate
R	Transmission range
	Random Variables for stage i
Θ_i	Direction of travel of the packet
Δ_i	Duration of the stage
N_i	Number of wireless transmissions (hops)
$X_{p,i}$	Progress due to physical transport
$X_{w,i}$	Progress due to wireless transmissions
C_i	Incurred cost

for their realizations. A list of symbols used throughout the text appears in Table 4.1.

The stage i, for $i = 1, 2, \ldots$, starts at time $t = T_{i-1}$, ends at time $t = T_i$, and is characterized by the direction of travel Θ_i, its duration $\Delta_i = T_i - T_{i-1}$, its net progress toward the destination X_i, its total transmission cost C_i, and a set of RVs related to the sequence of hops taken by the packet at the end of the stage.

During stage i the packet makes progress toward the destination in two ways: with physical transport and with wireless transmissions. Let $X_{p,i}$ be the progress in the direction of the x-axis, due to physical transport; its expression is $X_{p,i} = \Delta_i v_0 \cos \Theta_i$. On the other hand, let $X_{w,i}$ be the progress due to wireless transmissions. $X_{w,i}$ is the sum of the progress for each hop, i.e., $X_{w,i} = \sum_{j=1}^{N_i} X_{w,i}^{(j)}$, N_i being the number of hops taken in stage i. The total transmission cost for stage i is $C_i = \sum_{j=1}^{N_i} \left(X_{w,i}^{(j)^2} + Y_{w,i}^{(j)^2} \right)$. Note that

101
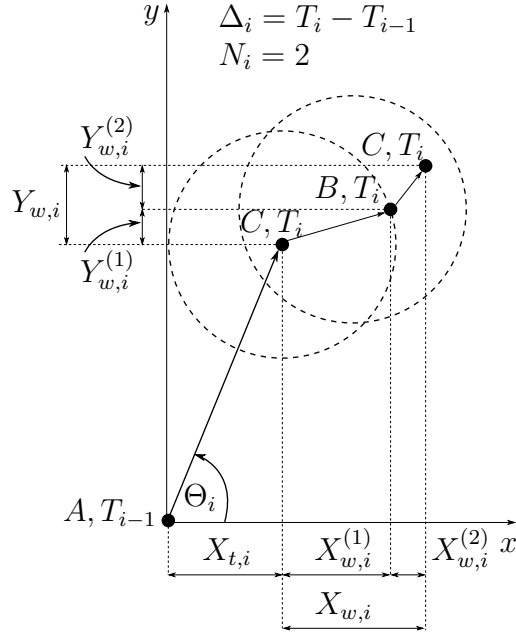
Figure 4.1: Illustration of an example stage i; the multihop packet forwarding depicted here has $N_i = 2$.

when a stage ends without transmissions, it is $N_i = 0$, $X_{w,i} = 0$ and $C_i = 0$.

Fig. 4.1 shows an example stage. At time T_{i-1} the carrier A is traveling along direction Θ_i. At time T_i A meets an eligible node B, so the packet is transmitted to B. Node B already has another eligible node C in its FR, thus the packet is transmitted to C. Node C does not have any eligible node in its FR; at this time, stage i is over and a new stage begins.

4.2.3 Performance Metrics

The metrics used to evaluate the routing rule are the average packet speed $\overline{V}$ at which the packet travels toward the destination, and the average packet cost $\overline{C}$.

To calculate the average packet speed, observe that the packet moves toward the destination by means of physical transport and wireless transmis-
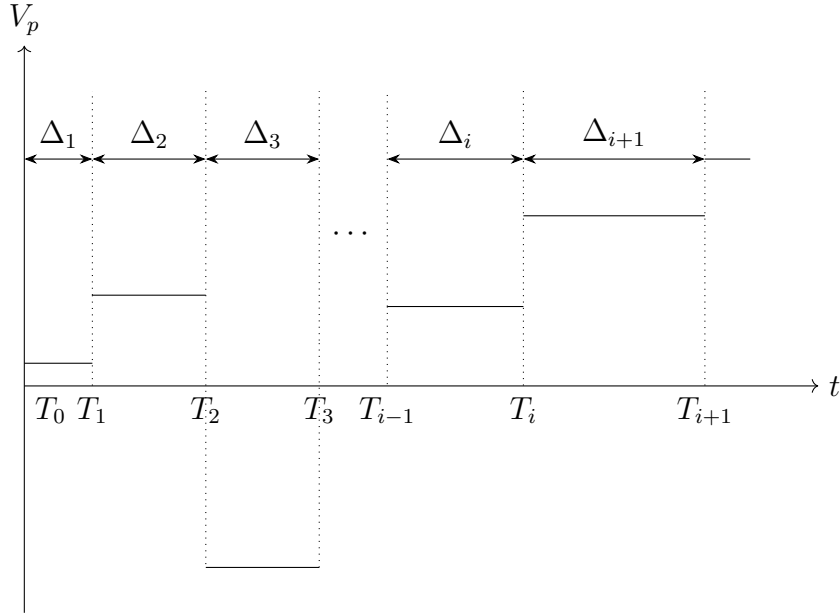
Figure 4.2: The random process $V_p(t)$ during a sequence of stages.

sions. Let $V_p(t)$ be the speed due to physical transport at time t, therefore the average speed due to physical transport is calculated as

$$\overline{V_p} = \lim_{t \to \infty} \left(\frac{1}{t} \int_0^t V_p(s)\, \mathrm{d}s \right). \tag{4.2.1}$$

As all the nodes move with constant speed v_0, the value of $V_p(t)$ depends only on the direction of travel of the packet $\Theta(t)$, therefore it is constant for the full duration of a stage. Fig. 4.2 shows the evolution of $V_p(t)$ for a sequence of stages.

The average speed due to wireless transmissions, which is denoted by $\overline{V_w}$ can be expressed as the fraction of the distance toward the destination covered due to wireless transmissions in the first K stages over the sum of the durations of those K stages as K goes to infinity:

$$\overline{V_w} = \lim_{K \to \infty} \frac{\sum_{i=1}^{K} X_{w,i}}{\sum_{i=1}^{K} \Delta_i}, \tag{4.2.2}$$

103

Note that there will be stages for which $X_{w,i} = 0$; as discussed, this happens when the stage ends because the carrier node changes its direction of travel and no eligible node is immediately found within the FR.

The overall average packet speed, $\overline{V}$ is obtained by summing the two components:

$$\overline{V} = \overline{V_p} + \overline{V_w}. \tag{4.2.3}$$

The average cost is calculated as

$$\overline{C} = \lim_{K \to \infty} \frac{\sum_{i=1}^{K} C_i}{\sum_{i=1}^{K} X_{p,i} + X_{w,i}}. \tag{4.2.4}$$

The average packet cost $\overline{C}$ is expressed in units of cost per meter. This metric tells how much does it cost to bring the packet one meter closer to the destination. As in the case of $\overline{V_w}$, there will be stages for which there are no wireless transmissions; for these stages, $C_i = 0$.

4.2.4 Routing Rule

A RR establishes the conditions that a node inside the FR of the carrier must satisfy to be eligible, and hence completely specifies, in conjunction with the node mobility process, the trajectory of the tagged packet.

Four RRs are proposed. In the definitions that follow, $\mathcal{F}$ is the FR of the current carrier, θ_c is the direction of the carrier, a generic neighboring node of the carrier has direction θ_n, and ϕ is the angle formed by the x-axis and the line segment connecting the node and the carrier, where $\phi \in [-\pi, \pi]$.

RR1: A node is eligible if its direction is better than the direction of the carrier node, i.e., $|\theta_i| < |\theta_c|$. If more than one node is eligible, the carrier selects the one with the best direction among the others.

RR2: A node is eligible if $|\theta_n| < |\theta_c|$, and it is located in the half of $\mathcal{F}$ that points toward the direction of the x-axis, i.e., $|\phi| \leq \frac{\pi}{2}$. If more that one node is eligible, the best one will be chosen as in RR1.

RR3: A node is eligible if $|\theta_n| < |\theta_c|$, and its direction is within a threshold $\tau \geq 0$, i.e., $|\theta_n| \leq \tau$. If more that one node is eligible, the best one will be chosen as in RR1.

RR4: A node is eligible if it is located in the half of $\mathcal{F}$ that points toward the direction of the x-axis, i.e., $|\phi| \leq \frac{\pi}{2}$. If there is more than one eligible node, the closest to the carrier will be chosen to minimize the transmission cost.

4.3 Methodology

This section presents the mathematical framework used to evaluate the average packet speed $\overline{V}$ and the average packet cost $\overline{C}$, for a given routing rule. In particular, it is shown that the evolution of the route taken by a packet can be modeled using finite-state continuous-time Markov chains (CTMCs) [84] and a number of simplifying approximations. The analysis can handle many different RRs; in Sections 4.5 and 4.4 the framework is used to evaluate the performance of RR1 under different simplifying approximations.

4.3.1 The Continuous-Time Markov Chain

Consider the speed due to physical transport $V_p(t)$. At time t its value is $V_p(t) = v_0 \cos \Theta(t)$. Since v_0 is constant and common to all nodes, $V_p(t)$ only depends on the direction of travel $\Theta(t)$; for this reason, from now on the problem is stated in terms of directions.

105

The random process $\Theta(t)$ is modeld as a CTMC in the state space $I = \{i\}_{i=1,2,\ldots,N}$. The CTMC is in state i at time t, if

$$\Theta(t) \in [\theta_i, \theta_{i+1}), \quad i = 1, 2, \ldots, N,$$

where the endpoints θ_i are defined by the discretization of the interval $[-\pi, \pi]$ in N subinterval of length $\frac{2\pi}{N}$. Therefore,

$$\theta_i = -\pi + (i-1)\frac{2\pi}{N}, \quad i = 1, 2, \ldots, N.$$

The set $\{\theta_i\}_{i=1,2,\ldots,N}$ is called S.

A consequence of the discretization is that the continuous random process $\Theta(t) \in [-\pi, \pi]$ is approximated by the discrete random process $\widetilde{\Theta}(t) \in S$. Thus, when $\Theta(t) \in [\theta_i, \theta_{i+1})$, it is $\widetilde{\Theta}(t) = \theta_i$. Later in the text, the generic state i is referred either through its index i, or through the direction θ_i.

The random process $\Theta(t)$ is modeled as a CTMC in the state space S. S is obtained discretizing the direction of travel of the packet, that is by the discretization of the interval $[-\pi, \pi]$ in N disjoint subintervals of width $\frac{2\pi}{N}$; this creates out of $\Theta(t)$ another discrete random process that is called $\widetilde{\Theta}(t)$. The direction of travel of the packet, i.e., the state of the CTMC, is θ_i, $i = 1, 2, \ldots, N$, if the direction of travel $\Theta(t)$ of the carrier node belongs to the i-th subinterval, i.e., if $\Theta(t) \in \left[-\pi + (i-1)\frac{2\pi}{N}, -\pi + i\frac{2\pi}{N}\right)$. The effect of the discretization can be summed up with the following approximation:

Approximation 1. The direction of travel $\Theta(t)$ of the carrier node is modified such that it coincides with $\widetilde{\Theta}(t)$.

Observe that the random process $\widetilde{\Theta}(t)$ is not Markovian by itself. According to the Markov property, the transition from the current state $\widetilde{\Theta}(t_0) = \theta_i$ to the next state $\widetilde{\Theta}(t_1) = \theta_j$, $j \neq i$, $t_1 > t_0$, depends only on $\widetilde{\Theta}(t_0)$ and not

on the previous history $\widetilde{\Theta}(t < t_0)$. To understand that $\widetilde{\Theta}(t)$ is not Markovian consider again Fig. 4.1 where the directions at time T_i of nodes A, B, and C are θ_A, θ_B and θ_C, respectively. When node A transmits the packet to node B, the latter transmits the packet immediately to the eligible node C which is already inside its FR $\mathcal{F}$; therefore the process has moved from state θ_A to θ_C. Assume that C changes direction after an amount of time short enough such that B is still inside $\mathcal{F}$; assume moreover that the new direction is such that B becomes eligible to C. The result is that C will immediately transmit the packet back to B. The probability of this event, does not depend only on the current state θ_C, but also on the fact that the packet went from node A to node C passing through node B, and node B is still in the forwarding region of node C.

The following approximation ensures that the Markov property is satisfied.

Approximation 2. Whenever a node receives the packet, or the carrier node changes its direction of travel, the entire process describing the position and the direction of travel of the other nodes is restarted.

It follows from this approximation that the time the system spends in each state is exponentially distributed. Indeed, the packet changes direction, i.e., state, according to three independent stochastic processes: the process with which the carrier node meets better nodes, which will be showed to be Poisson (see Proposition 3), the process with which the carrier node changes its direction, which is Poisson by definition, and the process with which the nodes inside the FR of the carrier node become eligible, which will also be showed to be Poisson (see Proposition 4).

The conclusion is that the random process $\widetilde{\Theta}(t)$ describing the direction of travel of the packet at time t, is a continuous-time Markov chain in the

state space $S = \{\theta_i\}_{i=1,2,\dots,N}$.

4.3.2 Limiting Distributions

This section is about how to derive the limiting distributions for the CTMC and for its Embedded Markov Chain (EMC), which will be used to calculate the metrics presented in Section 4.2.3. The existence and uniqueness of the limiting distributions will first be proved. through its index i, only for the rest of this section.

A sufficient condition for a CTMC with state space I to have a unique limiting distribution is [84]:

(a) The chain is *irreducible*, i.e., all the states communicate with each other, which means that starting at state i, the probability to visit state j at some time in the future is not null, $\forall i, j \in I$.

(b) The chain is *positive recurrent*. This happens when starting at state i, the mean value of the time needed to return at state i (mean return time) is finite, $\forall i \in I$.

When both conditions a) and b) are satisfied, the chain is said to be *ergodic*.

In our case, the Markov chain is ergodic. Indeed, the fact that sooner or later the carrier node will change direction, ensures that all the states communicate with each other. This, along with the fact that the state-space is finite, makes the mean return time finite [84, Corollary 4.2]. Therefore, the limiting distribution $\mathbf{\Pi} = [\pi_1, \pi_2, \dots, \pi_N]$ exists and is unique. π_i gives the probability that the CTMC is in state θ_i for $t \to \infty$; this probability is independent of the initial state. Equivalently, π_i represents the long-run proportion of time the chain is in state i.

The limiting distribution can be found by solving the global balance equations, which state that the rate at which the system leaves state i must be equal to the rate at which the system enters state i, $\forall i \in I$:

$$\begin{cases} q_i \pi_i = \sum_{j \neq i} q_{ji} \pi_j, & \forall i \in I, \\ \sum_i \pi_i = 1, \end{cases} \qquad (4.3.1)$$

where q_i is the rate at which the system exits from state i and q_{ji} is the rate at which the system, when in state j, makes transition to state i.

The first equation in (4.3.1) can be rewritten as

$$\sum_{j \neq i} \pi_j q_{ji} - \pi_i q_i = 0 \Leftrightarrow \sum_j \pi_j \widetilde{q}_{ji} = 0, \quad \forall i \in I,$$

where

$$\widetilde{q}_{ji} = \begin{cases} q_{ji}, & \text{if } j \neq i, \\ -q_j, & \text{if } j = i. \end{cases}$$

Note that $q_j = \sum_{i \neq j} q_{ji}$. Equations (4.3.1) can now be written in matrix form:

$$\begin{cases} \mathbf{\Pi Q} = 0, \\ |\mathbf{\Pi}| = 1, \end{cases} \qquad (4.3.2)$$

where $|\cdot|$ is the 1-norm and $\mathbf{Q}$ is the *generator matrix* defined as:

$$\mathbf{Q} = \begin{bmatrix} -q_1 & q_{12} & \cdots & q_{1N} \\ \vdots & \vdots & \ddots & \vdots \\ q_{N1} & q_{N2} & \cdots & -q_N \end{bmatrix}. \qquad (4.3.3)$$

Equation (4.3.2) shows that the limiting distribution can be found by solving a system of linear equations.

The EMC is a discrete-time Markov chain composed of the sequence of states visited by the CTMC when the amount of time spent in each state is ignored [84]. The process $\widetilde{\Theta}(n)$, $n \in \mathbb{Z}^+ = \{0, 1, 2, \dots\}$ is called the EMC associated to CTMC $\widetilde{\Theta}(t)$. $\widetilde{\Theta}(n)$ is defined on the same state space of $\widetilde{\Theta}(t)$ and is characterized by the transition matrix $\mathbf{P}$, whose elements p_{ij} represent the probability of going from state i to state j, $\forall i, j \in I$. The matrix $\mathbf{P}$ can be derived from the generator matrix $\mathbf{Q}$ in the following way:

$$
p_{ij} = \begin{cases} \frac{q_{ij}}{q_i}, & \text{if } i \neq j, \\ 0, & \text{if } i = j. \end{cases}
$$

It is easy to see that if the CTMC is ergodic, then the associated EMC is also ergodic. The ergodicity guarantees the existence and uniqueness of the limiting distribution of the EMC as well. Let $\boldsymbol{\Psi} = [\psi_1, \psi_2, \dots, \psi_N]$ denote the limiting distribution of $\widetilde{\Theta}(n)$. $\boldsymbol{\Psi}$ can be found as solution of the global balance equations:

$$
\begin{cases} \boldsymbol{\Psi}\mathbf{P} = \mathbf{P}, \\ |\boldsymbol{\Psi}| = 1. \end{cases} \tag{4.3.4}
$$

The probabilities ψ_i can be interpreted as the long run proportion of transitions that the discrete-time Markov chain $\widetilde{\Theta}(n)$ makes into state i.

By combining (4.3.2) and (4.3.4), it is possible to find the following relationship between ψ_i and π_i [85]:

$$
\psi_i = \frac{\pi_i q_i}{\sum_{j=1}^{N} \pi_j q_j}. \tag{4.3.5}
$$

Having the limiting distributions, it is possible to calculate the performance metrics defined in Section 4.2.3.

4.3.3 Performance Metrics

Having $\widetilde{\Theta}(t)$ modeled as a CTMC allows us to calculate the average speed due to physical transport using the ergodic theorem for positive recurrent CTMCs [86, Theorem 3.8.1]. Therefore (4.2.1) can be written as

$$\overline{V_p} = \lim_{t \to \infty} \left(\frac{1}{t} \int_0^t v_0 \cos \widetilde{\Theta}(s) \, \mathrm{d}s \right) = v_0 \sum_{\theta_i \in S} \pi_i \cos \theta_i. \qquad (4.3.6)$$

To calculate $\overline{V_w}$, (4.2.2) is rewritten as

$$\overline{V_w} = \lim_{K \to \infty} \frac{\frac{1}{K} \sum_{k=1}^K X_{w,k}}{\frac{1}{K} \sum_{k=1}^K \Delta_k}. \qquad (4.3.7)$$

The numerator can be written as

$$\sum_{k=1}^K \frac{X_{w,k}}{K} = \sum_{\theta_i \in S} \frac{k(\theta_i)}{K} \cdot \frac{\sum_{j=1}^{k(\theta_i)} X_{w,j}}{k(\theta_i)}.$$

The quantity $k(\theta_i)$ is the number of stages among stages $1, 2, \ldots, K$ for which the direction of travel of the packet is $\Theta = \theta_i$, therefore $K = \sum_{\theta_i \in S} k(\theta_i)$. By rewriting the denominator in the same way, and by letting K goes to infinity, it is

$$\overline{V_w} = \lim_{K \to \infty} \frac{\sum_{\theta_i \in S} \frac{k(\theta_i)}{K} \cdot \frac{\sum_{j=1}^{k(\theta_i)} X_{w,j}}{k(\theta_i)}}{\sum_{\theta_i \in S} \frac{k(\theta_i)}{K} \cdot \frac{\sum_{j=1}^{k(\theta_i)} \Delta_j}{k(\theta_i)}} = \frac{\sum_{\theta_i \in S} \psi_i \mathbb{E}[X_{w,j}; \Theta = \theta_i]}{\sum_{\theta_i \in S} \psi_i \mathbb{E}[\Delta_j; \Theta = \theta_i]}. \qquad (4.3.8)$$

The expected values result from the application of the Strong Law of Large Numbers, and $\psi_i = \frac{k(\theta_i)}{K}$ can be interpreted as the long-run proportion of transitions towards state θ_i, i.e., the limiting distribution of the EMC $\widetilde{\Theta}(n)$. $\mathbb{E}[\Delta_j; \Theta = \theta_i]$ is the expected duration of the stage j, given that the carrier is traveling along direction θ_i. $\mathbb{E}[X_{w,j}; \Theta = \theta_i]$ represents the expected value

of the progress towards the destination for the stage j, when the packet is transmitted from a node that is traveling along direction θ_i to another.

A simple way to calculate $\overline{C}$ is to calculate the average cost per unite of time similarly to (4.3.8) and, divide by $\overline{V}$. Therefore, by rewriting (4.2.4) and using the SLLN, as in (4.3.8), $\overline{C}$ becomes

$$\overline{C} = \frac{\sum_{\theta_i \in S} \psi_i \mathbb{E}[C_j; \Theta = \theta_i]}{\sum_{\theta_i \in S} \psi_i \mathbb{E}[\Delta_j; \Theta = \theta_i] \times \overline{V}}. \tag{4.3.9}$$

where $\mathbb{E}[C_j; \Theta = \theta_i]$ is the expected value of the transmission cost incurred in the stage j, given that the carrier node travels along direction θ_i.

To improve readability, from now on, the expected values that appear in (4.3.8) and (4.3.9) will be written as $\mathbb{E}[X_w|\theta_i]$, $\mathbb{E}[C|\theta_i]$ and $\mathbb{E}[\Delta|\theta_i]$.

This section showed that once the matrix $\mathbf{Q}$ is known for the routing rule that is under analysis, the limiting distributions $\mathbf{\Pi}$ and $\mathbf{\Psi}$ can be calculated, then the performance metrics $\overline{V}$ and $\overline{C}$ are derived using (4.3.6), (4.3.8) and (4.3.9).

4.3.4 Rates

To calculate the generator matrix $\mathbf{Q}$, four technical results need to be mentioned. Notice that they depend on the RR, here RR1 is considered, as it will be analyzed in details in the next sections.

Proposition 1. When the carrier node is traveling along direction θ, the counting process $\{N_{\chi;\theta}(t), t \geq 0\}$ of nodes arriving with a direction within $[\chi, \chi + \mathrm{d}\chi]$ at the boundary of its forwarding region is a Poisson process with rate $\gamma(\chi; \theta)\, \mathrm{d}\chi$ such that [79]

$$\gamma(\chi; \theta) = \beta \left| \sin\left(\frac{\chi - \theta}{2} \right) \right|, \qquad -\pi \leq \theta, \chi \leq \pi \tag{4.3.10}$$

Table 4.2: The interval $\mathcal{R}$ of Proposition 2 for the different subregions of $[-\pi, \pi] \times [-\pi, \pi]$.

Description	$\mathcal{R} = [\chi_A, \chi_B]$
$0 \leq \theta \leq \pi,\ \theta \leq \phi \leq \pi$	$[-\theta + 2\pi,\ \theta + 2\pi]$
$0 \leq \theta \leq \pi,\ 0 \leq \phi \leq \theta$	$[-\theta + 2\pi,\ 2\phi - \theta + 2\pi]$
$0 \leq \theta \leq \pi,\ \theta - \pi \leq \phi \leq 0$	$\emptyset$
$0 \leq \theta \leq \pi,\ -\pi \leq \phi \leq \theta - \pi$	$[2\phi - \theta + 4\pi,\ \theta + 2\pi]$
$-\pi \leq \theta \leq 0,\ \theta + \pi \leq \phi \leq \pi$	$[\theta,\ 2\phi - \theta - 2\pi]$
$-\pi \leq \theta \leq 0,\ 0 \leq \phi \leq \theta + \pi$	$\emptyset$
$-\pi \leq \theta \leq 0,\ \theta \leq \phi \leq 0$	$[2\phi - \theta,\ -\theta]$
$-\pi \leq \theta \leq 0,\ -\pi \leq \phi \leq \theta - \pi$	$[\theta,\ -\theta]$

where $\beta = \frac{2v_0 \lambda R}{\pi}$. β can be interpreted as the maximum value of the differential rate $\gamma(\chi; \theta)$, which is achieved for the nodes that are traveling along the opposite direction with respect to the carrier node, i.e., when $\chi = \theta \pm \pi$.

Proof. See [79]. $\qquad\square$

Proposition 2. When the carrier node is traveling along direction θ, the counting process $\{N_{\phi;\theta}(t),\ t \geq 0\}$ of nodes with a better direction of travel than the carrier node that enter the forwarding region at location $[\phi, \phi + d\phi]$, where $\phi \in [-\pi, \pi]$ is the angle formed between the positive x-axis and the line segment connecting the node and the boundary location, is a Poisson process with rate $\mu(\phi; \theta)\, d\phi$ such that:

$$\mu(\phi; \theta) = \frac{\beta}{4}\left[G(\chi_B) - G(\chi_A)\right], \quad \mathcal{R} = [\chi_A, \chi_B], \tag{4.3.11}$$

where $G(\chi) = \chi \cos(\phi - \theta) - \sin(\chi - \phi)$. The endpoints χ_A and χ_B of the interval $\mathcal{R}$ are defined according to the location on the (ϕ, θ) plane where the rate $\mu(\phi; \theta)$ is calculated; they are summarized in Table 4.2.

113

Proof. See Appendix 4.A □

Proposition 3. When the carrier node is traveling along direction θ, the counting process $\{N_\theta(t),\, t \geq 0\}$ of nodes with a better direction of travel than that of the carrier node that enter the forwarding region at any location of its boundary is a Poisson process with rate

$$\nu(\theta) = 2\beta \left[1 - \cos\theta\right]. \tag{4.3.12}$$

Proof. Equation (4.3.12) can be obtained either by integrating $\gamma(\chi;\theta)$, given in (4.3.10), or $\mu(\phi;\theta)$, given in (4.3.11). By integrating $\gamma(\chi;\theta)$, the result is

$$\nu(\theta) = \int_{-|\theta|}^{|\theta|} \gamma(\chi;\theta)\,\mathrm{d}\chi = 2\beta \left[1 - \cos\theta\right].$$

□

Proposition 4. The counting process $\{N_\sigma(t),\, t \geq 0\}$ of nodes that are inside the FR of the carrier node, and change their direction to a direction in $[\sigma, \sigma + \mathrm{d}\sigma]$, is a Poisson process with rate $\tau\,\mathrm{d}\sigma$ such that

$$\tau = \frac{1}{2}\lambda R^2 r_0. \tag{4.3.13}$$

Proof. The probability that a node inside the FR $\mathcal{F}$ changes its direction at time t, within the interval $[t_0, t_0 + \mathrm{d}t]$ can be calculated conditioned on N_p, i.e., the number of nodes inside $\mathcal{F}$, which is Poisson distributed with mean

114

$\lambda \pi R^2$. Therefore

$$
\begin{aligned}
P\{t_0 \leq t \leq t_0 + \mathrm{d}t\} &= \sum_{i=0}^{\infty} P\{t_0 \leq t \leq t_0 + \mathrm{d}t | N_p = i\} P\{N_p = i\} \\
&= \sum_{i=0}^{\infty} (ir_0 \, \mathrm{d}t) \frac{\exp(-\lambda \pi R^2)(\lambda \pi R^2)^i}{i!} \\
&= r_0 \, \mathrm{d}t \sum_{i=0}^{\infty} i \frac{\exp(-\lambda \pi R^2)(\lambda \pi R^2)^i}{i!} = r_0 \lambda \pi R^2 \, \mathrm{d}t.
\end{aligned}
$$

To calculate $P\{t_0 \leq t \leq t_0 + \mathrm{d}t | N_p = i\}$ in the second equation, the additive property of Poisson processes is used (i.e., the summation of independent Poisson processes is also a Poisson process, with a rate equal to the sum of the rates of the constituent Poisson processes [84]). In conclusion, the counting process of nodes changing their direction inside the FR is Poisson with rate $r_0 \lambda \pi R^2$.

Since each node selects its new direction of travel independently of the others and such that the new direction is uniformly distributed in $[-\pi, \pi]$, the probability to select a direction in $[\sigma, \sigma + \mathrm{d}\sigma]$ is $\frac{\mathrm{d}\sigma}{2\pi}$.

Using the independent thinning property of Poisson processes [83] (i.e., the process resulting from independently removing with probability α each arrival of an original Poisson process of density ρ is still a Poisson process with density $\alpha\rho$) leads to the result. □

4.4 Analysis of Routing Rule 1 without Multihop

The following simplifying approximation will be used throughout this section; however, it will be dropped in the next section in order to make a more realistic analysis.

Approximation 3. Whenever a node receives a packet or makes a turn, any node that is already in its FR is not considered by the routing rule. Eligible nodes that appears inside the FR are also neglected.

This approximation has two effects when the packet is transmitted: it limits the number of back-to-back wireless transmissions that can take place to one, and fixes the distance between transmitter and receiver to the deterministic value R.

Under this approximation the generator matrix element q_{ji} can be written as

$$q_{ji} = \begin{cases} \frac{r_0}{N}, & \text{if } |\theta_i| > |\theta_j|, \\ \frac{r_0}{N} + \frac{2\pi}{N}\gamma(\theta_i; \theta_j), & \text{if } |\theta_i| < |\theta_j|. \end{cases}$$

The case $|\theta_i| > |\theta_j|$ represents the fact that the direction can get worse only due to a change of direction of the carrier node. The other case corresponds to the case when the direction gets better due to changes in direction of the carrier nodes but also when the packet is transmitted to a node that is traveling with a better direction than the current one. Recall that $\frac{2\pi}{N}\gamma(\theta_i; \theta_j)$ is the rate at which the carrier node meets other nodes with direction θ_i, given that it is traveling with direction θ_j. Also note that Approximation 1 is used.

Now that the generator matrix $\mathbf{Q}$ is known, the limiting distributions $\mathbf{\Pi}$ and $\mathbf{\Psi}$ can be found numerically by solving the system (4.3.2) and using (4.3.5) respectively. Thus, the performance metrics can be calculated under Approximation 3.

The average speed due to physical transport $\overline{V_p}$ can be readily found with (4.3.6).

In order to calculate the average speed to wireless transmissions $\overline{V_w}$ and the average cost $\overline{C}$ through equations (4.3.8) and (4.3.9), the limiting dis-

tribution of the EMC $\widetilde{\Theta}(n)$ and the following conditional expectations are needed:

- $\mathbb{E}[X_w|\theta_i]$: the expected progress made by the packet due to wireless transmissions in the generic stage, when the carrier node travels along direction θ_i.

- $\mathbb{E}[\Delta|\theta_i]$: the expected duration of the generic stage when the carrier node travels along direction θ_i.

- $\mathbb{E}[C|\theta_i]$: the expected cost incurred in the generic stage when the carrier node travels along direction θ_i.

To calculate $\mathbb{E}[X_w|\theta_i]$ observe that under Approximation 3 the distance between transmitter and receiver is always R, therefore the average is taken over Φ only, i.e., the RV representing the location at the border of the FR $\mathcal{F}$ where the receiver enters $\mathcal{F}$ of the carrier (see Fig.4.9 in Appendix 4.A). The density of Φ conditioned on the direction of travel being θ_i, is given by

$$f_\Phi(\phi|\theta_i) = \frac{\mu(\phi;\theta_i)}{\nu(\theta_i)}. \tag{4.4.1}$$

Another element that is needed is the probability that the current state θ_i of the CTMC will change due to wireless transmission, i.e., $P_{TX,i}$. It is

$$P_{TX,i} = \frac{\nu(\theta_i)}{q_i}. \tag{4.4.2}$$

To calculate (4.4.1) and (4.4.2) it is used the fact that the probability that the minimum of a number of exponential RVs is equal to one of them is equal to its rate over the sum of all rates [84]. Therefore,

$$\mathbb{E}[X_w|\theta_i] = \int_{-\pi}^{\pi} R\cos\phi \frac{\mu(\phi;\theta_i)}{\nu(\theta_i)} \frac{\nu(\theta_i)}{q_i} \,\mathrm{d}\phi = \int_{-\pi}^{\pi} R\cos\phi \frac{\mu(\phi;\theta_i)}{q_i} \,\mathrm{d}\phi.$$

The average stage duration is the inverse of the rate at which the chain exits from state θ_i. Therefore

$$\mathbb{E}[\Delta|\theta_i] = \frac{1}{q_i}. \tag{4.4.3}$$

The resulting expression for $\overline{V_w}$ is

$$\overline{V_w} = \frac{R \sum_{\theta_i \in S} \frac{\psi_i}{q_i} \int_{-\pi}^{\pi} \cos \phi \mu(\phi; \theta_i) \, \mathrm{d}\phi}{\sum_{i=1}^{N} \frac{\psi_i}{q_i}} = R \sum_{\theta_i \in S} \pi_i \int_{-\pi}^{\pi} \cos \phi \mu(\phi; \theta_i) \, \mathrm{d}\phi, \tag{4.4.4}$$

where the last expression is obtained by substituting (4.3.5) and exploiting the fact that $\sum_{i=1}^{N} \pi_i = 1$. The integral in (4.4.4) is calculated by looking at Fig. 4.10 in Appendix 4.A. It can be written as

$$\int_{-\pi}^{\pi} \cos \phi \, \mu(\phi; \theta_i) \, \mathrm{d}\phi = \begin{cases} \displaystyle\int_{-\pi}^{\theta_i - \pi} \cos \phi \mu_{C1}(\phi; \theta_i) \, \mathrm{d}\phi \\ \quad + \displaystyle\int_{0}^{\theta_i} \cos \phi \mu_{B1}(\phi; \theta_i) \, \mathrm{d}\phi \\ \quad + \displaystyle\int_{\theta_i}^{\pi} \cos \phi \mu_{A3}(\phi; \theta_i) \, \mathrm{d}\phi & \text{if } \theta_i > 0 \\ \displaystyle\int_{-\pi}^{\theta_i} \cos \phi \mu_{B3}(\phi; \theta_i) \, \mathrm{d}\phi \\ \quad + \displaystyle\int_{\theta_i}^{0} \cos \phi \mu_{A1}(\phi; \theta_i) \, \mathrm{d}\phi \\ \quad + \displaystyle\int_{\theta_i + \pi}^{\pi} \cos \phi \mu_{D1}(\phi; \theta_i) \, \mathrm{d}\phi & \text{if } \theta_i \leq 0. \end{cases} \tag{4.4.5}$$

The rates $\mu_{\mathrm{xy}}(\phi; \theta_i)$ are calculated using (4.A.4) from Appendix 4.A. The

following expressions hold:

$$\mu_{C1}(\phi; \theta_i) = \frac{v_0 \lambda R}{\pi} \left[(\theta_i - \phi - \pi) \cos(\phi - \theta_i) + \sin(\phi - \theta_i) \right],$$

$$\mu_{B1}(\phi; \theta_i) = \frac{v_0 \lambda R}{\pi} \left[\phi \cos(\phi - \theta_i) - \sin \phi \cos \theta_i \right],$$

$$\mu_{A3}(\phi; \theta_i) = \frac{v_0 \lambda R}{\pi} \left[\theta_i \cos(\phi - \theta_i) - \sin \theta_i \cos \phi \right],$$

$$\mu_{B3}(\phi; \theta_i) = \frac{v_0 \lambda R}{\pi} \left[-\theta_i \cos(\phi - \theta_i) + \sin \theta_i \cos \phi \right],$$

$$\mu_{A1}(\phi; \theta_i) = \frac{v_0 \lambda R}{\pi} \left[-\phi \cos(\phi - \theta_i) + \sin \phi \cos \theta_i \right],$$

$$\mu_{D1}(\phi; \theta_i) = \frac{v_0 \lambda R}{\pi} \left[(\phi - \theta_i - \pi) \cos(\phi - \theta_i) + \sin(\theta_i - \phi) \right].$$

Now the integral in (4.4.5) can be solved and plugged in (4.4.4):

$$\overline{V_w} = \frac{v_0 \lambda R^2}{2} \sum_{\theta_i \in S} \pi_i \, \mathrm{sgn}(\theta_i)(\theta_i \cos \theta_i - \sin \theta_i). \qquad (4.4.6)$$

Observe that $\frac{v_0 \lambda R^2}{2}$ and π_i are non-negative $\forall \theta_i \in S$, and the function $\mathrm{sgn}(\theta_i)(\theta_i \cos \theta_i - \sin \theta_i)$ is non-positive $\forall \theta_i \in S$, therefore $\overline{V_w} \leq 0$.

Finally, the average packet speed can be written as

$$\overline{V} = \overline{V_p} + \overline{V_w} = v_0 \sum_{\theta_i \in S} \pi_i \left[\cos(\theta_i) + \frac{\lambda R^2}{2} \mathrm{sgn}(\theta_i) \left(\theta_i \cos \theta_i - \sin \theta_i \right) \right].$$

The calculation of the expected cost $\mathbb{E}[C|\theta_i]$ is made easy by the fact that under Approximation 3 the number of hops is limited to 1 and the distance between transmitter and receiver is always R. Therefore

$$\mathbb{E}[C|\theta_i] = \frac{R^2 P_{TX,i}}{\overline{V}} = \frac{R^2 \nu(\theta_i)}{\overline{V} \cdot q_i}.$$

Finally, by substituting the expressions for ψ_i and $\nu(\theta_i)$, the average packet

cost is

$$\overline{C} = \frac{\sum_{i=1}^{N} \psi_i R^2 \frac{\nu(\theta_i)}{q_i}}{\overline{V} \cdot \sum_{i=1}^{N} \frac{\psi_i}{q_i}} = \frac{4v_0 \lambda R^3}{\overline{V} \cdot \pi} \sum_{i=1}^{N} \pi_i (1 - \cos \theta_i).$$

4.4.1 Numerical and Simulation Results

This section presents the results of the validation of the model with the simulations.

In the simulations nodes move on a torus according to the mobility model described in Section 4.2.1. Their initial positions are uniformly distributed on the torus and one packet is generated and assigned to one node at random. Each simulation run lasts enough to have an estimate of all the quantities of interest with a small margin of error.

In order to implement the approximation made in this section, the simulator forces the node that received a packet at time t_r to not transmit it again to one of its eligible neighbor at t_r. The packet can be transmitted only to a node that will appear at the boundary of $\mathcal{F}$ after time t_r. A similar rule is followed for a node that wants to transmit the packet after a turn.

Fig. 4.3 shows the limiting distribution $\mathbf{\Pi}$ for different values of β, where $\beta = \frac{2v_0 \lambda R}{\pi}$. Notice the good agreement between simulation and analysis, despite the fact that the simulator does not implement Approximation 2. This means that assuming the system to be Markovian does not introduce a significant error, at least for the parameters that have been considered.

Observe from the previous section that the limiting distributions depend on the model parameters v_0, λ and R, only through β. As β increases $\mathbf{\Pi}$ gets concentrated around direction $\Theta = 0$, which is the direction of the packet destination. This means that the packet spends most of the time in preferred directions which are close to the direction of the destination. This is because when β is large, the rate at which the carrier node encounters other nodes
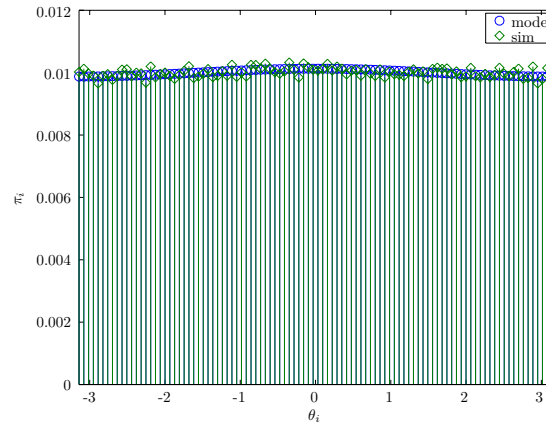
(a) $\beta = \frac{0.01}{\pi}$, $r_0 = 1$.
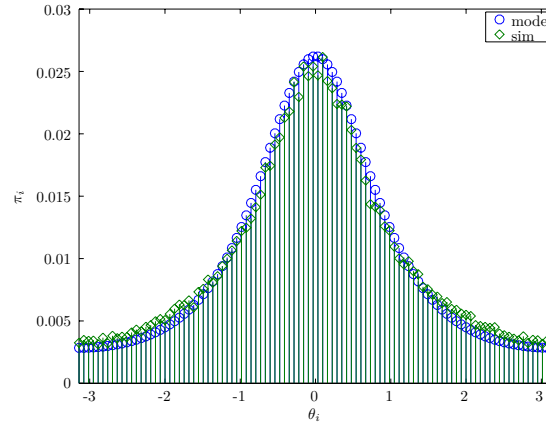
(b) $\beta = \frac{2}{\pi}$, $r_0 = 1$.
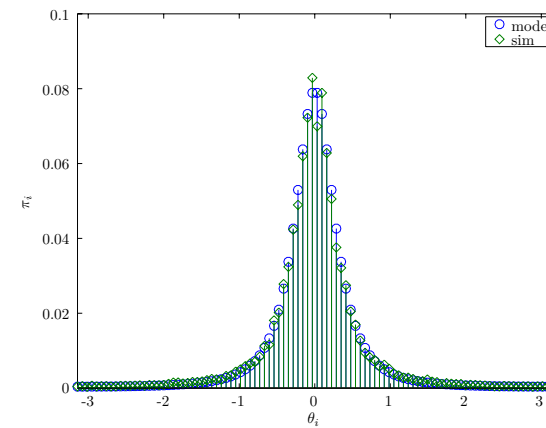
(c) $\beta = \frac{20}{\pi}$, $r_0 = 1$.

Figure 4.3: The limiting distribution $\mathbf{\Pi}$ for different value of β.

with a better direction is much larger than the turning rate. On the other hand, when $\beta \approx 0$, $\mathbf{\Pi}$ is almost flat, which means that there is no preferred direction for the packet. This is because the packet changes direction mostly because of the turns of its carrier nodes. Since the turning angle is uniformly distributed in $[-\pi, \pi]$, so is Θ.

(a) $\overline{V_p}$. $v_0 = 1$, $R = 1$.   (b) $\overline{V_w}$. $v_0 = 1$, $R = 1$.
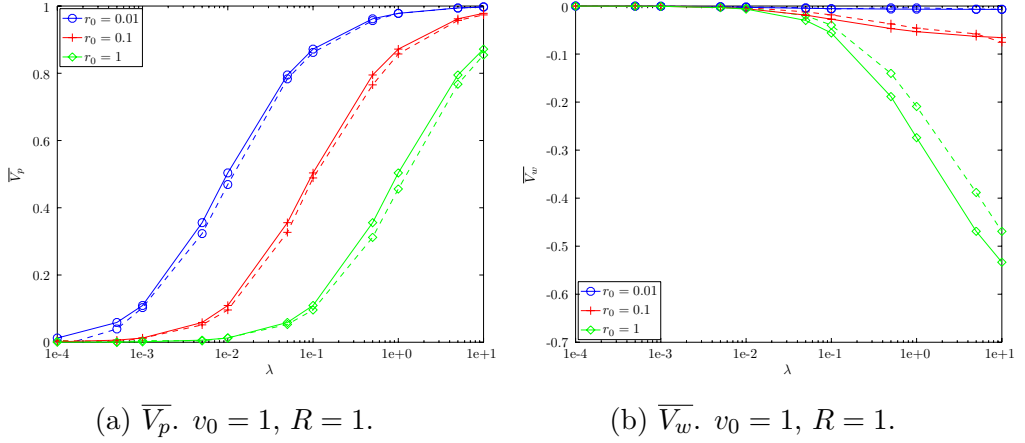
Figure 4.4: The average speeds $\overline{V_p}$ and $\overline{V_w}$ for different values of r_0. Analytic results are in solid lines, simulation results are in dashed lines.

The results for the performance metrics are now presentd. Fig. 4.4 shows the separate results for $\overline{V_p}$ and $\overline{V_w}$ as function of the density of nodes λ. The curves are obtained for different values of r_0; v_0 and R are both set to 1.

Fig. 4.4(a) shows that $\overline{V_p}$ is never negative, which means that the packet never goes backwards (on average) with respect to the destination when transported by the mobile nodes. In fact, when $\lambda \to 0$, as already said, the direction of the packet is uniformly distributed in $[-\pi, \pi]$: $\pi_i \approx \pi_0 = \frac{1}{2\pi}$, $\forall i$. Thus

$$\overline{V_p} \approx \pi_0 v_0 \sum_{\theta_i \in S} \cos \theta_i = 0.$$

Conversely, as $\lambda \to \infty$, the preferred directions are close to $\Theta = 0$, that is, $\pi_i \approx \delta(\theta_i)$, where $\delta(\theta_i)$ is the Kronecker delta function. Therefore, the value

of $\overline{V_p}$ is:

$$\overline{V_p} \approx v_0 \sum_{\theta_i \in S} \delta(\theta_i) \cos \theta_i = v_0.$$

The figure also shows that with the same value of λ, $\overline{V_p}$ increases as r_0 decreases. This is because a low turning rate makes the packet to stay on the best carrier for longer.

On the other hand, Fig. 4.4(b) shows that $\overline{V_w}$ is always negative. The reason for this is that, on average, the carrier node meets eligible nodes at a location on the boundary of the FR for which the progress X_w is negative.

The average packet speed $\overline{V}$ and the average packet cost $\overline{C}$ are showed together in Fig. 4.5 for different values of r_0. The cost grows faster for larger values of r_0 since a higher turning rate make the packet to "escape" from good directions more frequently; so more transmissions are required by the RR.

4.5 Analysis of Routing Rule 1 with Multihop

In this section the analysis is extended by taking into account multihop packet forwarding, and those packet transmissions that are triggered by a node that is inside the FR $\mathcal{F}$ of the carrier nodes and become eligible due to a change of direction. In this analysis only Approximations 1 and 2 hold.

At first, the elements q_{ji} of the generator matrix $\mathbf{Q}$ are calculated. For simplicity only non-negative values of the directions are considered, i.e., $\theta_j, \theta_i \geq 0$. This is not a limitation since the rates and the probabilities that are calculated are all symmetric with respect to direction 0. Therefore, the state index goes from 0 to $N/2$, and the corresponding direction goes
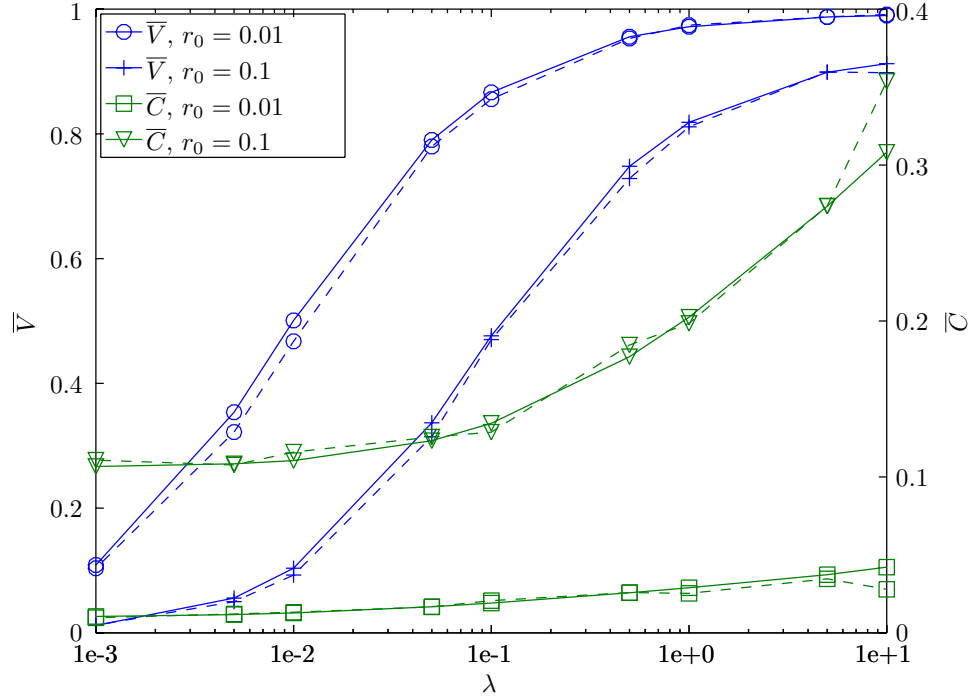
Figure 4.5: $\overline{V}$ and $\overline{C}$ for three values of r_0; $v_0 = 1$, $R = 1$. Analytic results are in solid lines, simulation results are in dashed lines.

from $\theta_0 = 0$ to $\theta_{\frac{N}{2}} = \pi$.

The elements of matrix $\mathbf{Q}$ can be written as

$$
q_{ji} = \begin{cases}
\frac{r_0}{N}\overline{P}_i, & \text{if } \theta_i > \theta_j, \\
\frac{r_0}{N}\overline{P}_i + \dfrac{\lambda\pi R^2 r_0}{N}\left(\overline{P}_i + \displaystyle\sum_{k=j-1}^{i+1} P_{ki}\right) \\
\qquad + \gamma(\theta_i;\theta_j)\overline{P}_i + \displaystyle\sum_{k=j-1}^{i+1}\gamma(\theta_k;\theta_j)P_{ki}\,, & \text{if } \theta_i < \theta_j.
\end{cases}
\tag{4.5.1}
$$

$\overline{P}_i = \exp(-\lambda R^2|\theta_i|)$ denotes the probability that there are no nodes in $\mathcal{F}$ with a direction of travel smaller that θ_i. P_{ki} is the probability for the packet to go from direction θ_k to direction θ_i in one or more hops instantaneously,

i.e., without stopping in any intermediate node. Each term of (4.5.1) is now explained. The case $\theta_i > \theta_j$ means that the packet goes to direction θ_i which is worse that its current direction θ_j. This happens only when the carrier makes a turn to θ_i and, after the restart of the node process (according to Approximation 2), there are no nodes with direction better then θ_i in $\mathcal{F}$. On the other hand, the term $\theta_i < \theta_j$ means that the packet goes to direction θ_i which is better than θ_j. This is triggered by three events, whose rates are the three terms of the second equation in (4.5.1):

1. The carrier makes a turn to direction θ_i and, after the restart of the node process, there are no nodes with direction better then θ_i in $\mathcal{F}$.

2. One of the nodes in $\mathcal{F}$ makes a turn to direction θ_k better than θ_j such that $\theta_i \leq \theta_k < \theta_j$, and the packet goes from θ_k to θ_i in one or more hops. The rate at which this event happens is equal to $\frac{\lambda \pi R^2 r_0}{N}$ (see Proposition 4). $\overline{P}_i$ is the probability that, given that the node that changes direction goes to $\theta_k = \theta_i$, no better nodes are in its FR, therefore the packet goes to θ_i in one hop. The summation term represents the probability that, given that the node that changes direction goes to $\theta_k \neq \theta_i$, the packet goes from θ_k to θ_i in more than one hop.

3. The carrier nodes meets an eligible node at the border of $\mathcal{F}$ and, either this node has direction θ_i and no better nodes are in its $\mathcal{F}$, or the encountered node has an intermediate direction θ_k such that $\theta_i < \theta_k < \theta_j$, such that the packet can go to θ_i in multihop.

The probability for the packet to go from direction θ_j to θ_i in one or more

hop instantaneously is equal to

$$
P_{ji} = \begin{cases} P_i + 2\sum_{k=i+1}^{j-1} P_{jk}P_{ki}, & \text{if } i < j, \\ 0, & \text{if } i \geq j. \end{cases}
\tag{4.5.2}
$$

P_i is the probability to go from θ_j to θ_i in one hop, that is, the probability that there is in $\mathcal{F}$ at least one node with direction θ_i, and no better nodes. Its expression is

$$
P_i = \left[1 - \exp\left(-\frac{\lambda \pi R^2}{N}\right)\right] \exp(-\lambda R^2 |\theta_i|).
$$

The summation term in (4.5.2) is the probability to go from θ_j to θ_i with more than one hops through intermediate nodes. The multiplicative factor 2 is needed to account for possible transitions to negative direction. Indeed, due to symmetry, the probability to go from θ_j to θ_k is equal to the probability to go from θ_j to $-\theta_k$. Observe that for $i \geq j$ it is $P_{ji} = 0$ since it is forbidden by the routing rule to go to a worse direction.

Having the matrix $\mathbf{Q}$ allows to derive the limiting distributions $\mathbf{\Pi}$ and $\mathbf{\Psi}$ which are needed to calculate the performance metrics $\overline{V}$ and $\overline{C}$.

First of all, notice that $\mathbb{E}[\Delta|\theta_i] = \frac{1}{q_i}$ since the duration of a stage, which coincides with the time spent in a state, is exponentially distributed.

The component of $\overline{V}$ due to physical transport, $\overline{V_p}$, can be calculated with (4.3.6) using the limiting distribution $\mathbf{\Pi}$.

To calculate $\overline{V_w}$ using (4.3.8), the limiting distribution $\mathbf{\Psi}$ of the EMC is needed, it can be found using (4.3.5) and $\mathbb{E}[X_w; \theta_i]$. Similarly, $\mathbb{E}[C|\theta_i]$ is needed to calculate $\overline{C}$ with (4.3.9). This two expected values are calculated in the next sections.

4.5.1 Calculation of $\mathbb{E}[C|\theta_i]$

To calculate $\mathbb{E}[C|\theta_i]$, i.e., the expected cost due to wireless transmissions for a generic stage given that the current carrier is traveling with direction θ_i, note that a stage ends when one of the following mutually exclusive events happens.

$\mathcal{A}$: The carrier changes its direction.

$\mathcal{B}$: The carrier meets an eligible node at the boundary of the FR.

$\mathcal{C}$: A neighbor of the carrier, i.e., a node inside the FR, becomes eligible.

When one of these event happens, there will be with some probability a multihop packet forwarding, at the end of which the stage ends. The expected cost for that packet forwarding, i.e., $\mathbb{E}[C|\theta_i]$, is now calculated.

Using the law of total expectation, $\mathbb{E}[C|\theta_i]$ can be written as

$$\mathbb{E}[C|\theta_i] = \mathbb{E}[C|\mathcal{A}, \theta_i]P(\mathcal{A}|\theta_i) + \mathbb{E}[C|\mathcal{B}, \theta_i]P(\mathcal{B}|\theta_i) + \mathbb{E}[C|\mathcal{C}, \theta_i]P(\mathcal{C}|\theta_i).$$

Although the methodology presented here is valid for any routing rule, the calculations that follow are done for RR1.

The following proposition will be used throughout this section.

Proposition 5. The expected cost of a multihop packet forwarding starting at a node with direction χ_i, given that given that Approximation 2, is equal to

$$\mathbb{E}[C_M|\chi_i] = \begin{cases} 0, & \text{if } i = 0, \\ cP_0, & \text{if } i = 1, \\ cP_0 + 2\sum_{j=1}^{i-1} \left(c + \mathbb{E}[C_M|\chi_j]\right) P_j, & \text{if } i > 1. \end{cases} \quad (4.5.3)$$

The term P_j, $j = 0, 1, \ldots, \lceil \frac{N}{2} \rceil$ is the probability to go immediately from χ_i to χ_j, $i > j$, in one hop; it is the probability that there is in $\mathcal{F}$ at least one node with direction χ_i, and no with direction smaller than χ_i in absolute value. Its expression is

$$P_j = \left[1 - \exp\left(-\frac{\lambda \pi R^2}{N} \right) \right] \exp(-\lambda R^2 |\chi_j|).$$

The quantity c is the expected cost of a transmission from the carrier to an eligible node uniformly distributed in $\mathcal{F}$, and its expression is

$$c = \frac{1}{\pi R^2} \int_{-\pi}^{\pi} \int_0^R r^2 r \, \mathrm{d}r \, \mathrm{d}\xi = \frac{R^2}{2}. \tag{4.5.4}$$

Calculations for event $\mathcal{A}$

The conditional probability $P(\mathcal{A}|\theta_i)$ can be calculated as the ratio between the rate at which event $\mathcal{A}$ happens and the rate at which the stages end, conditional on θ_i. This can be done because the events happen according to Poisson processes [84]. Therefore $P(\mathcal{A}|\theta_i) = \frac{r_0}{q_i}$. The rate r_0 is the turning rate, while the rate at which the stages end is q_i, which results from the Markov analysis.

In calculating the expected value of the cost conditional on event $\mathcal{A}$ and direction θ_i notice that there will be a non-zero cost only if the carrier turns to a direction ω_k such that $|\omega_k| > |\theta_i|$; since if $|\omega_k| < |\theta_i|$, there will be no eligible nodes in the FR of the carrier, thus no cost. Using the law of total

expectation recursively yields to

$$
\begin{aligned}
\mathbb{E}[C|\mathcal{A}, \theta_i] &= \sum_{|\omega_k|>|\theta_i|} \mathbb{E}[C|\omega_k, \mathcal{A}, \theta_i] P(\omega_k|\mathcal{A}, \theta_i) \\
&= \sum_{|\omega_k|>|\theta_i|} \sum_{|\theta_i|\le|\chi_j|<|\omega_k|} (c + \mathbb{E}[C|\chi_j, \omega_k, \mathcal{A}, \theta_i]) \\
&\quad \times P(\chi_j|\omega_k, \mathcal{A}, \theta_i) P(\omega_k|\mathcal{A}, \theta_i) \\
&\simeq \sum_{|\omega_k|>|\theta_i|} \sum_{|\theta_i|\le|\chi_j|<|\omega_k|} (c + \mathbb{E}[C_M|\chi_j]) \, P(\chi_j|\omega_k, \mathcal{A}, \theta_i) \\
&\quad \times P(\omega_k|\mathcal{A}, \theta_i)
\end{aligned}
$$

The approximation comes from the fact that when an eligible node receives the packet, the random process describing the position of nodes is restarted so that Proposition 5 applies. The term c is the average cost of the first transmission from the current carrier to the first relay, and its value is given by (4.5.4). The probability that the carrier turns to direction ω_k is uniformly and independently distributed, hence $P(\omega_k|\mathcal{A}, \theta_i|) = \frac{1}{N}$, where N is the number of discrete directions. Finally, the probability that the carrier finds an eligible node with direction χ_j, conditional on the new direction ω_j, θ_i and on the event $\mathcal{A}$, equals

$$
P(\chi_j|\omega_k, \mathcal{A}, \theta_i) = \left[1 - \exp\left(-\lambda R^2(\pi - |\theta_i|)\right)\right] \exp\left(-\lambda R^2(|\chi_j| - |\theta_i|)\right).
$$

The first multiplicative factor is the probability that there is in the FR a node with direction χ_j, given that the FR is empty of nodes with direction better than θ_i, as consequence of RR1; the second factor is the probability that in the FR there are no nodes with direction better than χ_j; in case there are, the packet will be transmit to one of them.

Calculations for event $\mathcal{B}$

The probability that the current stage ends because an eligible node is met at the border of the FR, conditional on the carrier direction being θ_i is $P(\mathcal{B}|\theta_i) = \frac{\nu(\theta_i)}{q_i}$. The term $\nu(\theta_i)$ is the rate at which eligible nodes enter the FR of a carrier traveling along direction θ_i, its expression is given by Proposition3.

When the carrier meets an eligible node with direction χ_j at the border of its FR, the cost of the first transmission is fixed to R^2. Once an eligible node receives the packet it assumed that the process describing the position of nodes restarts, therefore the expected cost for the next hops is given by Proposition 5. Therefore,

$$\mathbb{E}[C|\mathcal{B}, \theta_i] = R^2 + \sum_{|\chi_j|<|\theta_i|} \mathbb{E}[C_M|\chi_j] P(\chi_j|\mathcal{B}, \theta_i).$$

The probability that the eligible has direction χ_j, is given by

$$P(\chi_j|\mathcal{B}, \theta_i) = \frac{\gamma(\chi_j; \theta_i)}{\nu(\theta_i)} = \frac{\left|\sin\left(\frac{\chi_j - \theta_i}{2}\right)\right|}{2(1 - \cos\theta_i)}. \tag{4.5.5}$$

The expression for $\gamma(\chi_j; \theta_i)$, i.e., the rate at which the carrier meet a node with direction χ_j, given that it is traveling with direction θ_i, is given in [87].

Calculations for event $\mathcal{C}$

Similarly to the previous cases, the probability $P(\mathcal{C}|\theta_i)$ is calculated as the ratio between the rate at which event $\mathcal{B}$ happens and the rate at which stages end, conditional on θ_i. To calculate the first mentioned rate the definition of Poisson process is used. It states that the probability that the event happens

in the time interval $[t, t + \mathrm{d}t]$, is equal to its rate multiplied by $\mathrm{d}t$:

$$P\left(\mathcal{C}|\theta_i, [t, t + \mathrm{d}t]\right) = \pi R^2 \lambda \frac{\pi - |\theta_i|}{\pi} \cdot r_0 \cdot \frac{|\theta_i|}{\pi} \cdot \mathrm{d}t.$$

The first multiplicative factor is the average number of nodes in the FR of a node with direction θ_i when RR1 is used, the second term is the turning rate, therefore the product of the two is the rate at which the carrier sees its neighbors changing direction; the third term is the probability that the neighbor that changed direction becomes eligible, that is, its new direction χ_j is such that $|\chi_j| < |\theta_i|$. Finally,

$$P\left(\mathcal{C}|\theta_i\right) = \frac{r_0 R^2 \lambda (\pi - |\theta_i|)|\theta_i|}{\pi q_i}.$$

The expected cost related to event $\mathcal{C}$ is calculated as

$$\mathbb{E}[C|\mathcal{C}, \theta_i] = \sum_{|\chi_j| < |\theta_i|} \left(c + \mathbb{E}[C_M|\chi_j]\right) P(\chi_j|\mathcal{C}, \theta_i).$$

Also in this case, it is assumed the process describing the location of nodes restarts when an eligible node receives the packet, therefore Proposition 5 applies. The probability that the nodes that becomes eligible turns to direction χ_j conditional of event $\mathcal{C}$ and on the direction of the carrier θ_i, is

$$P(\chi_j|\mathcal{C}, \theta_i) = \frac{2\pi/N}{2|\theta_i|} = \frac{\pi}{N|\theta_i|}.$$

4.5.2   Calculation of $\mathbb{E}[X_w|\theta_i]$

In this section the expected progress due to wireless transmissions for a generic stage is calculated conditional on the direction of the carrier θ_i.

Notice that when RR1 is employed and it is assumed that the process

describing the position of nodes is restarted every time a node receives a packet, the expected progress due to multihop is zero, because the eligible nodes is uniformly distributed within the FR which is a circular disk. This is formalized by the following Proposition.

Proposition 6. The expected progress towards the destination of a multihop packet forwarding starting at a node with direction χ_i, given that Approximation 2 applies, is equal to

$$\mathbb{E}[X_{w,M}|\chi_i] = \begin{cases} 0, & \text{if } i = 0, \\ \alpha P_0, & \text{if } i = 1, \\ 2\sum_{j=1}^{i-1}\left(\alpha + \mathbb{E}[X_{w,M}|\chi_j]\right)P_j + \alpha P_0, & \text{if } i > 1. \end{cases} \quad (4.5.6)$$

The quantity α is the expected progress due to a transmission from the carrier to an eligible node uniformly distributed in $\mathcal{F}$. Due to symmetry it is $\alpha = 0$,

$$\alpha = \frac{1}{\pi R^2} \int_{-\pi}^{\pi} \int_0^R r\cos\xi\, r\, \mathrm{d}r\, \mathrm{d}\xi = 0, \quad (4.5.7)$$

which makes $\mathbb{E}[X_{w,M}|\chi_i] = 0$, $\forall i$.

As in Section 4.5.1, $\mathbb{E}[X_w|\theta_i]$ is calculated with the law of total expectation.

$$\mathbb{E}[X_w|\theta_i] = \mathbb{E}[X_w|\mathcal{A},\theta_i]P(\mathcal{A}|\theta_i) + \mathbb{E}[X_w|\mathcal{B},\theta_i]P(\mathcal{B}|\theta_i) + \mathbb{E}[X_w|\mathcal{C},\theta_i]P(\mathcal{C}|\theta_i).$$

Calculations for event $\mathcal{A}$

Using the same argument of Section 4.5.1 and Proposition 6, it is

$$\mathbb{E}[X_w|\mathcal{A}, \theta_i] = \sum_{|\omega_k|>|\theta_i|} \sum_{|\theta_i|\leq|\chi_j|<|\omega_k|} (\alpha + \mathbb{E}[X_{w,M}|\chi_j])$$
$$\cdot P(\chi_j|\omega_k, \mathcal{A}, \theta_i)\, P(\omega_k|\mathcal{A}, \theta_i) = 0.$$

Therefore it is

$$\mathbb{E}[X_w|\mathcal{A}, \theta_i] = 0.$$

Calculations for event $\mathcal{B}$

In this case:

$$\mathbb{E}[X_w|\mathcal{B}, \theta_i] = \mathbb{E}[X_{w,S}|\mathcal{B}, \theta_i] + \sum_{|\chi_j|<|\theta_i|} \mathbb{E}[X_{w,M}|\chi_j]P(\chi_j|\mathcal{B}, \theta_i) = \mathbb{E}[X_{w,S}|\mathcal{B}, \theta_i].$$

The term $\mathbb{E}[X_{w,S}|\mathcal{B}, \theta_i]$ is the expected value of the progress from a carrier with direction θ_i to an eligible node that appears at the border of its FR. It is calculated as

$$\mathbb{E}[X_{w,S}|\mathcal{B}, \theta_i] = \int_{-\pi}^{\pi} R\cos\phi f_\Phi(\phi)\, \mathrm{d}\phi$$
$$= \int_{-\pi}^{\pi} R\cos\phi \frac{\mu(\phi; \theta_i)}{\nu(\theta_i)}\, \mathrm{d}\phi. \tag{4.5.8}$$

The term $f_\Phi(\phi)$ is the PDF of the RV Φ representing the location of the eligible node on the border of $\mathcal{F}$, i.e., the angle formed between the x-axis and the line segment connecting the node and the carrier. The rate $\mu(\phi; \theta_i)$ is the rate at which eligible nodes enter the FR at location ϕ of a carrier traveling with direction θ_i, its expression is given in Appendix 4.A. The numerical results show that $\mathbb{E}[X_{w,S}|\mathcal{B}, \theta_i] < 0 \,\forall i$, since eligible nodes are met

only on the back of the FR, that is for $|\phi| > \frac{\pi}{2}$.

Calculations for event $\mathcal{C}$

Also in this case, thanks to Proposition 6, it is

$$\mathbb{E}[X_w|\mathcal{C}, \theta_i] = \sum_{|\chi_j|>|\theta_i|} \left(\alpha + \mathbb{E}[X_{w,M}|\chi_j]\right) P(\chi_j|\mathcal{C}, \theta_i) = 0.$$

Therefore

$$\mathbb{E}[X_w|\mathcal{C}, \theta_i] = 0.$$

All the elements to calculate $\overline{V}$ and $\overline{C}$ with (4.3.6,4.3.8,4.3.9) are now available.

4.5.3 Numerical and Simulation Results

The results of the numerical analysis and simulations are reported in this section.

Fig. 4.6 shows the expected packet speed $\overline{V}$ and expected packet cost $\overline{C}$ as function of the transmission range R, for two values of the node speed v_0.

The simulations and the model show that for $R > 8$ the packet is traveling on the perfect direction for most of the time, therefore the cost is mainly due to transmissions that take place after the carrier makes a turn, i.e., stages ends due to event $\mathcal{A}$ almost always. To prove this, consider $R = 55$ and $v_0 = 5$; if it is assumed that the cost is due to event $\mathcal{A}$ only, it is

$$\overline{C}_{R=55} = \frac{r_0 R^2}{2\overline{V}_{R=55}} \left[1 - \exp\left(-\pi R^2 \lambda \frac{1}{N}\right)\right] = 30.2,$$

as confirmed by Fig.4.6. The term inside brackets is the probability that once the carrier has changed direction it will find another node in its FR traveling
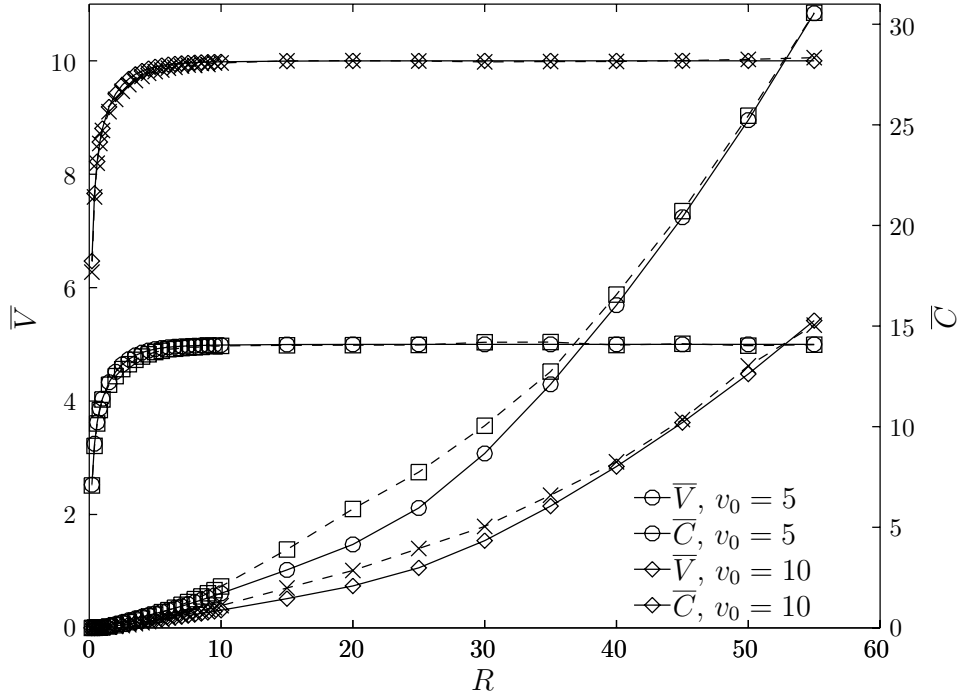
Figure 4.6: Expected packet speed and cost for two values of node speed v_0; $\lambda = 0.1$, $r_0 = 0.1$, $N = 101$. Simulation results are in dashed line.

with the perfect direction, therefore there will be only one transmission, whose expected cost is $R^2/2$.

From the mismatch between the analysis and simulation, it can be seen that the model is more conservative than the simulation. This is due to the fact that the process describing the nodes location is restarted whenever a packet is received. By restarting the process the average number of transmissions is lower, thus the average cost is smaller as well. This is because, when the process is restarted, the new carrier "forgets" about the fact that the intersection between the FRs of the former carrier and the new one is empty of nodes with direction better that the direction of the former carrier; so in average the new carrier has a larger area full of possibly eligible nodes. This

135
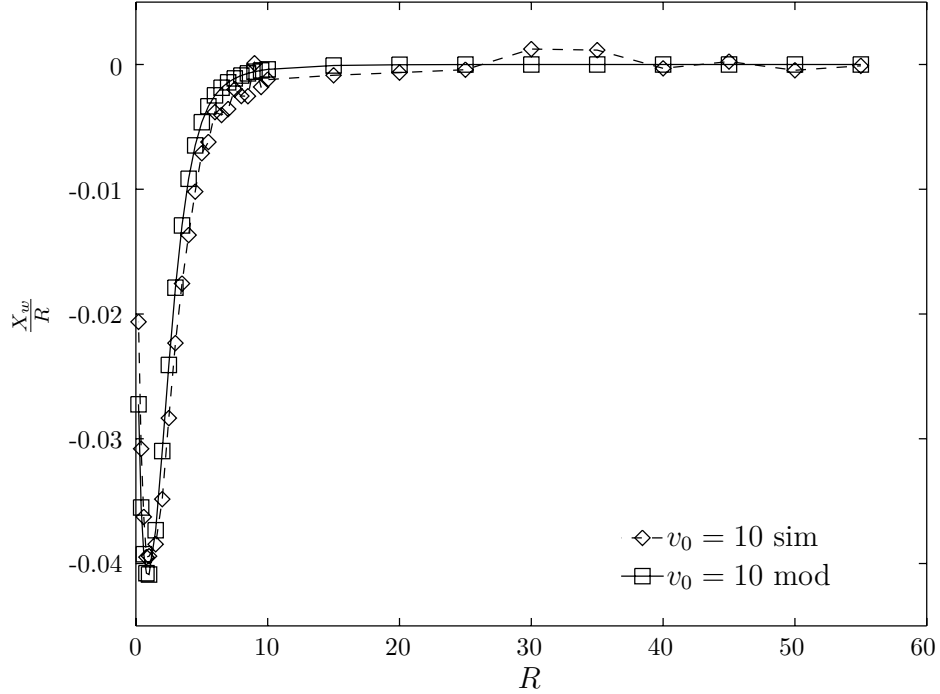
Figure 4.7: $\mathbb{E}[X_w]$ normalized with respect to R; $v_0 = 10$, $\lambda = 0.1$, $r_0 = 0.1$, $N = 101$.

mismatch disappears when R becomes larger enough such that the packet is traveling almost always along the perfect direction, in this case the carrier will transmit the packet in one hop only towards a node inside its FR.

Fig. 4.6 shows that for $R > 8$ the packet speed does not improve, which however is limited by the node speed v_0; as already said this is because for such values of R the packet is almost always traveling on the node with perfect direction and the contribution to the speed due to wireless transmission is on average zero, when event $\mathcal{A}$ dominates.

It is interesting to see the only contribution to the packet speed due to wireless transmissions, that is $\mathbb{E}[X_{w,S}|\mathcal{B}, \theta_i]$ given by (4.5.8). Fig. 4.7 shows that when R increases from 0, the number of transmissions towards eligible
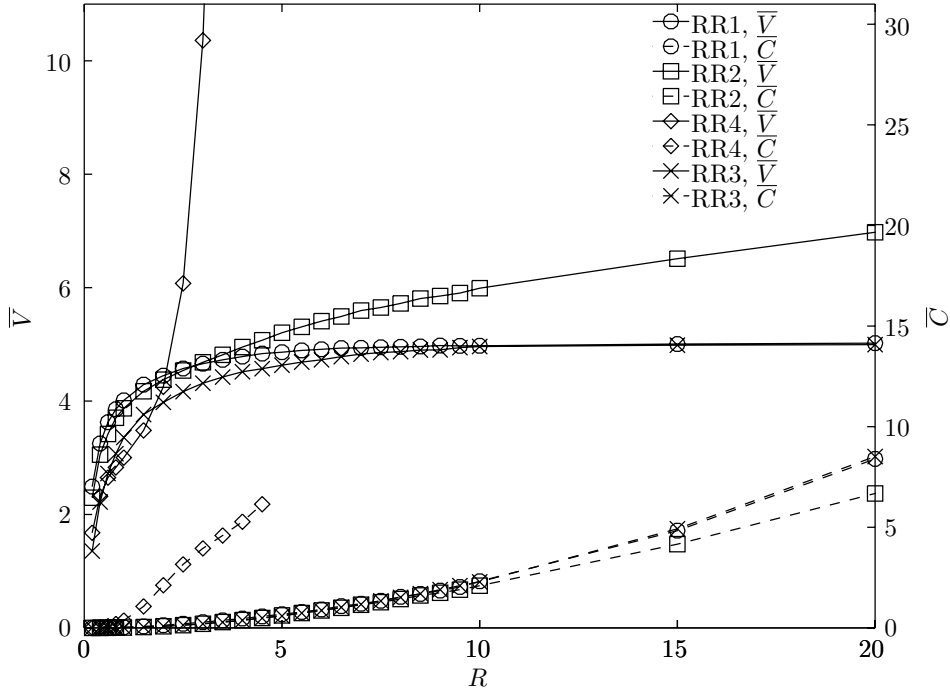
Figure 4.8: Simulated performance metrics $\overline{V}$ and $\overline{C}$ for the four RRs presented in Section 4.2.4. $v_0 = 5$, $\lambda = 0.1$, $r_0 = 0.1$, $\tau = \pi/8$ in RR3.

nodes met on the border of the FR increases as well; this results in an average negative progress since eligible nodes always hit the back of the FR region. After a certain value of R the packet is traveling mostly on directions very close to the perfect one, thus the rate of transmissions towards eligible node met on the border of the FR decreases, until it becomes zero for $R > 10$.

4.6 Other Routing Rules

This section contains the simulation results for the other RRs presented in Section 4.2.4.

One of the conclusions that can be drawn from the analysis of RR1 per-

formed in the previous sections, is that RR1 has the drawback that eligible nodes always hit the FR of the carrier on the opposite side with respect to the destination; as a result, the packet will go backwards. Moreover, when the packet is transmitted to eligible nodes inside the FR, the average progress is 0 (see (4.5.7)). To overcome this limitation, RR2 adds the condition that a node to be eligible shall be located in front of the current carrier. Fig. 4.8 shows, as expected, that RR2 has overall improved performance with respect to RR1. When R is smaller than 3, however, RR1 is slightly better; in this case, in fact, there will be on average more transmissions, as a consequence the packet will reach the perfect direction sooner. When R is bigger that 3, the expected progress due to transmissions towards eligible nodes that are inside the FR is positive and increase linearly with R, while it is null for RR1. This makes $\overline{V}$ a linear function of R; moreover, since RR2 avoids useless transmissions, also $\overline{C}$ is improved with respect to $RR1$.

RR3 is similar to RR1, it has the additional constraint that a node, to be eligible, must be traveling on a direction that is in absolute value smaller than a threshold τ. This has the advantage of reducing the cost on the expenses of the speed; however there is no significant improvement with respect to RR1. Once the transmission range becomes large enough, the probability to have an eligible node traveling on the perfect direction, when needed, is close to one. This nullify the effect of the threshold, hence, RR1 and RR3 behave the same.

One rule that differs significantly from the others is RR4. In this case, for a node to be eligible is enough to be in front of the carrier, that is the directions of travel are not accounted for. As expected, as the transmission range becomes larger that a certain value (4 in case of Fig. 4.8), both $\overline{V}$ and $\overline{C}$ explodes to infinite, since at any moment there will be an eligible node

in front of the carrier with probability 1. Since transmissions would never stop, the simulations could not proceed further than $R = 5$. The value of the transmission range for which $\overline{V}$ and $\overline{C}$ goes to infinite can be found by calculating the value of R for which the probability to have a node in the semicircular disk in front of the carrier is close to 1. For example, by setting this probability to 0.99 and using the parameters of Fig 4.8, it is

$$R_{99\%} = \sqrt{-\frac{2}{\lambda\pi}\log(1 - 0.99)} = 5.41,$$

which is in line with the result reported in Fig 4.8.

4.7   Conclusions

This chapter considers the problem of modeling the performance of routing in a DTN where mobile nodes move according to a RWP mobility model. A mathematical framework based on stochastic geometry and Markov chains theory is developed to model the average speed with which the packet moves toward the destination, and the average cost. In Section 4.5 the framework is used to model one of the four RRs proposed in Section 4.2.4; simulation results confirm the validity of the model. Although only one RR is studied analytically, it is straightforward to use the framework to evaluate the performance of other RRs.

4.A   Calculation of rate $\mu(\phi; \theta)$

The approach used to calculate the incidence rate for RR1 $\mu(\phi; \theta)\,\mathrm{d}\phi$ is the same as the one adopted in [87]; moreover, some results contained therein will be reused. Notice that the directions θ, ϕ and χ involved in the calculation,

are assumed to be continuous RVs.

The following notation will be used:

- $\theta \in [-\pi, \pi]$: direction of travel of the carrier node.

- $\phi \in [-\pi, \pi]$: a location on the boundary of the forwarding region of the carrier node. The forwarding region is a cicular disk of radius R centered at the carrier node.

- $\chi \in [\theta, \theta + 2\pi]$: the direction of travel of a node that that enters the forwarding region of the carrier node. The interval of definition of χ is for reasons of mathematical convenience (see [87]).

- $\gamma(\chi, \phi; \theta)\, d\chi\, d\phi$: the rate at which nodes with direction of travel in $[\chi, \chi + d\chi]$ enter the forwarding region of the carrier node at location $[\phi, \phi + d\phi]$, given that the carrier node travels with direction θ.

- $\mu(\phi; \theta)\, d\phi$: the rate at which nodes with a direction of travel better than the one of the carrier node, arrive at the boundary of the forwarding region of the latter, at location $[\phi, \phi + d\phi]$, given that the carrier node travels with direction θ. Recall that, if a node is traveling with direction χ, its direction is better than direction θ if $-|\theta| < \chi < |\theta|$; the latter double inequality is called the routing condition.

The directions discussed so far are described graphically in Fig. 4.9. It is necessary to recall from [87], that the condition for which a node that travels with direction χ enters the forwarding region of a node that travels with direction θ at location $[\phi, \phi + d\phi]$ from the outside, is:

$$\phi + \frac{\pi}{2} \leq \frac{\chi + \theta + \pi}{2} + 2k\pi \leq \pi + \frac{3\pi}{2}, \quad k \in \mathbb{Z}. \qquad (4.A.1)$$
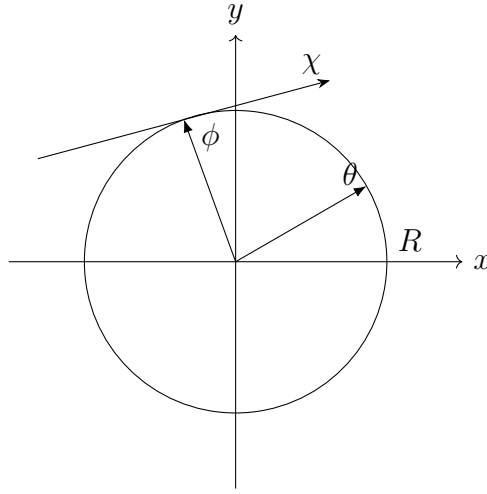
Figure 4.9: Illustration of the directions used in this section. The angles θ, ϕ and χ are taken with respect to the positive x-axis.

To calculate $\mu(\phi;\theta)$ is enough to integrate $\gamma(\chi,\phi;\theta)$:

$$
\mu(\phi;\theta) = \int_{\mathcal{R}} \gamma(\chi,\phi;\theta)\, \mathrm{d}\chi = \frac{v_0\lambda R}{2\pi} \int_{\mathcal{R}} \sin\left(\frac{\chi-\theta}{2}\right) \sin\left(\frac{\chi+\theta}{2} - \phi\right) \mathrm{d}\chi
$$

$$
= \frac{v_0\lambda R}{2\pi} \int_{\mathcal{R}} [\chi\cos(\phi-\theta) - \sin(\chi-\phi)]'\, \mathrm{d}\chi. \tag{4.A.2}
$$

The expression for $\gamma(\chi,\phi;\theta)$ is taken from [87, Eq. 2]. $\mathcal{R}$ is the set of values of $\chi \in [\theta, \theta+2\pi]$ for which $\gamma(\chi,\phi;\theta)$ is not zero. It is worth to mention that (4.A.1) is satisfied for a set of χ composed of periodic intervals of length 2π. Indeed, (4.A.1) can be written as

$$
2\phi - \theta - 4k\pi \leq \chi \leq 2\phi - \theta - 4k\pi + 2\pi, \quad k \in \mathbb{Z}. \tag{4.A.3}
$$

Thus, $\mathcal{R}$ can be found as the intersection of the set composed of the values of $\chi \in [\theta, \theta+2\pi]$ such that $-|\theta| < \chi < |\theta|$, with the periodic set defined in (4.A.3).

In order to find $\mathcal{R}$ we will take cases. Let χ_1 and χ_2 be the smallest and the

largest values, respectively, of $\chi \in [\theta, \theta + 2\pi]$ for which the nodes arrive at the location $[\phi, \phi + \mathrm{d}\phi]$ of the forwarding region from the outside. Observe that, since χ is defined within an interval of length 2π, for any value of ϕ there will be defined either χ_1 or χ_2, but not both of them. It is: $\chi_1 = 2\phi - \theta - 4k\pi$ and $\chi_2 = 2\phi - \theta - 4k\pi + 2\pi$. By applying the condition $\theta \leq \chi_1, \chi_2 \leq \theta + 2\pi$, the regions where χ_1 and χ_2 are defined on the (θ, ϕ) plane within the intervals of definition of θ and ϕ, i.e., $-\pi \leq \theta \leq \pi$, $-\pi \leq \phi \leq \pi$.

Consider χ_1, for $k = 0$ it is $\chi_1 = 2\phi - \theta$. Therefore, the region where χ_1 is defined for $k = 0$ is defined by the following inequalities:

$$\begin{cases} \theta \leq 2\phi - \theta \leq \theta + 2\pi \\ -\pi \leq \theta \leq \pi \\ -\pi \leq \phi \leq \pi \end{cases} \Leftrightarrow \begin{cases} \theta \leq \phi \leq \theta + \pi \\ -\pi \leq \theta \leq \pi \\ -\pi \leq \phi \leq \pi \end{cases}$$

The same can be done for $k = -1$, where is $\chi_1 = 2\phi - \theta + 4\pi$, in this case it is

$$\begin{cases} \theta \leq 2\phi - \theta + 4\pi \leq \theta + 2\pi \\ -\pi \leq \theta \leq \pi \\ -\pi \leq \phi \leq \pi \end{cases} \Leftrightarrow \begin{cases} -\pi \leq \phi \leq \theta - \pi \\ -\pi \leq \theta \leq \pi. \\ -\pi \leq \phi \leq \pi \end{cases}$$

For χ_2 and $k = 0$ it is $\chi_2 = 2\phi - \theta + 2\pi$, and the region where χ_2 is defined for $k = 0$ is defined by:

$$\begin{cases} \theta \leq 2\phi - \theta + 2\pi \leq \theta + 2\pi \\ -\pi \leq \theta \leq \pi \\ -\pi \leq \phi \leq \pi \end{cases} \Leftrightarrow \begin{cases} \theta - \pi \leq \phi \leq \theta \\ -\pi \leq \theta \leq \pi \\ -\pi \leq \phi \leq \pi \end{cases}$$

In the case of $k = 1$ it is $\chi_2 = 2\phi - \theta - 2\pi$, and χ_2 is defined in:

$$
\begin{cases}
\theta \leq 2\phi - \theta - 2\pi \leq \theta + 2\pi \\
-\pi \leq \theta \leq \pi \\
-\pi \leq \phi \leq \pi
\end{cases}
\Leftrightarrow
\begin{cases}
\theta + \pi \leq \phi \leq \pi \\
-\pi \leq \theta \leq \pi \\
-\pi \leq \phi \leq \pi.
\end{cases}
$$

The regions defined for other values of k are outside the domain $[-\pi, \pi] \times [-\pi, \pi]$.

Eight different subregions can be identified in the domain $[-\pi, \pi] \times [-\pi, \pi]$ where to find the boundaries of the interval $\mathcal{R}$. These subregions appears graphically in Fig. 4.10.

- **A3**: in this case is $\chi_1 = 2\phi - \theta$. $\mathcal{R}$ is composed of the values of $\chi \in [\theta, \theta + 2\pi]$ that satisfy the following inequalities:

$$
\begin{cases}
0 \leq \theta \leq \pi \\
\theta \leq \phi \leq \pi \\
-\theta + 2\pi < \chi < \theta + 2\pi
\end{cases}
\Rightarrow
\begin{cases}
0 \leq \theta \leq \pi \\
\theta \leq \chi_1 \leq -\theta + 2\pi \\
-\theta + 2\pi < \chi < \theta + 2\pi.
\end{cases}
$$

The first two double inequalities define the subregion A3, while the third is the routing condition when $0 \leq \theta \leq \pi$. At this point is important to remind that χ_1 is the smallest value of $\chi \in [\theta, \theta + 2\pi]$ for which the nodes arrive at the location $[\phi, \phi + d\phi]$ from the outside. Thus

$$
\mathcal{R} = [-\theta + 2\pi, \, \theta + 2\pi].
$$

- **B1**: in this case is $\chi_2 = 2\phi - \theta + 2\pi$. $\mathcal{R}$ is composed of the values of

$\chi \in [\theta, \theta + 2\pi]$ that satisfy the following inequalities:

$$\begin{cases} 0 \leq \theta \leq \pi \\ 0 \leq \phi \leq \theta \\ -\theta + 2\pi < \chi < \theta + 2\pi \end{cases} \Rightarrow \begin{cases} 0 \leq \theta \leq \pi \\ -\theta + 2\pi \leq \chi_2 \leq \theta + 2\pi \\ -\theta + 2\pi < \chi < \theta + 2\pi. \end{cases}$$

At this point is important to remind that χ_2 is the largest value of $\chi \in [\theta, \theta + 2\pi]$ for which the nodes arrive at the location $[\phi, \phi + \mathrm{d}\phi]$ from the outside. Thus

$$\mathcal{R} = [-\theta + 2\pi, \, \chi_2] = [-\theta + 2\pi, \, 2\phi - \theta + 2\pi].$$

- **B2**: in this case is $\chi_2 = 2\phi - \theta + 2\pi$. $\mathcal{R}$ is composed of the values of $\chi \in [\theta, \theta + 2\pi]$ that satisfy the following inequalities:

$$\begin{cases} 0 \leq \theta \leq \pi \\ \theta - \pi \leq \phi \leq 0 \\ -\theta + 2\pi < \chi < \theta + 2\pi \end{cases} \Rightarrow \begin{cases} 0 \leq \theta \leq \pi \\ \theta \leq \chi_2 \leq -\theta + 2\pi \\ -\theta + 2\pi < \chi < \theta + 2\pi. \end{cases}$$

Thus

$$\mathcal{R} = \emptyset.$$

- **C1**: in this case is $\chi_1 = 2\phi - \theta + 4\pi$. $\mathcal{R}$ is composed of the values of $\chi \in [\theta, \theta + 2\pi]$ that satisfy the following inequalities:

$$\begin{cases} 0 \leq \theta \leq \pi \\ -\pi \leq \phi \leq \theta - \pi \\ -\theta + 2\pi < \chi < \theta + 2\pi \end{cases} \Rightarrow \begin{cases} 0 \leq \theta \leq \pi \\ -\theta + 2\pi \leq \chi_1 \leq \theta + 2\pi \\ -\theta + 2\pi < \chi < \theta + 2\pi. \end{cases}$$

Thus

$$\mathcal{R} = [\chi_1, \, \theta + 2\pi] = [2\phi - \theta + 4\pi, \, \theta + 2\pi].$$

- **D1**: in this case is $\chi_2 = 2\phi - \theta - 2\pi$. $\mathcal{R}$ is composed of the values of $\chi \in [\theta, \theta + 2\pi]$ that satisfy the following inequalities:

$$\begin{cases} -\pi \le \theta \le 0 \\ \theta + \pi \le \phi \le \pi \\ \theta < \chi < -\theta \end{cases} \Rightarrow \begin{cases} -\pi \le \theta \le 0 \\ \theta \le \chi_2 \le -\theta \\ \theta < \chi < -\theta. \end{cases}$$

Note that the routing condition changes since negative values of θ are considered. In this case it is

$$\mathcal{R} = [\theta, \, \chi_2] = [\theta, \, 2\phi - \theta - 2\pi].$$

- **A2**: in this case is $\chi_1 = 2\phi - \theta$. $\mathcal{R}$ is composed of the values of $\chi \in [\theta, \theta + 2\pi]$ that satisfy the following inequalities:

$$\begin{cases} -\pi \le \theta \le 0 \\ 0 \le \phi \le \theta + \pi \\ \theta < \chi < -\theta \end{cases} \Rightarrow \begin{cases} -\pi \le \theta \le 0 \\ -\theta \le \chi_1 \le \theta + 2\pi \\ \theta < \chi < -\theta. \end{cases}$$

Thus

$$\mathcal{R} = \emptyset.$$

- **A1**: in this case is $\chi_1 = 2\phi - \theta$. $\mathcal{R}$ is composed of the values of

$\chi \in [\theta, \theta + 2\pi]$ that satisfy the following inequalities:

$$
\begin{cases}
-\pi \leq \theta \leq 0 \\
\theta \leq \phi \leq 0 \\
\theta < \chi < -\theta
\end{cases}
\Rightarrow
\begin{cases}
-\pi \leq \theta \leq 0 \\
\theta \leq \chi_1 \leq -\theta \\
\theta < \chi < -\theta.
\end{cases}
$$

Thus

$$
\mathcal{R} = [\chi_1, \, -\theta] = [2\phi - \theta, \, -\theta].
$$

- **B3**: in this case is $\chi_2 = 2\phi - \theta + 2\pi$. $\mathcal{R}$ is composed of the values of $\chi \in [\theta, \theta + 2\pi]$ that satisfy the following inequalities:

$$
\begin{cases}
-\pi \leq \theta \leq 0 \\
-\pi \leq \phi \leq \theta - \pi \\
\theta < \chi < -\theta
\end{cases}
\Rightarrow
\begin{cases}
-\pi \leq \theta \leq 0 \\
-\theta \leq \chi_2 \leq \theta \\
\theta < \chi < -\theta.
\end{cases}
$$

Thus

$$
\mathcal{R} = [\theta, \, -\theta].
$$

The intervals $\mathcal{R}$ and the boundaries of the corresponding subregions are summarized in Table 4.3.

It follows from (4.A.2) that

$$
\mu(\phi; \theta) = \frac{v_0 \lambda R}{2\pi}[G(\chi_B) - G(\chi_A)], \qquad \mathcal{R} = [\chi_A, \chi_B], \tag{4.A.4}
$$

where $G(\cdot)$ is defined as

$$
G(\chi) = \chi \cos(\phi - \theta) - \sin(\chi - \phi),
$$
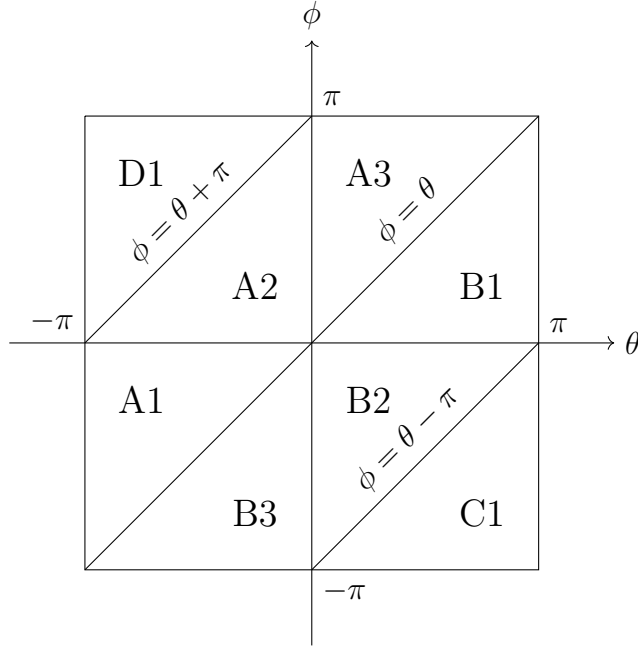
Figure 4.10: Subregions considered when calculating $\mathcal{R}$.

Table 4.3: The interval $\mathcal{R}$ for the different subregions of $[-\pi, \pi] \times [-\pi, \pi]$.

Subregion	Description	$\mathcal{R}$
A3	$0 \leq \theta \leq \pi,\ \theta \leq \phi \leq \pi$	$[-\theta + 2\pi,\ \theta + 2\pi]$
B1	$0 \leq \theta \leq \pi,\ 0 \leq \phi \leq \theta$	$[-\theta + 2\pi,\ 2\phi - \theta + 2\pi]$
B2	$0 \leq \theta \leq \pi,\ \theta - \pi \leq \phi \leq 0$	$\emptyset$
C1	$0 \leq \theta \leq \pi,\ -\pi \leq \phi \leq \theta - \pi$	$[2\phi - \theta + 4\pi,\ \theta + 2\pi]$
D1	$-\pi \leq \theta \leq 0,\ \theta + \pi \leq \phi \leq \pi$	$[\theta,\ 2\phi - \theta - 2\pi]$
A2	$-\pi \leq \theta \leq 0,\ 0 \leq \phi \leq \theta + \pi$	$\emptyset$
A1	$-\pi \leq \theta \leq 0,\ \theta \leq \phi \leq 0$	$[2\phi - \theta,\ -\theta]$
B3	$-\pi \leq \theta \leq 0,\ -\pi \leq \phi \leq \theta - \pi$	$[\theta,\ -\theta]$

Figure 4.11: $\mu(\phi; \theta)$, $v_0 = 1$, $\lambda = 1$, $R = 1$

and the values of χ_A and χ_B are taken from Table 4.3. Fig 4.11 shows the plot of the rate $\mu(\phi; \theta)$.
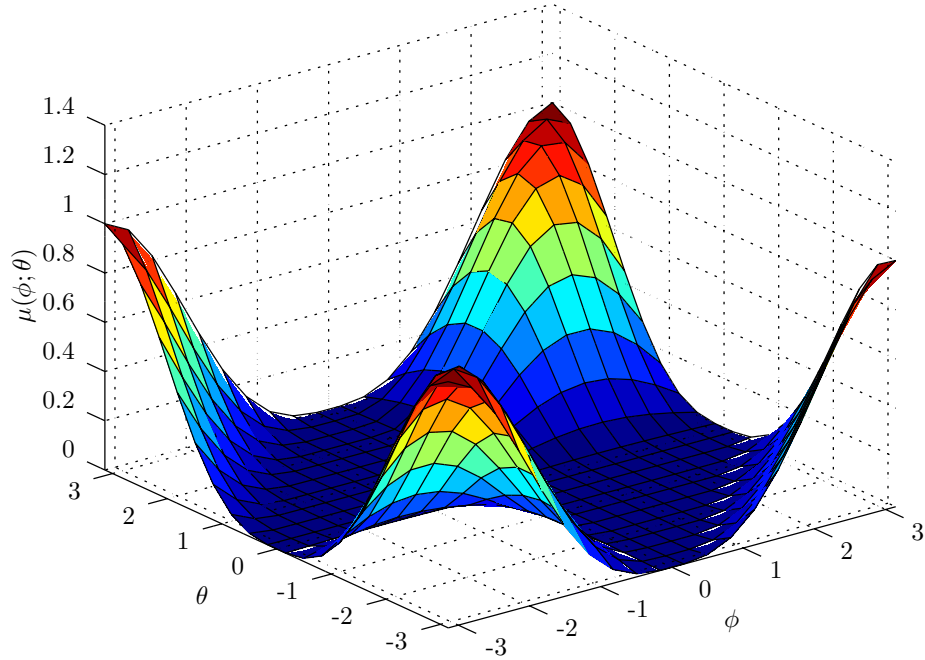
Conclusions

This work investigates two major topics: WBANs (Part I) and DTNs (Part II). The research presented in Part I is characterized by an experimental approach, while in Part II, problems are addressed with simulation techniques and mathematical analysis. This heterogeneity of approaches gave me the opportunity to understand the strengths and the limitations of each of them.

The research on WBAN has been driven by the needs of the WiserBAN project: a complete evaluation of the performance of a real WBAN implemented according to the WiserBAN specifications, taking into account three of the major challenges that characterize the design of such a network; namely, the impact of the human body on the radio channel characteristics, the energy consumption, and coexistence with other wireless technologies. These issues, along with an introduction to the WBAN concept, are described in Chapter 1. Chapter 2 presents the architecture of the WBAN realized for the WiserBAN project, an analytic model for the CSMA/CA with priorities defined in the IEEE 802.15.6 standard, where a query-based traffic is established, and the results of the measurement campaign performed to evaluate the PLR, average delay and energy consumption of the reference WBAN. The effects of the issues presented in Chapter 1 are highlighted, and novel solutions to mitigate their negative effects are presented and evaluated.

The amount of possible future work on this subject is abundant. Regarding the characterization of the radio channel in the presence of the human body, an experimental campaign has already started aiming at the evaluation of the characteristics of the *body-to-body* radio channel. The idea is to fill the gap in the literature for models describing the propagation channel between devices located on different human subjects. This information will be exploited to develop collaboration schemes at the MAC and/or network layer between WBANs deployed on different persons. The energy consumption of a WBAN can be further optimized by harvesting the energy produced by the human body, mainly by movement. Some work has already been done in this direction: the nodes of the WBAN simulate the arrival of energy packets coming from an harvester; the coordinator of the network queries the nodes according to a sequence that guarantees that the queried node has enough energy to reply. It would be interesting to make the coordinator able to predict the amount of energy available at any node, at any instant of time, by *learning* their energy harvesting patters. With respect to the coexistence issues, future work may be oriented to the experimental evaluation of the features of the WBAN-oriented IEEE 802.15.6 standard that deal with this issue, i.e., channel hopping and beacon shifting [43, Section 6.1.3]. Moreover the investigation should not be limited to the coexistence with other wireless technologies (e.g., Wi-Fi, being the most aggressive), but also to the coexistence with other WBANs. Channel hopping, introduced in an amendment to the IEEE 802.15.4 standard [54], is also worth to be evaluated experimentally. Another issue that is not investigated in this thesis is security. Virtually all the data that are exchanged in a WBAN are sensitive to privacy concerns; think of ECG data, or glucose levels. Moreover, the ability to wirelessly control biomedical instruments like an implanted defibrillator or an insulin

pump, makes it possible to "hack" these devices and even cause the death of the WBAN user [88]. These problems call for the adoption of strong security techniques, some of them already defined in the cited standards; see [7] for an overview. WBANs, as well as many other Internet-of-Things applications, will never be widely adopted as long as security remains a critical issue.

Part II of the thesis introduces the concept of DTN in the first section of Chapter 3. The rest of the chapter presents an idea that consists in using a DTN composed of pedestrians and vehicles moving in a urban area, to assist a low-range wireless backbone for the delivery of data from one location to another within the same urban area. Under some circumstances the wireless backbone may be unable to handle all its traffic; this happens when the offered data traffic is larger than the maximum throughpout that the network can support. When this happens, part of the traffic is offloaded to the DTN composed of pedestrians and vehicles that is in the proximity of the wireless backbone. Simulation results show that the throughput can be increased in this way, even without using any DTN routing protocol. The effect of the interference generated by the DTN on the backbone is also evaluated. This work can be considered preliminary, and there is room for further developments. Among them, a more realistic mobility model for pedestrians can be considered in order to replicate the social aspects of human mobility; for example: groups of friends moving together, nodes that periodically move from home to the working place, etc. When [11] was written, the SUMO simulator [77] allowed to model vehicles mobility only; its latest release includes a feature that allows us to model microscopically the mobility of pedestrians on sidewalks. Another next step would be to implement a routing algorithm for the DTN in order to further increase the throughput and decrease the average delay. Among the routing algorithms

available in the literature it is worth focusing on those that consider the sociability aspects of human mobility, since they are the best performing ones; for a survey, see [89]. Finally, it would be interesting to move towards a more realistic scenario with more backbones, sources and sinks, and use a real city map instead of an artificial Manhattan grid.

Chapter 4 concludes the investigation on on DTN. The work presented in this chapter establishes a mathematical framework for modeling the performance of a DTN under a RWP mobility model. The framework uses tools from stochastic geometry and Markov chain theory to model the average speed with which a generic packet moves towards the destination and the average cost per meter when a given routing rule is used. In fact, the packet travels towards the destination by means of a combination of physical transports in the buffers of the carrier nodes, which involve no cost, and wireless transmissions, which on the other hand, involve a cost equal to the square of the distance between transmitter and receiver. Four routing rules are defined, but only one of them is analyzed, while the other three are just simulated. However, it should be clear that the framework can be applied to a large number of routing rules. The simulation results match well with the analytic results, and mismatch, when present, is due to the approximations made to make the analysis tractable. Also in this case, many ways to improve the work are possible. For example, it would be interesting to apply the framework to the other routing rules presented in Section 4.2.4; to use a more realistic mobility model, which confines the nodes on bounded regions representing the streets of a urban area. In this case, the challenge would be to keep the model mathematically tractable and simple, its simplicity being its main strength.

Bibliography

[1] WiserBAN - smart miniature low-power wireless microsystem for body area. `http://wiserban.eu/`, 2013.

[2] Carlos Cordeiro. Use cases, applications, and requirements for bans, January 2007.

[3] Scott Burleigh, Adrian Hooke, Leigh Torgerson, Kevin Fall, Vint Cerf, Bob Durst, Keith Scott, and Howard Weiss. Delay-tolerant networking: an approach to interplanetary internet. *Communications Magazine, IEEE*, 41(6):128–136, 2003.

[4] Riccardo Cavallari, Eugenio Guidotti, Chiara Buratti, and Roberto Verdone. Experimental characterisation of data aggregation in BANs with a walking subject. In *Proceedings of the 7th International Conference on Body Area Networks*, pages 191–194. ICST (Institute for Computer Sciences, Social-Informatics and Telecommunications Engineering), 2012.

[5] Alfonso Panunzio, Marco Pietro Caria, Stefan Mijovic, Riccardo Cavallari, and Chiara Buratti. Experimental characterisation of an IEEE 802.15. 6-based body area network. In *Proceedings of the 8th International Conference on Body Area Networks*, pages 116–119. ICST (Insti-

tute for Computer Sciences, Social-Informatics and Telecommunications Engineering), 2013.

[6] Stefan Mijovic, Andrea Stajkic, Riccardo Cavallari, and Chiara Buratti. Experimental characterization of Low Power Listening in BAN. *e-Health Networking, Applications & Services (Healthcom), 2013 IEEE 15th International Conference on*, pages 145–149, 2013.

[7] Riccardo Cavallari, Flavia Martelli, Ramona Rosini, Chiara Buratti, and Roberto Verdone. A survey on wireless body area networks: technologies and design challenges. *Communications Surveys & Tutorials, IEEE*, 16(3):1635–1657, 2014.

[8] R. Cavallari and C. Buratti. On the performance of IEEE 802.15.6 CSMA/CA with priority for query-based traffic. In *Networks and Communications (EuCNC), 2014 European Conference on*, pages 1–5, June 2014.

[9] Stefan Mijovic, Riccardo Cavallari, and Chiara Buratti. Experimental characterisation of energy consumption in body area networks. In *2015 IEEE World Forum on Internet of Things (WF-IoT) (WF-IoT 2015)*, Milano, Italy, December 2015.

[10] Stefan Mijovic, Andrea Stajkic, Riccardo Cavallari, and Chiara Buratti. Low Power Listening in BAN: Experimental Characterisation. *International Journal of E-Health and Medical Communications (IJEHMC)*, 5(4):52–66, 2014.

[11] Riccardo Cavallari and Roberto Verdone. Performance of a lamp post wireless backbone with Delay Tolerant offload. In *Euro Med Telco Conference (EMTC), 2014*, pages 1–5. IEEE, 2014.

[12] Riccardo Cavallari, Roberto Verdone, and Stavros Toumpis. Cost/Speed analysis of mobile wireless DTNs under random waypoint mobility. In *2016 14th International Symposium on Modeling and Optimization in Mobile, Ad Hoc, and Wireless Networks (WiOpt'16)*, Tempe, USA, May 2016.

[13] H. Li, Y. Schwoerer, J. Yoon, J. Farserotu, W. Yang, K Sayrafian, D. Miniutti, and D. Lewis. IEEE 802.15.6 regulation subcommittee report, May 2010.

[14] H.S. Savci, A. Sula, Zheng Wang, N.S. Dogan, and E. Arvas. Mics transceivers: regulatory standards and applications [medical implant communications service]. In *SoutheastCon, 2005. Proceedings. IEEE*, pages 179–182, 2005.

[15] Peter D. Bradley. Implantable ultralow-power radio chip facilitates in-body communications. *RF DESIGN*, 30(6):20, 2007.

[16] ITU - Radio Regulations, Volume 1, Sectio iv. `http://life.itu.int/radioclub/rr/rindex.htm`, 2012.

[17] FCC - Medical Body Area Networks - small entity compliance guide. `http://www.fcc.gov/document/medical-body-area-networks`, May 2013.

[18] M Seyedi, Behailu Kibret, Daniel TH Lai, and M Faulkner. A survey on intrabody communications for body area network applications. 2013.

[19] Joonsung Bae, Hyunwoo Cho, Kiseok Song, Hyungwoo Lee, and Hoi-Jun Yoo. The signal transmission mechanism on the surface of human body for body channel communication. *Microwave Theory and Techniques, IEEE Transactions on*, 60(3):582–593, 2012.

[20] Ian F. Akyildiz, Fernando Brunetti, and Cristina Blázquez. Nanonetworks: A new communication paradigm. *Comput. Netw.*, 52(12):2260–2279, August 2008.

[21] L. Galluccio, T. Melodia, S. Palazzo, and G.E. Santagati. Challenges and implications of using ultrasonic communications in intra-body area networks. In *Wireless On-demand Network Systems and Services (WONS), 2012 9th Annual Conference on*, pages 182–189, 2012.

[22] B. Atakan, O.B. Akan, and S. Balasubramaniam. Body area nanonetworks with molecular communications in nanomedicine. *Communications Magazine, IEEE*, 50(1):28–34, 2012.

[23] Y. Davilis, A. Kalis, and A. Ifantis. On the use of ultrasonic waves as a communications medium in biosensor networks. *Information Technology in Biomedicine, IEEE Transactions on*, 14(3):650–656, 2010.

[24] Min Chen, Sergio Gonzalez, Athanasios Vasilakos, Huasong Cao, and Victor C. Leung. Body area networks: A survey. *Mob. Netw. Appl.*, 16(2):171–193, Apr. 2011.

[25] M. Ghovanloo. An overview of the recent wideband transcutaneous wireless communication techniques. In *Engineering in Medicine and Biology Society,EMBC, 2011 Annual International Conference of the IEEE*, pages 5864 –5867, 30 2011-sept. 3 2011.

[26] Songping Mai, Chun Zhang, Mian Dong, and Zhihua Wang. A cochlear system with implant dsp. In *Acoustics, Speech and Signal Processing, 2006. ICASSP 2006 Proceedings. 2006 IEEE International Conference on*, volume 5, page V, may 2006.

[27] D.B. Shire, S.K. Kelly, Jinghua Chen, P. Doyle, M.D. Gingerich, S.F. Cogan, W.A. Drohan, O. Mendoza, L. Theogarajan, J.L. Wyatt, and J.F. Rizzo. Development and implantation of a minimally invasive wireless subretinal neurostimulator. *Biomedical Engineering, IEEE Transactions on*, 56(10):2502 –2511, oct. 2009.

[28] Fred Dijkstra. Requirements for ban and ban standardization from the point of view of gaming. In *BODYNETS2012, 7th International Conference on Body Area Networks*, Sept. 2012.

[29] NATO network enabled capability, Nov. 2012.

[30] Sebastiano Schillaci. BAN in defence applications. In *BODYNETS2012, 7th International Conference on Body Area Networks*, Sept. 2012.

[31] B. Zhen, M. Patel, S. Lee, E. Won, and A. Astrin. TG6 technical requirements document (TRD). IEEE p802. 15-08-0644-09-0006, September 2008.

[32] M. Patel and J. Wang. Applications, challenges, and prospective in emerging body area networking technologies. *IEEE Trans. on Wireless Communications*, 17(1):80–88, Feb. 2010.

[33] Mouhcine Guennoun, Marjan Zandi, and Khalil El-Khatib. On the use of biometrics to secure wireless biosensor networks. In *Information and Communication Technologies: From Theory to Applications, 2008. ICTTA 2008. 3rd International Conference on*, pages 1–5. IEEE, 2008.

[34] C. C Y Poon, Yuan-Ting Zhang, and Shu-Di Bao. A novel biometrics method to secure wireless body area sensor networks for telemedicine and m-health. *Communications Magazine, IEEE*, 44(4):73–81, 2006.

[35] Chia-Hsien Lin, K. Saito, M. Takahashi, and K. Ito. A compact planar inverted-f antenna for 2.45 GHz on-body communications. *Antennas and Propagation, IEEE Transactions on*, 60(9):4422–4426, 2012.

[36] R. Rosini and R. D'Errico. Comparing on-body dynamic channels for two antenna designs. In *Antennas and Propagation Conference (LAPC), 2012 Loughborough*, nov. 2012.

[37] H. Giddens, D.-L. Paul, G.S. Hilton, and J.P. McGeehan. Influence of body proximity on the efficiency of a wearable textile patch antenna. In *Antennas and Propagation (EUCAP), 2012 6th European Conference on*, pages 1353–1357, 2012.

[38] Venkateswara Sarma Mallela, V Ilankumaran, and N Srinivasa Rao. Trends in cardiac pacemaker batteries. *Indian pacing and electrophysiology journal*, 4(4):201, 2004.

[39] Fan Zhang, Yanqing Zhang, J. Silver, Y. Shakhsheer, M. Nagaraju, A. Klinefelter, J. Pandey, J. Boley, E. Carlson, A. Shrivastava, B. Otis, and B. Calhoun. A batteryless 19uw MICS/ISM-band energy harvesting body area sensor node soc. In *Solid-State Circuits Conference Digest of Technical Papers (ISSCC), 2012 IEEE International*, pages 298 –300, feb. 2012.

[40] Vladimir Leonov, Paolo Fiorini, and Ruud J.M. Vullers. Theory and simulation of a thermally matched micromachined thermopile in a wearable energy harvester. *Microelectronics Journal*, 42(4):579 – 584, 2011.

[41] Zigbee Alliance. http://www.zigbee.org/.

[42] IEEE 802.15.4 Standard. *Part 15.4: Wireless Medium Access Control (MAC) and Physical Layer (PHY) Specifications for Low-Rate Wireless*

Personal Area Networks (LR-WPANs). IEEE, Piscataway, New Jersey, 08855-1331, 2006.

[43] IEEE standard for local and metropolitan area networks part 15.6: Wireless body area networks. *IEEE Std 802.15.6-2012*, pages 1 –271, February 2012.

[44] Abdelmalik Bachir, Mischa Dohler, Thomas Watteyne, and Kin K Leung. MAC essentials for wireless sensor networks. *Communications Surveys & Tutorials, IEEE*, 12(2):222–248, 2010.

[45] Amre El-Hoiydi and Jean-Dominique Decotignie. Low power downlink mac protocols for infrastructure wireless sensor networks. *Mob. Netw. Appl.*, 10(5):675–690, October 2005.

[46] Michael Buettner, Gary V. Yee, Eric Anderson, and Richard Han. X-MAC: a short preamble MAC protocol for duty-cycled wireless sensor networks. In *Proceedings of the 4th international conference on Embedded networked sensor systems*, SenSys '06, pages 307–320, New York, NY, USA, 2006. ACM.

[47] D. Kurup, W. Joseph, G. Vermeeren, and L. Martens. In-body path loss model for homogeneous human tissues. *Electromagnetic Compatibility, IEEE Transactions on*, 54(3):556–564, 2012.

[48] Raffaele D'Errico and Laurent Ouvry. A statistical model for on-body dynamic channels. *International Journal of Wireless Information Networks*, 17:92–104, 2010.

[49] R. Rosini and R. D'Errico. Off-body channel modelling at 2.45 GHzfor two different antennas. In *Antennas and Propagation (EUCAP), 2012 6th European Conference on*, pages 3378–3382, 2012.

[50] R. Rosini, R. D'Errico, and R. Verdone. Body-to-body communications: A measurement-based channel model at 2.45 GHz. In *Personal Indoor and Mobile Radio Communications (PIMRC), 2012 IEEE 23rd International Symposium on*, pages 1763–1768, 2012.

[51] Javier Bonny. Investigating MAC power consumption in wireless sensor network. *project report for the course of Self Organized Mobile Networks*, pages 1–5, 2004.

[52] R. de Francisco, Li Huang, and G. Dolmans. Coexistence of WBAN and WLAN in medical environments. In *Vehicular Technology Conference Fall (VTC 2009-Fall), 2009 IEEE 70th*, pages 1–5, Sep. 2009.

[53] Flavia Martelli and Roberto Verdone. Coexistence issues for wireless body area networks at 2.45 GHz. *European Wireless, 2012. EW. 18th European Wireless Conference*, pages 1 –6, april 2012.

[54] IEEE standard for local and metropolitan area networks–part 15.4: Low-rate wireless personal area networks (LR-WPANs) amendment 1: MAC sublayer. *IEEE Std 802.15.4e-2012 (Amendment to IEEE Std 802.15.4-2011)*, pages 1–225, 2012.

[55] CC2530, Texas Instruments. `http://www.ti.com/product/cc2530`, 2012.

[56] E. Le Roux, N. Scolari, B. Banerjee, C. Arm, P. Volet, D. Sigg, P. Heim, J.-F. Perotto, F. Kaess, N. Raemy, A. Vouilloz, D. Ruffieux, M. Contaldo, F. Giroud, D. Severac, M. Morgan, S. Gyger, C. Monneron, Thanh-Chau Le, C. Henzelin, and V. Peiris. A 1V RF SoC with an 863-to-928 MHz 400 kb/s radio and a 32b dual-MAC DSP core for wireless sensor and body networks. In *Solid-State Circuits Conference Digest*

of Technical Papers (ISSCC), 2010 IEEE International, pages 464–465, 2010.

[57] S. Rashwand, J. Misic, and H. Khazaei. Performance analysis of IEEE 802.15.6 under saturation condition and error-prone channel. In *Wireless Communications and Networking Conference (WCNC), 2011 IEEE*, 2011.

[58] S. Rashwand and J. Misic. Performance evaluation of IEEE 802.15.6 under non-saturation condition. In *Global Telecommunications Conference (GLOBECOM 2011), 2011 IEEE*, pages 1–6, 2011.

[59] Jamil Yusuf Khan, Mehmet R Yuce, Garrick Bulger, and Benjamin Harding. Wireless body area network (WBAN) design techniques and performance evaluation. *Journal of medical systems*, 36(3):1441–1457, 2012.

[60] Changle Li, Huan-Bang Li, and R. Kohno. Performance evaluation of IEEE 802.15.4 for Wireless Body Area Network (WBAN). In *Communications Workshops, 2009. ICC Workshops 2009. IEEE International Conference on*, pages 1–5, June 2009.

[61] Adam Dunkels, Fredrik Osterlind, Nicolas Tsiftes, and Zhitao He. Software-based on-line energy estimation for sensor nodes. In *Proceedings of the 4th workshop on Embedded networked sensors*, pages 28–32. ACM, 2007.

[62] Yong Li, Pan Hui, Depeng Jin, and Sheng Chen. Delay-tolerant network protocol testing and evaluation. *Communications Magazine, IEEE*, 53(1):258–266, 2015.

[63] Kevin Fall. A delay-tolerant network architecture for challenged internets. In *Proceedings of the 2003 conference on Applications, technologies, architectures, and protocols for computer communications*, pages 27–34. ACM, 2003.

[64] Kevin Fall and Stephen Farrell. DTN: an architectural retrospective. *Selected Areas in Communications, IEEE Journal on*, 26(5):828–836, 2008.

[65] Amin Vahdat, David Becker, et al. Epidemic routing for partially connected ad hoc networks. Technical report, Technical Report CS-200006, Duke University, 2000.

[66] Yue Cao and Zhili Sun. Routing in delay/disruption tolerant networks: A taxonomy, survey and challenges. *Communications Surveys & Tutorials, IEEE*, 15(2):654–677, 2013.

[67] Nabil Benamar, Kamal D. Singh, Maria Benamar, Driss El Ouadghiri, and Jean-Marie Bonnin. Routing protocols in Vehicular Delay Tolerant Networks: A comprehensive survey. *Computer Communications*, 48(0):141 – 158, 2014. Opportunistic networks.

[68] Fang Dong, Yuxiang Hu, Min Tong, and Xiaomin Ran. Supporting emergency service by retasking delay-tolerant network architecture. In *Mobile Ad-hoc and Sensor Networks, 2009. MSN'09. 5th International Conference on*, pages 360–365. IEEE, 2009.

[69] Opengarden. Firechat, 2015. `http://opengarden.com/`.

[70] The new trouble for oppressive regimes: FireChats. `http://www.todayszaman.com/anasayfa_`

`the-new-trouble-for-oppressive-regimes-firechat_370062.` `html`. Accessed: 16-01-2016.

[71] Cisco Visual Networking Index: Forecast and Methodology, 2013-2018. `http://newsroom.cisco.com/release/1197391/`, June 2014.

[72] Roberto Verdone, Davide Dardari, Gianluca Mazzini, and Andrea Conti. *Wireless sensor and actuator networks: technologies, analysis and design.* Academic Press, 2010.

[73] Savio Dimatteo, Pan Hui, Bo Han, and Victor OK Li. Cellular traffic offloading through wifi networks. In *Mobile Adhoc and Sensor Systems (MASS), 2011 IEEE 8th International Conference on*, pages 192–201. IEEE, 2011.

[74] Yong Li, Guolong Su, Pan Hui, Depeng Jin, Li Su, and Lieguang Zeng. Multiple mobile data offloading through delay tolerant networks. In *Proceedings of the 6th ACM workshop on Challenged networks*, pages 43–48. ACM, 2011.

[75] Joohyun Lee, Yung Yi, Song Chong, and Youngmi Jin. Economics of WiFi Offloading: Trading Delay for Cellular Capacity. *Wireless Communications, IEEE Transactions on*, 13(3):1540–1554, March 2014.

[76] Xuejun Zhuo, Wei Gao, Guohong Cao, and Sha Hua. An Incentive Framework for Cellular Traffic Offloading. *Mobile Computing, IEEE Transactions on*, 13(3):541–555, March 2014.

[77] Daniel Krajzewicz, Jakob Erdmann, Michael Behrisch, and Laura Bieker. Recent development and applications of SUMO - Simulation of Urban MObility. *International Journal On Advances in Systems and Measurements*, 5(3&4):128–138, December 2012.

[78] Ari Keränen, Jörg Ott, and Teemu Kärkkäinen. The ONE Simulator for DTN Protocol Evaluation. In *SIMUTools '09: Proceedings of the 2nd International Conference on Simulation Tools and Techniques*, New York, NY, USA, 2009. ICST.

[79] Anna Sidera and Stavros Toumpis. On the delay/cost tradeoff in wireless mobile delay-tolerant networks. In *Modeling and Optimization in Mobile, Ad Hoc, and Wireless Networks (WiOpt), 2014 12th International Symposium on*, pages 452–459. IEEE, 2014.

[80] P. Jacquet, B. Mans, and G. Rodolakis. Information Propagation Speed in Mobile and Delay Tolerant Networks. *Information Theory, IEEE Transactions on*, 56(10):5001–5015, Oct 2010.

[81] Argyrios G. Tasiopoulos, Christos Tsiaras, and Stavros Toumpis. Optimal and achievable cost/delay tradeoffs in delay-tolerant networks. *Computer Networks*, 70:59–74, 2014.

[82] Christian Bettstetter. Mobility modeling in wireless networks: categorization, smooth movement, and border effects. *ACM SIGMOBILE Mobile Computing and Communications Review*, 5(3):55–66, 2001.

[83] François Baccelli and Bartlomiej Blaszczyszyn. *Stochastic geometry and wireless networks: Theory*, volume 1. Now Publishers Inc, 2009.

[84] Sheldon M Ross. *Introduction to probability models*. Academic press, 2014.

[85] Vidyadhar G Kulkarni. *Modeling and analysis of stochastic systems*. CRC Press, 2009.

[86] James R Norris. *Markov chains.* Number 2008. Cambridge university press, 1998.

[87] Anna Sidera and Stavros Toumpis. Incidence Rates Calculations in Wireless Mobile Delay-Tolerant Networks. Unpublished. Available: `http://pages.cs.aueb.gr/~toumpis/research.html`, 2014.

[88] Medical devices vulnerable to hackers. `http://www.bbc.com/news/technology-34390165`. Accessed: 27-12-2015.

[89] Kaimin Wei, Xiao Liang, and Ke Xu. A survey of social-aware routing protocols in delay tolerant networks: applications, taxonomy and design-related issues. *Communications Surveys & Tutorials, IEEE*, 16(1):556–578, 2014.